Transportation Consortium of South-Central States

Solving Emerging Transportation Resiliency, Sustainability, and Economic Challenges through the Use of Innovative Materials and Construction Methods: From Research to Implementation

Assessing the Impacts of Super Storm Flooding in the Transportation Infrastructure – Case Study: San Antonio, Texas

Project No. 18HSTSA02

Lead University: University of Texas at San Antonio

Collaborative Universities: Texas A&M University

Final Report

August 2019

Disclaimer

The contents of this report reflect the views of the authors, who are responsible for the facts and the accuracy of the information presented herein. This document is disseminated in the interest of information exchange. The report is funded, partially or entirely, by a grant from the U.S. Department of Transportation's University Transportation Centers Program. However, the U.S. Government assumes no liability for the contents or use thereof.

Acknowledgements

The authors express gratitude to Mr. Nefi Garza, Assistant Director of the Transportation and Capital Improvement (TCI) Department of the City of San Antonio for the support to this research project. We also express appreciation for San Antonio River Authority (SARA) for sharing data and insights for this project. We thank also the reviewers and the staff and Director of Tran-SET.

TECHNICAL DOCUMENTATION PAGE

1. Project No.	2. Government Accession No.	3. Recipient's Catalog No.
18HSTSA02		

4. Title and Subtitle	5. Report Date
Assessing the Impacts of Super Storm Flooding in the Transportation Infrastructure – Case Study: San Antonio, Texas	Aug. 2019
	6. Performing Organization Code
7. Author(s)	**8. Performing Organization Report No.**
PI: Marcio H. Giacomoni https://orcid.org/0000-0001-7027-4128 Co-PI: Francisco Olivera https://orcid.org/0000-0003-0919-6815 GRA: Cesar do Lago https://orcid.org/0000-0002-0387-0226	
9. Performing Organization Name and Address	**10. Work Unit No. (TRAIS)**
Transportation Consortium of South-Central States (Tran-SET) University Transportation Center for Region 6 3319 Patrick F. Taylor Hall, Louisiana State University, Baton Rouge, LA 70803	**11. Contract or Grant No.** 69A3551747106
12. Sponsoring Agency Name and Address	**13. Type of Report and Period Covered**
United States of America Department of Transportation Research and Innovative Technology Administration	Final Research Report Mar. 2018 – Mar. 2019
	14. Sponsoring Agency Code

15. Supplementary Notes

Report uploaded and accessible at Tran-SET's website (http://transet.lsu.edu/).

16. Abstract

Flooding are likely to increase worldwide due to climate change. Large storms, referred here as superstorms, defined as events with return period equal or larger than 100 years, can lead to an increase of property damages and loss of life. The ability to predict and plan for the impacts of superstorms on transportation infrastructure is key to mitigate future damages and losses. This study analyzed 51 combinations of future projections for representative concentration pathways (RCP) 4.5 and 8.5 scenarios, which were used to calculate future 1st and 3rd quartiles, median, minimum and maximum intensity-duration-frequency curves (IDF). A HEC-HMS and GSSHA models were built for Leon Creek and Upper San Antonio watersheds. HEC-RAS 1D and 2D were used to evaluate flooding in 20 bridges and the extent of flooded area and roads in both watersheds and to test flood control scenarios. Land use modification with 5, 10 and 15% of LID areas in the watersheds were simulated. The use of levees and altering channels were evaluated. In addition, we evaluated how an increasing the storage capacity of the Olmos Dam would contribute to reduce flood impacts downstream. Results show that the 3rd quartile of projected IDF is closest to the one originated with observed precipitation, which is likely to increase in the future. The near future (2025-2049) under RCP 4.5 scenario presented the greatest increase in intensity. HEC-HMS models showed that discharge peak will increase for all future periods under both scenarios, for the 100- and 500-years storms. Flood projections generated by GSSHA for 100- and 500-years and future precipitation showed that flooded area can increase significantly. For instance, the increase in flooded roads can be more than 80% in near future for 500-year storm in Leon Creek watershed. HEC-RAS analysis showed that all 20 analyzed bridges can be flooded with 500-years storm with climate change and 15 with the 100-year storm. Simulation showed that LID implementation and the elevation of the Olmos Dam's crest were ineffective to protect transportation infrastructure. Enhancing cross-sections of the main channels and the use of levees can mitigate the impact in some bridges. This study illustrates the need for updates in the design criteria of current and future transportation infrastructure.

17. Key Words	18. Distribution Statement
Super storms, flooding, climate change, hydrologic modeling	No restrictions. This document is available through the National Technical Information Service, Springfield, VA 22161.

19. Security Classif. (of this report)	20. Security Classif. (of this page)	21. No. of Pages	22. Price
Unclassified	Unclassified	65	

Form DOT F 1700.7 (8-72) **Reproduction of completed page authorized.**

SI* (MODERN METRIC) CONVERSION FACTORS

APPROXIMATE CONVERSIONS TO SI UNITS

Symbol	When You Know	Multiply By	To Find	Symbol
		LENGTH		
in	inches	25.4	millimeters	mm
ft	feet	0.305	meters	m
yd	yards	0.914	meters	m
mi	miles	1.61	kilometers	km
		AREA		
in^2	square inches	645.2	square millimeters	mm^2
ft^2	square feet	0.093	square meters	m^2
yd^2	square yard	0.836	square meters	m^2
ac	acres	0.405	hectares	ha
mi^2	square miles	2.59	square kilometers	km^2
		VOLUME		
fl oz	fluid ounces	29.57	milliliters	mL
gal	gallons	3.785	liters	L
ft^3	cubic feet	0.028	cubic meters	m^3
yd^3	cubic yards	0.765	cubic meters	m^3
		NOTE: volumes greater than 1000 L shall be shown in m^3		
		MASS		
oz	ounces	28.35	grams	g
lb	pounds	0.454	kilograms	kg
T	short tons (2000 lb)	0.907	megagrams (or "metric ton")	Mg (or "t")
		TEMPERATURE (exact degrees)		
^oF	Fahrenheit	5 (F-32)/9 or (F-32)/1.8	Celsius	^oC
		ILLUMINATION		
fc	foot-candles	10.76	lux	lx
fl	foot-Lamberts	3.426	$candela/m^2$	cd/m^2
		FORCE and PRESSURE or STRESS		
lbf	poundforce	4.45	newtons	N
lbf/in^2	poundforce per square inch	6.89	kilopascals	kPa

APPROXIMATE CONVERSIONS FROM SI UNITS

Symbol	When You Know	Multiply By	To Find	Symbol
		LENGTH		
mm	millimeters	0.039	inches	in
m	meters	3.28	feet	ft
m	meters	1.09	yards	yd
km	kilometers	0.621	miles	mi
		AREA		
mm^2	square millimeters	0.0016	square inches	in^2
m^2	square meters	10.764	square feet	ft^2
m^2	square meters	1.195	square yards	yd^2
ha	hectares	2.47	acres	ac
km^2	square kilometers	0.386	square miles	mi^2
		VOLUME		
mL	milliliters	0.034	fluid ounces	fl oz
L	liters	0.264	gallons	gal
m^3	cubic meters	35.314	cubic feet	ft^3
m^3	cubic meters	1.307	cubic yards	yd^3
		MASS		
g	grams	0.035	ounces	oz
kg	kilograms	2.202	pounds	lb
Mg (or "t")	megagrams (or "metric ton")	1.103	short tons (2000 lb)	T
		TEMPERATURE (exact degrees)		
^oC	Celsius	1.8C+32	Fahrenheit	^oF
		ILLUMINATION		
lx	lux	0.0929	foot-candles	fc
cd/m^2	$candela/m^2$	0.2919	foot-Lamberts	fl
		FORCE and PRESSURE or STRESS		
N	newtons	0.225	poundforce	lbf
kPa	kilopascals	0.145	poundforce per square inch	lbf/in^2

TABLE OF CONTENTS

LIST OF FIGURES

LIST OF TABLES

ACRONYMS, ABBREVIATIONS, AND SYMBOLS

BCCAv2	Bias-Correction and Constructed Analogs Version 2
CMIP5	Coupled Model Intercomparison Project Phase 5
DBC	Daily Bias Correction
DEM	Digital Elevation Model
DT	Daily Translation
ERDC	Engineering Research and Development Center
FEMA	Federal Emergency Management Agency
GCM	General Climate Model
GEV	Generalized Extreme Value
GIS	Geographic Information System
GSSHA	Gridded Surface Subsurface Hydrologic Analysis
HEC	Hydrologic Engineering Center
HMS	Hydrologic Modeling System
IDF	Intensity-Duration-Frequency
LOCA	Localized Analogs (LOCA)
LOCI	Local Intensity
LU	Land Use
MPE	Multisensor Precipitation Estimation
NED	United States Elevation Data
NOAA	National Oceanic and Atmospheric Administration
NSE	Nash-Sutcliffe Efficiency
NWET	Number of Wet Days
P90	90th Percentile
P95	95th Percentile
P99	99th Percentile
RAS	River Analysis System
RCP	Representative Concentration Pathway

RCM	Regional Climate Model
SARA	San Antonio River Authority
SCS	Soil Conservation Services
SGS	United States Geological Survey
SSURGO	Soil Survey Geographic Database
TOPAZ	Topographic Parameterization Program
TxDOT	Texas Department of Transportation
USCOE	United States Army Corps of Engineers
WCRP	World Climate Research Program
WMS	Water Modeling System

EXECUTIVE SUMMARY

The frequency and severity of flooding from superstorm events are likely to increase worldwide due to climate change. A superstorm is defined in this investigation as an extreme rain event with a return period equal or higher than 100 years. Damages to property and loss of life can get significantly worse if the transportation infrastructure is vulnerable to flooding. Therefore, improving the understanding of how the transportation infrastructure is affected by large-scale floods is of vital importance, especially when massive evacuations are needed. This study analyzed 51 future projections of 33 General Climate Models (GCM) obtained in the Coupled Model Intercomparison Project Phase 5 (CMIP5) and downscaled with the Localized Analogs (LOCA) and Bias-Correction and Constructed Analogs Version 2 (BCCAv2) for representative concentration pathways (RCP) 4.5 and 8.5 scenarios. The projections were divided in three future periods: near future (2025-2049), mid future (2050-2074), and far future (2075-2099). Future projections were bias-corrected using the Daily Bias Correction (DBC) method. The bias-correction calibration used observed precipitation records between 1950 and 1974 and it was validated with historical data from 1975 to 1999. The future intensity-duration-frequency curves (IDF) were estimated with the generalized extreme value (GEV) method with yearly maximum rainfall depth in 1, 2, 3, 5 and 7 days. Intensities with durations less than one day were estimated by applying empirical factors calculated from the existing IDFs. The 1st and 3rd quartiles, median, minimum and maximum intensities of the projections were determined for both scenarios and each period. Subsequently, a HEC-HMS, HEC-RAS 1D, 2D and a GSSHA models were built for Upper San Antonio and Leon Creek watersheds. GSSHA was built with grid cells of 150m. The HEC-HMS and GSSHA models were calibrated and validated with six observed rainfall events that generated the greatest peak flow in the Upper San Antonio watershed in the last 15 years. GSSHA floodplain for 100-years storm was compared to Federal Emergency Management Agency (FEMA) 100-year floodplain map. HEC-RAS 1D model was used to evaluate the water surface elevation on 20 bridges in critical locations. A HEC-RAS 2D model was built with 3m cell size, with calculations performed over a terrain with 0.5m resolution. Alternative scenarios with Low Impact Development (LID) were evaluated with 5%, 10% and 15% of implemented area. In addition, we have analyzed how an increased storage capacity of the Olmos Dam would help to mitigate flood from future superstorms. Finally, levees and channel alterations were simulated in the Upper San Antonio watershed. Results show that the 3rd quartile of projected IDF is closest to the one originated with observed precipitation. The median and 1st quartiles from GCM sub estimated the intensities. The 3rd quartile intensity is likely to increase in the future, especially for storms longer than 1 day duration. The near future (2025-2049) under RCP 4.5 scenario presented the greatest increase in intensity. HEC-HMS showed that the peak discharge will increase for all future periods under both scenarios, for the 100- and 500-years storms in the 3rd quartile. The peaks from 1st quartile precipitations were consistently below the ones generated by the historical 100- and 500-years storm. Flood projections for 100- and 500-years with GSSHA and 3rd quartile precipitation showed that flooded areas can increase significantly in the near future under RCP 4.5, especially in the Leon Creek where the increase in flooded roads is estimated to increase more than 80%. The increase of flooded area and length of flooded roads was approximately linear, with a higher slope in Upper San Antonio where urbanization is more intense. HEC-RAS analysis showed that climate change can reduce from 9 to 5 the number of safe bridges subjected to 100-year storm in the near future in the selected studied location. In addition, all the 20 analyzed bridges are likely to be flooded with 500-year on the same scenario and future period. LID scenarios simulation suggests that LID implementation to protect the transportation infrastructure was

ineffective in mitigating the increase of surface runoff due to climate change. Only one bridge in Leon Creek would be reverted to normal condition with 100-year storm with 5% area with LIDS, and two bridges if the percentage of LID is 10%. Enhancing the cross-sectional area of the main channels was relatively efficient in reducing flood impacts. The number of bridges flooded in the near future was the same as current conditions for a 100-year storm when this strategy was tested. The projected flooded roads and area was almost as the same level as the predicted with the current 100-year storm and existing channel cross section. However, the flood damages of the future 500-year were still significantly higher. Increasing the Olmos Dam capacity reduced its overflow. However, it showed no effect in reducing flooding in the area located downstream. Its original configuration delays the hydrograph peak supporting flood protection. The runoff from other areas is responsible for the maximum flooding occurring in the critical area studied in Upper San Antonio. Implementing levees along the San Antonio river provides the highest level of protection against flooding. This control scenario was sized to prevent flooding for 100-year storm. This configuration reduced the 500-year flooding to approximately the 100-year level. Maps of central-south and central-north regions of San Antonio exemplify the impacts of climate change in San Antonio and how the reliability of existing infrastructure can be compromised. This report indicates that climate change is likely to increase flood damages in the transportation infrastructure at San Antonio and illustrates the need for an update in the design criteria of hydraulic manuals used in the region.

1. INTRODUCTION

Multiple studies indicate that climate change is likely to produce multiple negative economic, environmental, and social impacts, as a result in the increase of the frequency and intensity of extreme events, such as rain storms and consequently flooding *(1–5)*. Such impacts are exacerbated by the growth of urban population and impervious land cover. Hydrologically, climate change accelerates the hydrologic responses of urban watersheds, increasing the generation of stormwater runoff volume and peak flows. Yet, the non-stationary effects of climate change on rainfall patterns pose an obstacle to hydrologists in predicting damages from future floods because of the uncertainties of climate projections.

The evidences that climate change is increasing flood damages are strong since many intense storm events have been observed in the recent years. According to *(6)*, the United States has experienced 16 flood events in the past 10 years that exceeded $1 billion in losses, totalizing adjusted $51.2 billion in economic damages; these flood events also resulted in 224 deaths. Besides economic losses, floods can affect public health by spreading diseases *(7, 8)*. In 2017, the State of Texas registered Hurricane Harvey as a 1,000-year storm event. Tropical storm Harvey broke all the rainfall records for the U.S. (more than 50 inches) and produced unprecedented flooding in Eastern Texas, with a total damage estimation of $160 billion and at least 60 deaths. In 2016, the region around Baton Rouge, Louisiana, flooded as a consequence of a 500-year storm *(9)*. As a result of this storm, the City of Baton Rouge received approximately 25.5 inches of rainfall from August 12-14, 2016, which caused unprecedented flooding, damaged around 60,000 houses, and killed at least 13 people. In 2012, the Superstorm Sandy is believed to represent a storm with a return period between 150 to 1,000 years *(10)*. Sandy impacted more than 570,000 houses in the East Coast of the U.S., caused more than $75 billion in damages and resulted in at least 233 fatalities. Figure 1 show the exponential growth of adjusted costs from 1969 to 2019 that resulted from superstorms in the United States.

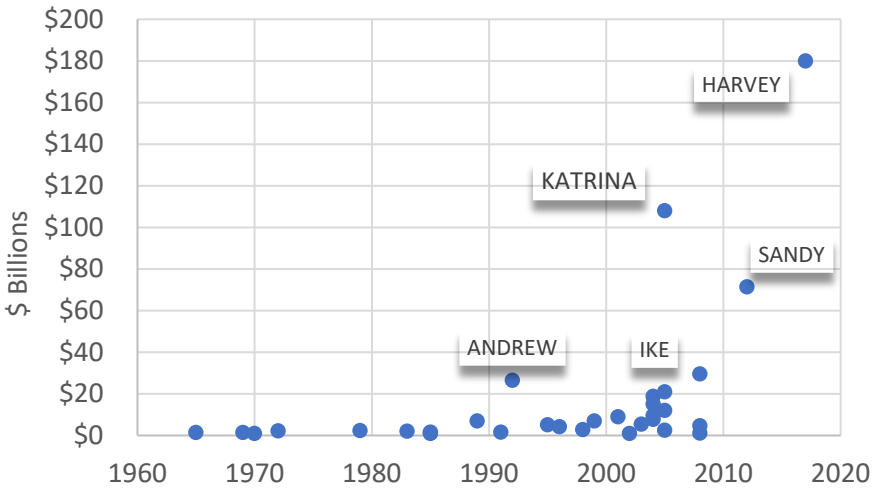

Figure 1. Cost of hurricanes in the United States since 1965.

Understanding how superstorms impact transportation infrastructure and communities, and how to better predict the future effects of climate change is of the utmost importance for society. Most critical infrastructure built in urban areas, including that for transportation and flood protection are designed to handle a design storm with a 1% probability of occurrence in one year or 100-year

return period. Moreover, the impacts of storm events and the design of flood protection structures are typically assessed using hydrologic and hydraulic simulation models. Many of these models are one-dimensional simplifications of complex drainage and riverine networks that simulate flow in these systems under steady flow conditions. In recent years, due to the increase of computing capacity, the use of 2 dimensional models (2D) has become more accessible. For instance, the U.S. Army Corps of Engineers released a new version of the software HEC-RAS which now incorporated 2D modeling capabilities and the Hydraulics Laboratory of the US Army Engineering Research and Development Center released the model Gridded Surface Subsurface Hydrologic Analysis.

2. OBJECTIVES

The main goal of this project is to develop and apply a computational framework capable of predicting the impacts of super storms in the transportation infrastructure and evaluating flood protection strategies that alleviate some of the impacts in highly populated urban areas. Four objectives are proposed:

- Objective 1: the first objective is to assess the impacts of super storms flooding in the transportation infrastructure. A suite of hydrologic and hydraulic simulation models were tested and used to evaluate flood impacts with a focus to the main transportation infrastructure, such as highways and bridges.
- Objective 2: the second objective is to explore alternative flood protection structures that can minimize damages and maximize the resilience of transportation systems in large metropolitan areas. The models were updated and flood control structures, such as levees, dams and alternative land cover were tested.
- Objective 3: the third objective is to train city and transportation officials and watershed managers to better delineate floodplain mapping of super storms and incorporate potential climate change impacts in future city planning.
- Objective 4: the last objective of this project is to enhance the public awareness of about the impacts of super storms in the built environment, with an emphasis in the main transportation infrastructure.

The current report presents the results obtained by the technical components, represented by Objectives 1 and 2.

3. LITERATURE REVIEW

Future climate predictions have many uncertainties, posing a major challenge for the development of strategies to mitigate storm impacts *(12, 13)*. The study published by *(14)* compared the performance of the GCMs included in the Coupled Model Intercomparison Project Phase 5 (CMIP5). The study included 27 indices to evaluate the models which compromise temperature, rainfall, droughts and others. We have summarized their results for six indices which can directly influence the uncertainty of predicting future flood events: (1) Maximum precipitation depth in one day, (2) maximum precipitation depth in five consecutive days, (3) the 95^{th} and (4) the 99^{th} percentiles of the greatest rainfall events, (5) the number of days with rainfall above 10mm, and (6) 20mm. The performance of 33 GCM for these six indices are shown in Figure 2 as root square mean error (RSME) between the models and four reanalysis datasets.

Intensity-duration frequency (IDF) curves are commonly used to estimate the frequency of damages caused by intense precipitations. The uncertainties in Figure 2 varies widely between the models, which directly influences the IDF parameters. This figure also shows that indexes related to more intense events are more uncertain. For instance, the prediction of the number of days with precipitation over 10mm was usually more precise. *(15)* used a Bayesian approach including 26 General Climate Model (GCM) contained in CMPI5 and found that the uncertainties of IDF parameters are more significant than those from the GCM. *(16)* discussed the types of uncertainties related to climate change and water resources with possible ways to diminish them. If the uncertainties are irreducible, there are two ways to manage them. The first is by precaution, which considers the worst scenario for the mitigation plans. The second is by the multi-model probabilistic approach, which may present different solutions based on the results presented by various global models. Because of high uncertainties of climate change models, it is advisable to include an array of future projections from different GCMs, as each may lead to alternative results.

GCM projections generate future precipitation series based on greenhouse gases emission scenario. These series are used to estimate future IDFs with the same methodology that is applied to historical records. The most common method is to find the yearly maximum intensities, adjust the values into a distribution function and then extrapolate them according to the probability. *(17)* used a combination of 50 GCM and Regional Climate Model (RCM) to generate future IDF for New York State. They found that the median increase of rainfall intensity is between 20 and 30% for RCP 8.5 scenario. *(18)* used 24 GCMs on their study and found that the frequency of extreme rainfalls is decreasing in central-south region of India. *(19)* found that the increase in 10-years storms is evident in southern Ontario under RCP 8.5. *(20)* used 9 GCMs to generate IDFs and found that all the projections presented an increase in intensity for all return periods in Thailand. *(21)* created IDFs with 3 GCMs for north of Vietnam, their results show a significant increase in rainfall intensity. *(22)* used 5 GCMs to analyze the changes in IDFs in Barcelona (Spain) and observed an increasing trend in rainfall intensity.

The literature suggests that an increase in rainfall intensity with direct impact on engineer structures is likely and expected worldwide. *(23)* modeled the impacts of climate change in Boston and found that the delay in trips caused by floods is likely to almost double between 2003 and 2025. *(24)* found that climate change will increase the frequency and extent of flooded roads in Oregon, which is estimated to cause up to 10% increase in travel delay. *(25)* investigated how extreme events effects transportation through data acquired from transit agencies. The authors found that, in most cases, the agencies take reactive measures, like sending alerts to avoid areas

with high risk of flooding. Just a few of them take a proactive approach to mitigate floods, and the reason is the lack of funding. Changes in policy making is required to prevent major impacts on transportation infrastructure as a result of climate changes.

These studies show that climate change projections present high related uncertainties and require proper methodology to maximize the efficiency of management actions. There is a voluminous number of studies involving the impacts of climate change. Few, however, address these impacts on transportation infrastructure. This report can guide decision makers to better manage of transportation infrastructure in the future of San Antonio as well as enhance scientific knowledge of climate change impacts in urban area on the built environment.

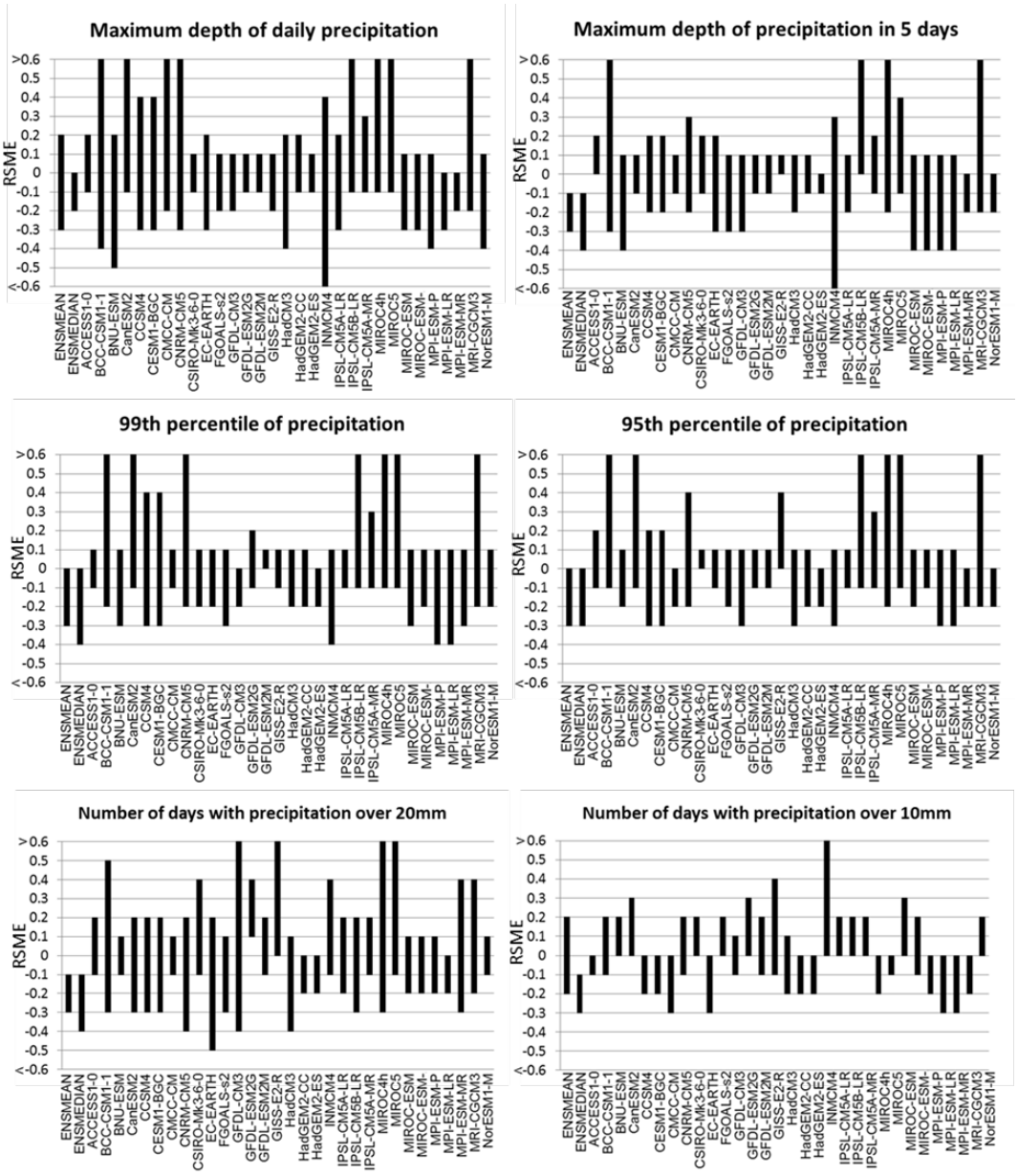

Figure 2. Performance of the General Climate Models measured as RSME, participating in the Coupled Model Intercomparison Project Phase 5 (CMIP5) on extreme precipitation indices. Based on *(14)*.

4. METHODOLOGY

4.1. Case Study

The case study is the City of San Antonio, TX, which lays within the flood prone region of Texas referred to as the *Flash Flood Alley*. This region is particularly vulnerable to super storms because: 1) it is experiencing one the fastest population growth rates in the U.S. (the population in 2016 was 1.6 million inhabitants and projected to reach 2.5 million residents in 2050 *(26)*; and 2) it is partially located in the *Balcones Escarpment*, which is characterized by a geomorphology with rugged natural drainage and intense rainfall events. The *Flash Flood Alley* constitute one of the most flood prone areas of the North American continent. Previous research conducted at UTSA shows that Bexar County leads the country in flood related deaths *(27)*.

San Antonio has a warm climate with an average temperature of 20.5ºC. The city has an annual average of 680mm of precipitation. Its climate is classified as humid subtropical Cfa according to Koppen. Examples of Superstorms with 100 and 500 years of return period calculated by NOAA's Atlas 14 *(28)* and USGS *(29) (30)* are shown in Figure 3. IDFs for Superstorms in San Antonio. The intensities calculated by two agencies differ. The intensity shows better agreement for shorter duration. The difference between the curves is highlighted with duration over 1 day. This figure shows how IDFs can also aggregate error to future estimations discussed in Section 3.

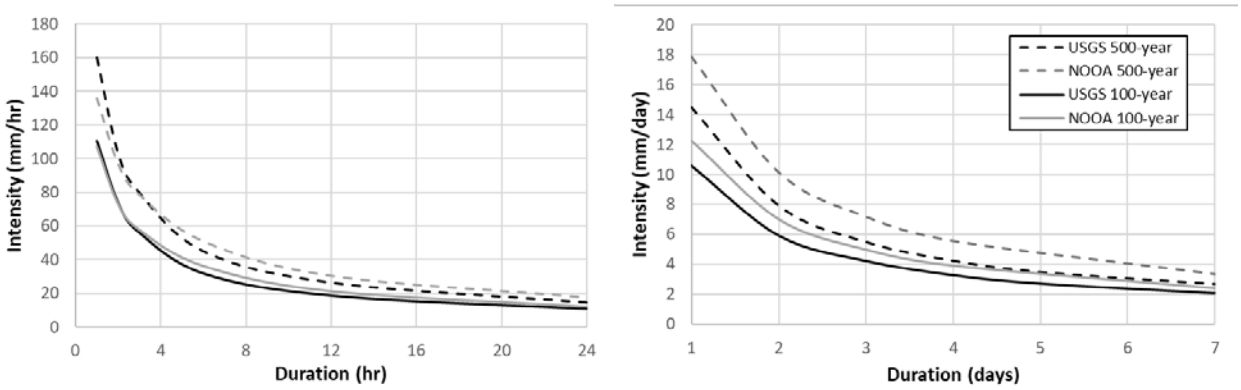

Figure 3. IDFs for superstorms in San Antonio.

Two watersheds within the City of San Antonio were selected: the Upper San Antonio and Leon Creek watersheds, located in the central and west portions of the City (Figure 4). The drainage area of Leon Creek and Upper San Antonio watersheds are 336.9 and 133.02 mi², respectively. These two watersheds were selected because of two significant differences. First, while Leon Creek watershed is fairly unprotected against large storm events, the Upper San Antonio watershed is heavily regulated and contains one of the most developed flood control systems in urban areas in the U.S. The Upper San Antonio flood control system includes the Olmos Dam and reservoir that was designed to regulated two consecutive 100-year 24 hours design storms, and two underground tunnels that divert water from the San Antonio River and San Pedro Creek bypassing the downtown area of the city.

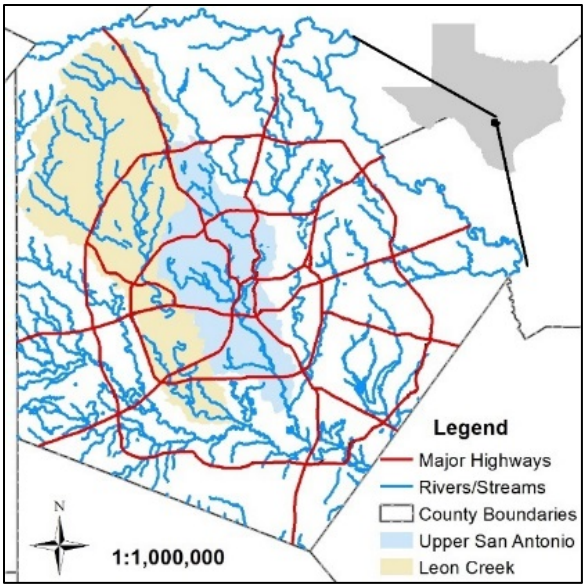

Figure 4. Location of Leon and Upper San Antonio.

The Olmos Dam was built in 1925-1927 at a cost of $1.5 million. This structure has a storage capacity of approximately 19,000,000 m^3 at its crest elevation of 207 m above sea level. The crest height is 16.5 m from the Olmos Creek bottom. The spillway has 351 m of length. The dam contains six gates. The dam's outflow varies little if only dependent on the gates, as Figure 4 shows. This figure also shows that its outflow only increases significantly if the water elevation surpasses 207 m (crest elevation).

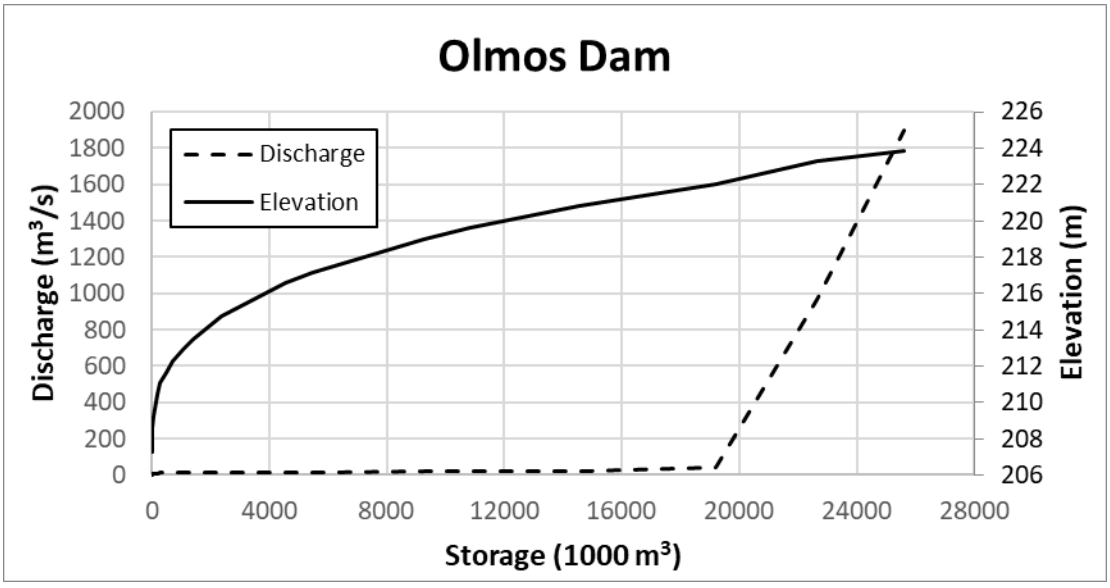

Figure 5. Olmos Dam discharge and elevation in function to storage.

The tunnels are located below the San Pedro Creek and San Antonio River (details in Figure 6). The tunnels have 24 ft of diameter. San Pedro Creek and San Antonio River tunnels are located 43 and 46 m on average below surface and are 1,824 and 4,945 m long, respectively. The San Pedro

Creek tunnel is able to divert almost all inflow below 100 m^3/s, while the San Antonio river tunnel diverts up to 180 m^3/s (Figure 7). Besides the greater capacity of the tunnel in San Antonio River up to 180 m^3/s when compared to the San Pedro's, the excess of runoff above this value tend to flow almost entirely on the surface.

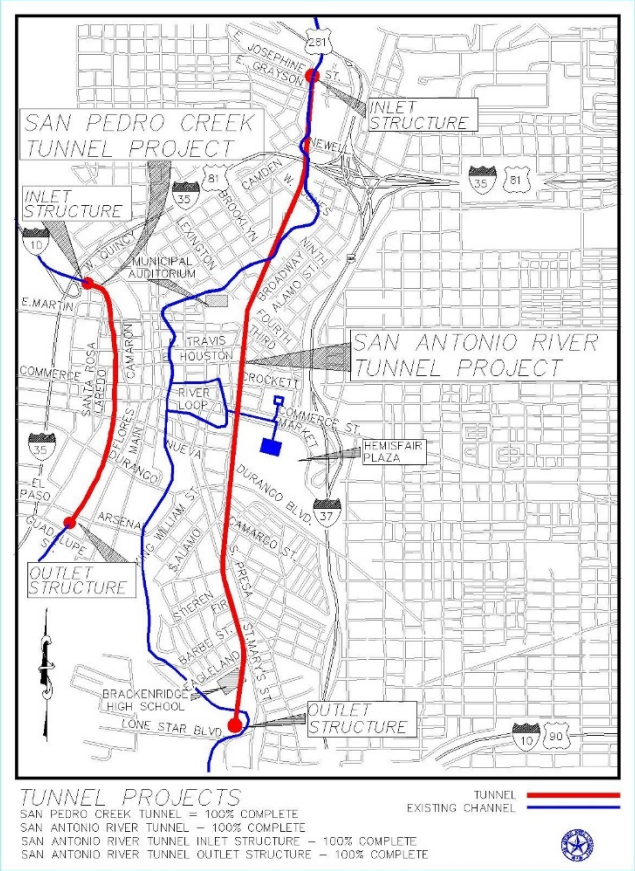

Figure 6. Tunnels in Upper San Antonio *(57)*.

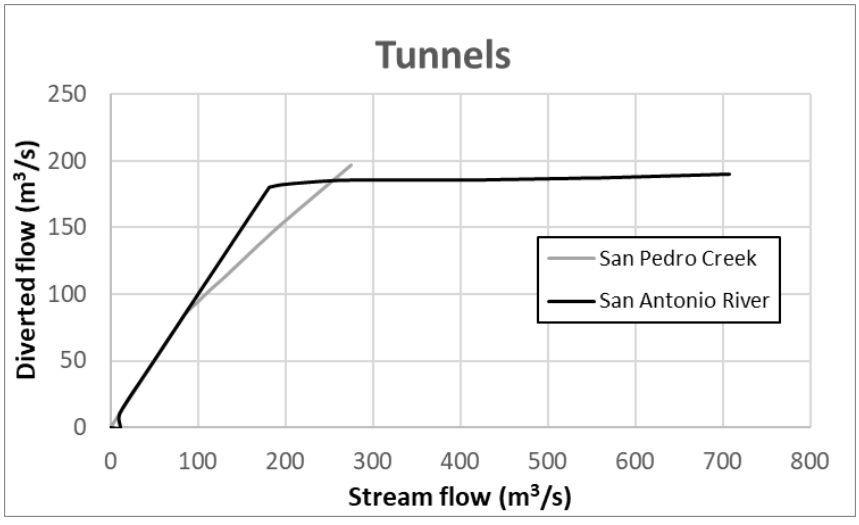

Figure 7. Bypass functions of the San Pedro and San Antonio tunnels.

4.2. Data Acquisition and Preparation

4.2.1. Precipitation and Flow

Flow data was acquired from USGS website for both Leon Creek and Upper San Antonio watersheds (USGS ID 08181480 and 08178565, respectively). The flow gauges and the watershed delineation can be observed in Figure 8. These are the closest flow gauges to the watersheds outlet. The six greatest observed runoff peaks over the last 15 years were selected to calibrate and validate the models. These were selected by subtracting the river base flow by the observed peak. The events 1, 2, and 3 were used for calibration and 4, 5, and 6 for validation. The most intense events were set for calibration to adjust better the models for the most extreme rainfalls.

Table 1. Rain events selected for calibration and validation.

	Upper San Antonio				
Event	**Date**	**Total Depth (in)**	**Duration (hr)**	**Maximum Intensity (in/hr)**	**Peak - Base Flow (cfs)**
1	5/25/2013	9.42	26	2.06	81,300
2	8/16/2007	5.17	12	1.71	63,132
3	9/26/2016	5.62	22	1.6	53,288
4	5/23/2015	3.23	24	0.83	45,968
5	6/2/2016	3.04	24	0.84	42,903
6	12/3/2016	3.79	32	0.78	29,617
	Leon Creek				
Event	**Date**	**Total Depth (in)**	**Duration (hr)**	**Maximum Intensity (in/hr)**	**Peak - Base Flow (cfs)**
1	5/25/2013	9.42	26	2.06	49,970
2	4/17/2010	4.71	21	1.86	16,264
3	10/30/2015	4.14	11	1.75	10,875
4	9/9/2018	1.6	5	1.38	10,207
5	9/8/2010	3.31	29	0.65	7,759
6	9/4/2018	5.47	28	1.08	6,297

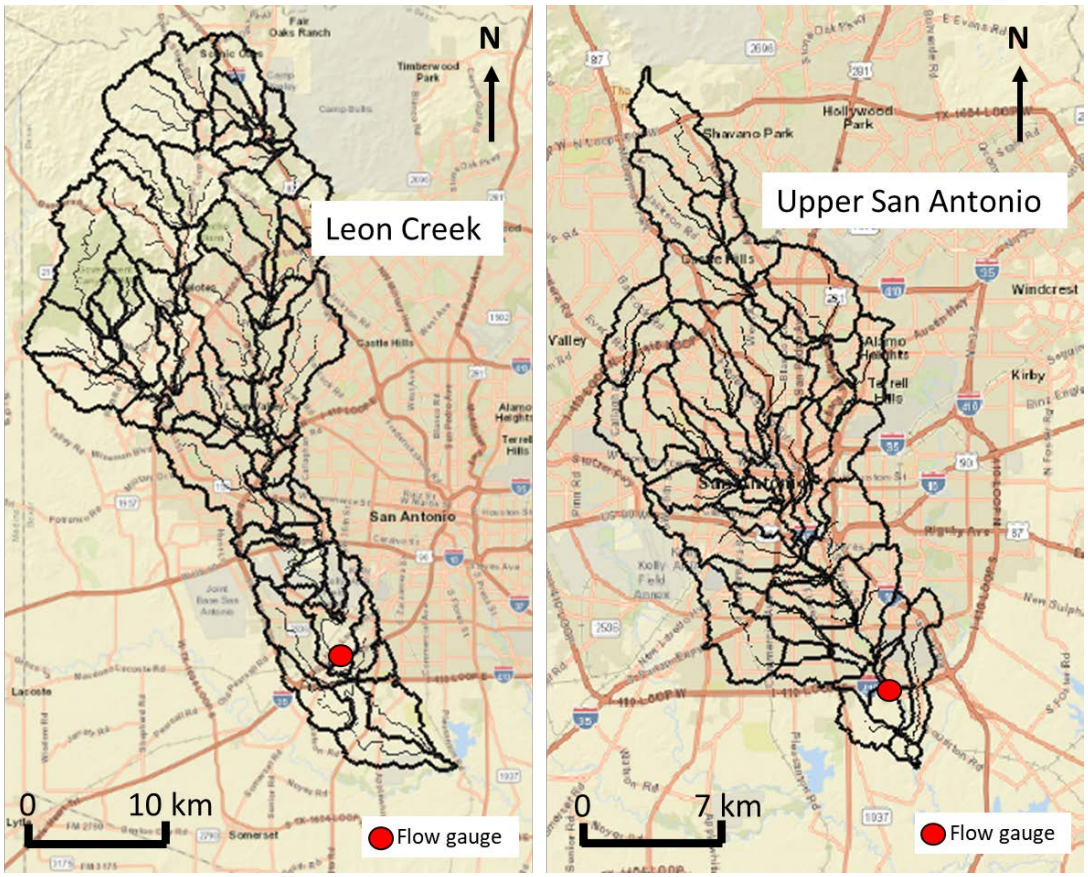

Figure 8. Leon Creek and Upper San Antonio watersheds.

Radar precipitation data was used for calibrating and validating the models. Level 4 radar precipitation data was used due to Multisensor Precipitation Estimation (MPE) adjustment. Radar data is available at Earth Observing Laboratoy's website *(31)* as Z file with 4 km spatial and 1 hour time resolution. The NOAA's Weather and Climate Toolkit (WCT) version 4.3.1 software was used to select the region of interest and convert the data to ASCII format *(58)*. The data covers the selected events plus seven prior days to warm the models up.

4.2.2. Geographic Information Systems (GIS)

The National Elevation Dataset (NED) of 10 m resolution was used to delineate the watershed and sub-basins, calculate the time of concentration, estimate the elevation-storage curve for Olmos Dam, generate the elevation grids for GSSHA model and estimate channels cross-sections. LiDAR (Light Detection and Ranging) with high 50 cm resolution data was obtained from the database of the San Antonio River Authority (SARA). This databased totals 3.0 Terabytes of information. LiDAR was used to support the estimation parameters for channels cross-section values.

The SSURGO (Soil Survey Geographic Database) soil map for San Antonio was used in the models. The landuse map (.tif file) was downloaded from City of San Antonio website *(32)* and converted to gridded map of 30 m resolution. Channels and street delineation shapefiles were also obtained from the City's website. The visualization of the flood maps was displayed upon World Street maps.

QGIS v 3.4.4 and Water Modeling System (WMS) v10.1 were the software used to manage and process GIS data. WMS was used to prepare the data for the hydrological modelling and QGIS to compute flood extension in area and length of flooded streets. The 10m resolution DEM, soil type and World Street map were directly downloaded through WMS interface.

4.2.3. Climate Change Data

Intensity-duration curves were generated for 4.5 and 8.5 RCPs. Rainfall projections from 32 different General Climate Models (GCM) were used here. The Bias-Correction and Constructed Analogs version 2 (BCCAv2) and the Localized Analogs (LOCA) downscaling methods were included. All GCMs were downscaled with LOCA and 19 with BCCAv2, totaling 51 different projection for both RCPs. The list of all GCMs is shown in Table 2. These climate change scenarios were obtained from the World Climate Research Programme's (WCRP's) Coupled Model Intercomparison Project Phase 5 (CMIP5) *(33)*.

The rainfall data was acquired from 1950 to 1999 (historical) and from 2025 to 2099 (future). Future projections were analyzed for near (2025-2059), medium (2050-2074), and far futures (2075-2099). The historical was used to compare the models to the observed rainfall data of that same period (Station ID: GHCND:USW00012921).

An additional bias correction was performed with the Daily Bias Correction (DBC) method. This hybrid method combines the Local Intensity (LOCI) *(34)* and Daily Translation (DT) *(35)* bias corrections. The LOCI method corrects the frequency of rainfall by setting a threshold so that the number of wet days is equal between observed and projected series. For an observed precipitation series with n wet days, the threshold is the n^{th} highest depth modeled and all depths below it is considered a noise in the climate model. Then, this method corrects the precipitation depths based on the average of observed daily precipitation and the projected series that are above the threshold. The DT adjusts the rainfall depths by finding the ratio of each percentile between observed and projected series. However, we have aim to identify the most extreme events and the factor to each percentile was encompassing many wet days. Therefore, a factor for each per thousand was determined in this bias-correction (Equation 1). The threshold and the percentile ratios were found with rainfall between 1950 and 1974. These same parameters were applied to correct the bias of 1975-1999 data for validation. So, 25 years were used to calibrate and validate this method, which is the same duration as the future time series.

$$f_i = \frac{Do_i}{Dgcm_i} \qquad [1]$$

where f is the correction factor, Do (mm) is the observed daily depth $Dgcm$ (mm) is the daily depth from the climate model after the LOCI correction and i is the correspondent per thousand (1 to 1000).

Table 2. GCMs and corresponding downscaling methods.

GCM	LOCA	BCCAv2
ACCESS1-0.1	X	X
ACCESS1-3.1	X	
BCC-CSM1-1.1	X	X
BCC-CSM1-1-M.1	X	
CANESM2.1	X	
CCSM4.6	X	
CESM1-BGC.1	X	X
CESM1-CAM5.1	X	
CMCC-CM.1	X	
CMCC-CMS.1	X	
CNRM-CM5.1	X	X
CSIRO-MK3-6-0.1	X	
EC-EARTH.2	X	
FGOALS-G2.1	X	
GFDL-CM3.1	X	
GFDL-ESM2G.1	X	X
GFDL-ESM2M.1	X	X
GISS-E2-H.2	X	
GISS-E2-R.2	X	
HADGEM2-AO.1	X	
HADGEM2-CC.1	X	
HADGEM2-ES.1	X	
INMCM4.1	X	X
IPSL-CM5A-LR.1	X	
IPSL-CM5A-MR.1	X	X
MIROC5.1	X	
MIROC-ESM.1	X	X
MIROC-ESM-CHEM.1	X	X
MPI-ESM-LR.1	X	
MPI-ESM-MR.1	X	X
MRI-CGCM3.1	X	X
NORESM1-M.1	X	X
Total	32	19

4.3. Future IDF Generation

The maximum rainfall depth in 1, 2, 3, 5 and 7 days for each of the 25 years within the 1975-1999 and the three future periods were calculated after the bias correction. Subsequently, the Generalized Extreme Value (GEV) method was used to estimate the rainfall depth for 2, 5, 10, 25, 50, 100 and 500 years of return period. This distribution was used to compare the IDF previously generated in Texas *(29, 30).* The GEV quantile can be calculated with Equation 2:

$$Q = \xi + \frac{\alpha}{\kappa}\{1 - [-\ln(F)]^{\kappa}\} \qquad [2]$$

where Q is the quantile, ξ is the location α is the scale, κ is the shape, and F is the yearly non-exceedance probability. The parameters ξ, α and κ can be estimated with L-moments *(36).* Sub-daily extremes for durations of 1, 6 and 12 hours were estimated using empirical factors *(37). (17)* also applied these factors to find future IDFs in the state of New York. The IDF estimated for all projections were summarized by the first and third quartiles, the median, and the minimum and maximum intensity values. The precision of the projections was verified with relative error to the observed, by developing boxplot with maximum, minimum, first, second and third quartile from all GCMs with both downscaling methods.

4.4. Models Development and Simulation

Three hydrologic model frameworks were developed in this investigation: 1) GSSHA, 2) HEC-HMS+HEC-RAS 1D, and 3) HEC-HMS+HEC-RAS 2D. The HEC-HMS and HEC-RAS models were obtained from SARA website. SARA's HEC-HMS was tested and after verifying that it overpredicts peaks of those 6 selected events, and a new one model was developed. The HEC-RAS 1D model from SARA was used here without significant alterations.

4.4.1. Gridded Surface Subsurface Hydrologic Analysis (GSSHA)

The Gridded Surface Subsurface Hydrologic Analysis (GSSHA) model was developed by the Watershed Systems Group within the Coastal and Hydraulics Laboratory of the US Army Engineering Research and Development Center (ERDC) *(11).* GSHAA is a fully distributed physically-based hydrologic model that represents watersheds using a structure grid and defined hydro-meteorological inputs *(11).* GSHAA is a reformulation of the two-dimensional model CASC2D *(11),* which failed to reproduce reliable results in saturation excess runoff condition, when groundwater plays a relevant influence in the generation of surface runoff. GSSHA represents precipitation distribution, snowfall accumulation and melting, precipitation interception, overland water retention, infiltration, overland flow routing, evapotranspiration, soil moisture in the vadose zone, lateral groundwater flow, stream/groundwater interaction and exfiltration. The model utilizes mass-conserving solutions of partial differential equations to solve many of the dynamic processes. GSSHA has been applied to several studies to analyze hydrologic and sedimentation processes, planning and design of flood control structures, land-use change, environmental restoration, best management practices, and climate change. GSSHA has been recently certified by Federal Emergency Management Agency (FEMA) to be used in National Flood Insurance Program studies as a hydrologic model.

The GSSHA model is built following a series of steps inside the WMS software. First, GSSHA computes flow paths using the algorithm Topographic Parameterization Program (TOPAZ) *(38).* The input for TOPAZ includes a DEM obtained from the National Elevation Dataset with resolution of 10 m. The algorithm fills depressions, and generates flow direction and flow accumulation layers in order to obtain stream segments. The streams had to be adjusted to their actual location in the watershed, which were redrawn based on San Antonio's channels shapefile. Then the arcs were smoothed using simple interpolation between the vertices. The channel bottom width, depth and side slope of each arc was set. Manning's roughness values were estimated by observing satellite images of the channel's surfaces. Finally, the elevation of each arc was set based on the digital elevation model. Satellite image was used to identify culverts weir and reservoir in each watershed. The Upper San Antonio watershed contains the Olmos Dam reservoir, which was represented as an embankment with culverts in GSSHA.

After the streams and subwatersheds were delineated, the resolution of the model was reduced from 10 to 150m. The resolution was reduced to decrease computational efforts, as GSSHA model with a grid of 10 m would require significant computational run time. The 150m resolution grid was interpolated to the river arcs to incorporate their depth to the grid. During the interpolation process, *Dam* grid cells, which have lower elevation than its neighbors, are generated and need to be removed. In TOPAZ, these are excluded by using a smoothing function before executing the model.

Grids for land use (LU) and soil type were computed, shown in Figures 9 and 10 for Leon Creek and Upper San Antonio watersheds, respectively. The map color representation and the percentage of each soil and LU characteristics are presented in Tables 3 and 4. LU indicates the characteristics of imperviousness and roughness of each grid, while soil type defines the infiltration parameters. It can be observed that that Upper San Antonio watershed is almost fully urbanized, while Leon Creek has a significant green area percentage of its watershed on the north west. Leon Creek has a higher percentage of bedrock formation than the Upper San Antonio watershed. The bedrock formation matches with the Edwards Trinity aquifer system area. Land use and soil type information was used to parameterize the Green and Ampt infiltration method *(39)* with moisture redistribution used in GSSHA.

Table 3. Soil type percentages for Leon and Upper San Antonio watersheds.

Soil	Leon Creek (%)	Upper San Antonio (%)
Loam	0.8	0.7
Silty clay	19.3	28.2
Sandy clay	0.04	0.3
Variable	1.1	0.7
Clay	20.4	41.0
Very gravelly loam	0.3	1.6
Clay loam	8.6	8.3
Bedrock	41.1	17.3
Gravelly clay loam	7.9	1.9
Fine sandy loam	0.6	0.6

Table 4. Land use percentages for Leon and Upper San Antonio watersheds.

Land Use	Leon Creek (%)	Upper San Antonio (%)
Barren Land (Rock/Sand/Clay)	0.00	0.7
Cultivated Crops	3.3	0.3
Deciduous Forest	5.0	1.3
Developed, High Intensity	9.4	15.1
Developed, Low Intensity	11.6	30.2
Developed, Medium Intensity	10.6	21.6
Developed, Open Space	15.3	22.9
Evergreen Forest	22.3	2.6
Grassland/Herbaceous	5.1	0.7
Mixed Forest	9.0	0.7
Open Water	0.5	0.5
Pasture/Hay	1.0	1.3
Shrub/Scrub	10.0	3.3
Woody Wetlands	1.3	0.04

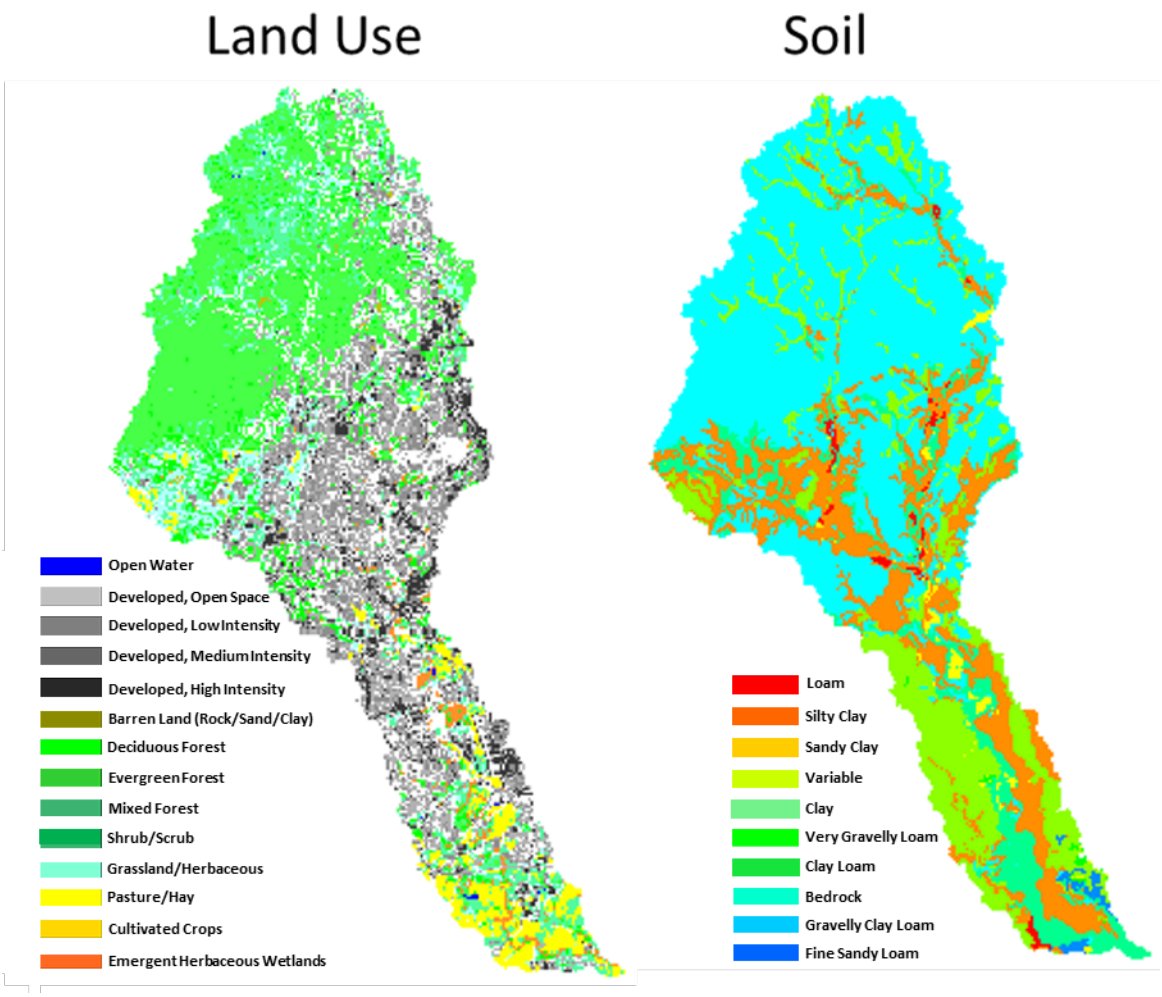

Figure 9. Land use (right) and soil type (left) grids for Leon Creek.

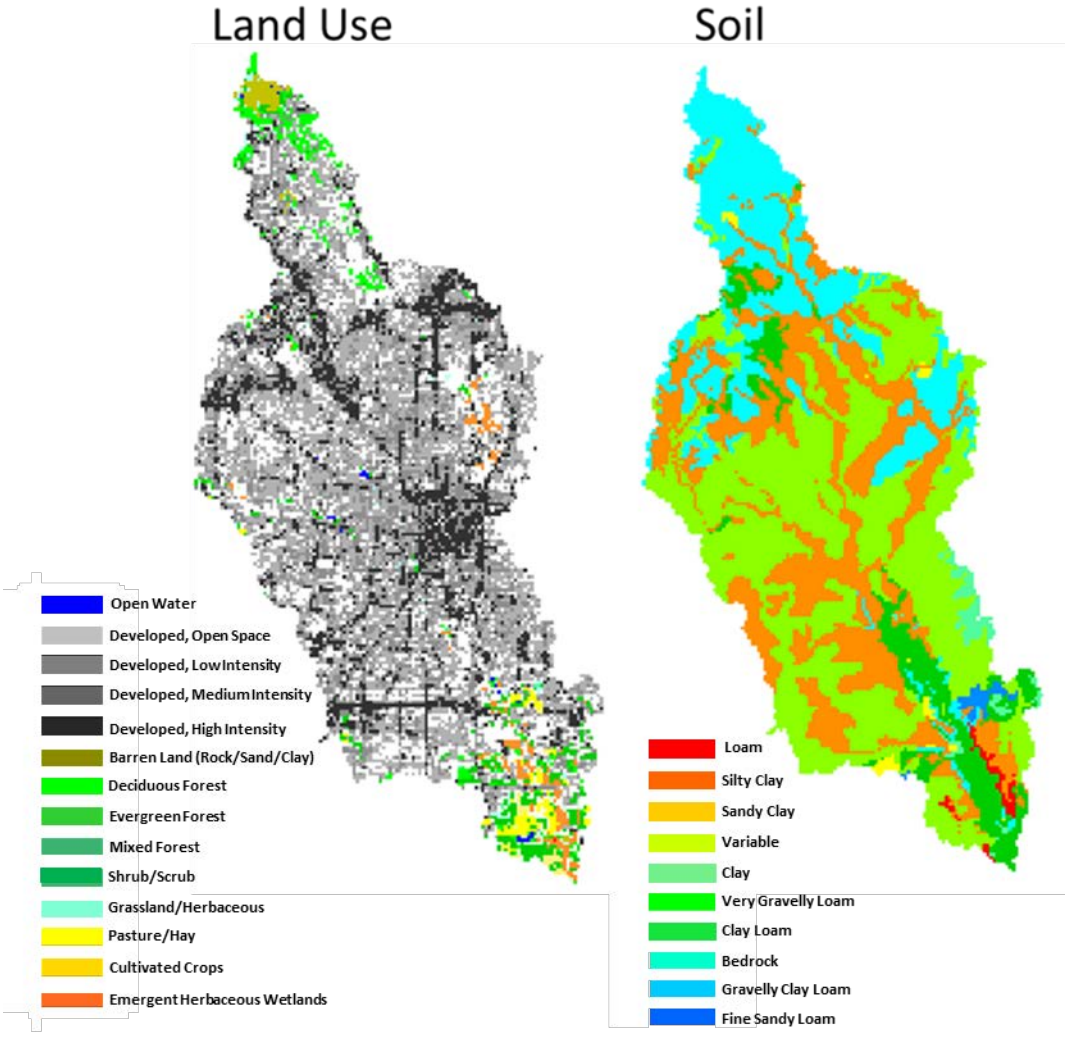

Figure 10. Land use (right) and soil (left) grids for Upper San Antonio.

An embankment was created to represent the Olmos Dam in Upper San Antonio. It was drawn in the correspondent location of the dam with the correspondent location as described in Subsection 4.1. Two culverts with 3.5m and 6m in width and height were inserted to represent two open gates, as it normally occurs.

The representation of the tunnels was done using initial boundary conditions at their inlet and outlet. In this case, the overflow was represented using the diverted and non-diverted flow modeled with HEC-HMS (described in Subsection 4.4.2.). The flow between the tunnel inlet and outlet was correspondent the non-diverted flow into the tunnels. The diverted flow modeled with the HEC-HMS was added at the grid where the outlet is located. This methodology represents a loss of runoff at the inlet, which is added latter at the grid correspondent to the outlet.

4.4.2. HEC-HMS + HEC-RAS 1D

The Hydrologic Modeling System (HMS) and River Analysis System (RAS) are, respectively, hydrologic and hydraulic computer applications developed by the Hydrologic Engineering Center (HEC) of the U.S. Corps of Engineers (USACE). HMS is a watershed rainfall-runoff tool that has

precipitation time series at different watershed locations and watershed physical characteristics as input, and estimates flows at a number of different locations in the system. It uses a semi-distributed approach in which the watershed is subdivided into a number of elements (i.e., sub-basins, reaches, junctions, sources, sinks, reservoirs and diversions) dendritically connected, with the exception of the case of the diversions. For the sub-basins, HMS includes a number of runoff depth estimation models to choose from, including the Curve Number method, Green and Ampt method, and initial plus constant rate, among others. Estimated runoff depths are then routed to the sub-basins' outlets using a unit hydrograph approach for which there are also a number of options to choose from, including the Soil Conservation Service's (SCS), and Clark's, among others. Calculated flows at the sub-basins' outlets are then routed through a stream network. Again, a number of routing options are available, including the Muskingum's and level pool routing, among others. Hydrographs are calculated at the upstream and downstream points of each element.

The HEC-RAS 1D is a flow-stage tool that has flows and the physical characteristics of the reach as input, and estimates the water depth at different reach cross sections. When combined with Geographic Information System (GIS) software and detailed terrain data, RAS is able to generate floodplain maps. RAS uses a semi-distributed approach in which the reach is subdivided into segments, defined by cross-sections, composed of a middle main channel and bound by a floodplain on each side. RAS can also include a number of different infrastructure features that affect the flow such as bridges and culverts. RAS supports steady and unsteady one-dimensional flow (i.e., along the reach axis). In steady flow, time-invariant flow values at different locations are used; in unsteady flow, instead of entering a time-invariant flow value, a hydrograph is used. The unsteady option is of particular use when the travel time in the reach is significantly longer than the timeframe in which the flows vary.

A new HEC-HMS model was built for both watersheds. The HEC-HMS models for the Leon Creek (236 mi^2) contains 98 sub-basins and 97 reaches. The HEC-HMS model for the Upper San Antonio River watersheds (134 mi^2) was divided into 40 sub-basins, 40 reaches, and 1 reservoir. See Figure 4 for sub-basin boundaries of the Leon Creek and Upper San Antonio watersheds. The models uses the Green and Ampt infiltration model and the SCS Unit Hydrograph for the transformation of rainfall excess into runoff. The river routing is computed using the Muskingun-Cunge model. The parameters estimation for Green and Ampt and impervious area were computed using the weighted average based on the area of land use and soil types.

The Olmos Dam was modeled using a elevation-storage function and a storage-discharge function for its outlet (Figure 5). The San Pedro and San Antonio tunnels were modeled with inflow-diversion functions (Figure 7). Therefore, the discharge diverted in the tunnels is function of the stream flow at the inlet. The Olmos Dam and the tunnels functions were downloaded from SARA's website *(57)*.

The HEC-RAS 1D model was also downloaded from SARA's website. This model was used in critical areas in terms of transportation infrastructure with higher flooded area identified with GSSHA model. The location of HEC-RAS 1D analysis for Leon Creek and Upper San Antonio watersheds are represented in Figures 11 and 12. For the Leon Creek, the HEC-RAS 1D models contained 286 cross sections, three lateral structures, two culverts and nine bridges. The Upper San Antonio river was modeled using HEC-RAS containing two inline structures, two culverts, 185 cross sections and 20 bridges. The HEC-RAS upstream initial boundary condition flows was obtained from the HEC-HMS output. The downstream boundary condition was set to be normal

depth. The Upper San Antonio contains two upstream boundary condition, one for San Antonio River and another for San Pedro Creek. In addition, a lateral inflow from Apache Creek into San Pedro Creek was also included. Unsteady flow simulations were run with 10 s-time step and a 15 min time resolution of the input flow.

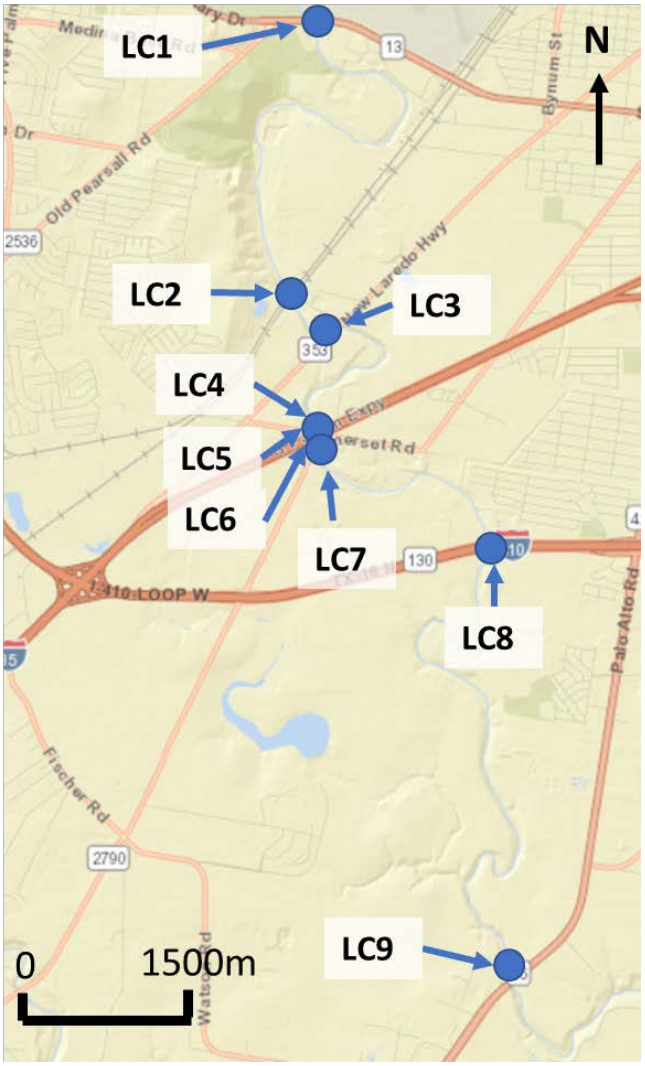

Figure 11. Area and bridges of HEC-RAS analysis in the Leon Creek.

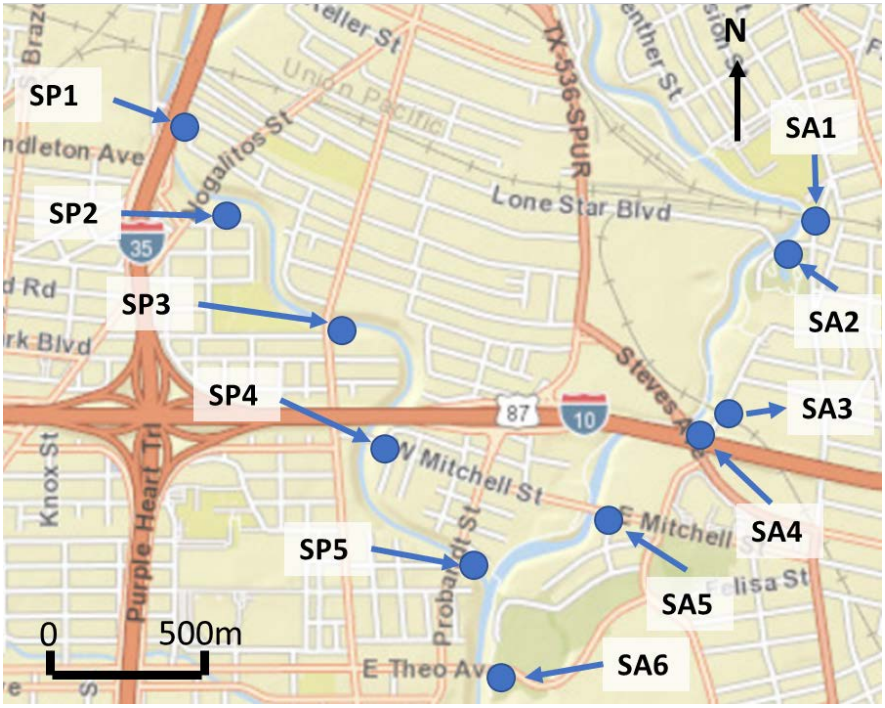

Figure 12. Area and bridges of HEC-RAS analysis in Upper San Antonio river and the tributary San Pedro Creek.

The name of all analyzed bridges is shown in Table 5. For each bridge, the difference between the water surface elevation and the elevation of bridge deck was calculated to assess the flood depth. Bridges that crosses over the San Antonio river and San Pedro creek were included in the analysis. In this watershed, the Inter-State 10 (I-10) and the Highway U.S. 87 were not included in the analysis, as the water elevation did not reach them even in the worst-case scenario.

Table 5. Analyzed bridges located in the San Antonio, San Pedro and Leon Creek.

Leon Creek		San Antonio River		San Pedro Creek	
Bridge Name	**Code**	**Bridge Name**	**Code**	**Bridge Name**	**Code**
SW Military Drive	LC1	S.P. Co. Railroad	SA1	Furnish Street	SP1
Quintana	LC2	Lone Star Boulevard	SA2	Nogalitos Street	SP2
New Laredo Highway	LC3	MKT & So. Pacific Railroad	SA3	South Flores Street	SP3
IH 35 S Access Road	LC4	Steves Avenue	SA4	West Mitchell Street	SP4
IH 35 S	LC5	E. Mitchell Street	SA5	Probandt Street	SP5
IH 35 S Access Road 2	LC6	E. Theo Avenue	SA6		
Somerset Road	LC7				
SW Loop 410	LC8				
State Highway 16	LC9				

4.4.3. HEC-RAS 2D

Some scenarios simulated with HEC-RAS 1D extrapolated the cross section limits, which reduces the precision of the floodplain estimation. HEC-RAS also supports unsteady 2D dimensional flow in which the terrain is represented by a grid of cells from which and to which the water flows. HEC-RAS 2D simulations were carried out to estimate the extent of flooded area in the locations showed the section 4.4.2. The input to a HEC-RAS 2D can be of two types: (1) hydrographs at the reach and tributary headwaters; and (2) precipitation hyetographs at the different elements of the terrain grid. This study used HEC-RAS 2D as a routing model, similarly to the HEC-RAS 1D. In the former case, HEC-RAS routes the flow and estimates water depths, supporting the case of overflow of the main channel. In the latter case, HEC-RAS estimates runoff depths and routes them across the landscape within and outside the main channel.

The 0.5 m resolution lidar DEM was used to represent the terrain in HEC-RAS 2D. Than, 3 m grids were created for the simulation base of the model, as recommended by FEMA (10 ft maximum grid). The same land use file (.tif) used for GSSHA model was inserted in the HEC-RAS 2D for setting the roughness along the area. In addition, left and right river embankments were drawn to designate a separate roughness within its limits. The simulations were performed with 1 second time step. The same boundary conditions used in the 1D model were applied to the 2D model.

4.5. Model Assessment and Simulations

The developed models were assessed via calibration and validation steps. The calibration was performed manually with the three most intense events and the validation with the other three intense storm events (see Table 1). The calibration was performed to minimize the difference between observed and simulated peak flows. The performance of the model was evaluated with the difference in peaks and in volume, NSE (Equation 3) and R^2. The initial parameters related to land use and soil are shown in Tables 6 and 7. The floodplains generated with GSSHA above 0.1m depth with 100-years storm were compare to Federal Emergency Management Agency (FEMA) predictions for the same frequency *(57)*. The flooded area and flooded roads were calculated for depths above 0.3m, which can float many common vehicles according to FEMA.

$$NSE = 1 - \frac{\sum_{t=1}^{T}(Q_m^t - Q_o^t)^2}{\sum_{t=1}^{T}(Q_o^t - Q_o^A)^2} \quad [3]$$

where $Q_m^t$is the modeled flow in time *t*, Q_o^t is the observed flow in time *t*, Q_o^A is the average of observed flow and *T* is the total simulated period.

The land use initial parameters was based on *(40)*, shown in Table 6. The soil parameters for infiltration was based on *(41)* and is shown in Table 7. The hydraulic conductivity, suction head and porosity for limestone (bedrock) were based on *(42–44)*, respectively.

After calibration and validation, a series of simulation runs were performed using design storms. The SCS type III of rainfall distribution was applied to the rainfall depth of different IDF curves, for both existing IDF used by USGS *(29, 30)* and the future IDFs. The 24 hours storm duration was chosen because of the time of concentration of the watersheds that are in the same order of magnitude and because many hydraulic structures are designed to handle 24 hours long storm events.

Table 6. Initial land use parameters.

Land Use Type	Roughness ($s/m^{1/3}$)	Impervious Area (%)
Water	0.045	99.99
Developed, Open Space	0.3	20
Developed, Low Intensity	0.07	45
Developed, Medium Intensity	0.013	75
Developed, High Intensity	0.011	90
Barren land	0.4	0
Deciduous forest	0.492	0
Evergreen Forest	0.492	0
Mixed Forest	0.492	0
Shrub/Scrub	0.48	0
Grassland/Herbaceous	0.45	0
Pasture/Hay	0.45	0
Cultivated Crops	0.45	0
Woody Wetlands	0.45	0
Herbaceous wetlands	0.45	0

Table 7. Initial soil parameters.

Soil	Hydraulic Conductivity (cm/hr)	Suction Head (cm)	Total Porosity (cm^3/cm^3)	Effective Porosity (cm^3/cm^3)	Residual Saturation (cm^3/cm^3)	Field Capacity Saturation (cm^3/cm^3)	Wilting Point Saturation (cm^3/cm^3)
Bedrock	0.02	1.00	0.06	0.05	0.01	0.01	0.006
Clay	0.03	31.63	0.48	0.39	0.09	0.40	0.27
Clay loam	0.10	20.88	0.46	0.39	0.08	0.32	0.20
Fine sandy loam	1.09	11.01	0.45	0.41	0.04	0.21	0.10
Gravelly clay loam	0.10	20.88	0.46	0.39	0.08	0.32	0.20
Loam	0.66	8.89	0.46	0.43	0.03	0.27	0.12
Sandy clay	0.06	23.90	0.43	0.32	0.11	0.34	0.24
Silty clay	0.05	29.22	0.48	0.42	0.06	0.39	0.25
Variable	0.31	17.37	0.42	0.36	0.06	0.28	0.17
Very gravelly loam	0.66	8.89	0.46	0.43	0.03	0.27	0.12

4.6. Low Impact Development Scenarios

An alternative strategy to mitigate the impacts of urbanization is the use of stormwater Green Infrastructure, such as Low Impact Development (LID), which are decentralized strategies that control runoff by better mimicking pre-development or natural hydrologic processes *(45, 46)*. LID strategies include structural Best Management Practices (BMPs), such as, bioretentions (also known as rain gardens), sand filters, permeable pavement, green roofs, rainwater harvesting, bioswales, infiltration trenches, retention basins, extended detention basins, grassy swales,

vegetative filter strips, and constructed wetlands. LIDs better mimic natural flow regime by restoring infiltration and retaining water for longer durations on the site it is generated from. Besides the benefits of restoring the pre-development hydrology, many LID structures provide water quality enhancement by treating water and thus reducing nutrients, metals, and thermal pollution concentrations.

A total of three LID scenarios were created and implemented in the HEC-HMS and GSSHA models. The scenarios assumed that a total of 5%, 10% and 15% of the sub-basins areas would be retrofitted or implement LID controls that allow infiltration. To represent infiltration BMPs, the parameters were changed in the HEC-HMS models. The altered flows were than inserted into HEC-RAS 1D and 2D to estimate the impacts on the flood waves and in the bridges, as well as, on the roads within flooded areas. In addition to the parameter change, an initial storage was inserted in the model. The infiltration BMP characteristics are listed on Table 8. The parameters values were obtained from *(47)*. The percentage of impervious of each sub-basin was updated. The new imperviousness was calculated with Equation 4, assuming that the LID practices are inserted uniformly in the subbasins. This approach considers that the LIDs are placed uniformly between pervious and impervious area. The surface storage was calculated by multiplying the surface storage by the percentage of LID placed.

$$Imp_{LID} = Imp(1 - f_{LID}) \quad [4]$$

where Imp_{LID} is the updated imperviousness, Imp is the original calibrated imperviousness and f_{LID} is the fraction of modeled LID scenario (0.05, 0.1 and 0.15).

Table 8. Adopted low impact development parameters.

Parameter	Value
Hydraulic conductivity (cm/hr)	0.43
Suction Head (cm)	11.00
Porosity	0.40
Residual Saturation	0.04
Initial Moisture	0.35
Surface Storage (cm)	30

4.7. Floodplain Widening

Floodplain widening was analyzed in the upper San Antonio critical area (Figure 12). This technique was not evaluated in Leon Creek area as the analyzed area is mostly natural at its surroundings. The San Pedro creek and San Antonio River cross-sections were altered from a natural to a rectangular cross section in HEC-RAS 1D. Due to the lack of space in the surrounding area to expand the rivers width, we maintained their original depth and distance between river banks (example in Figure 13). A rectangular shape has the maximum cross-sectional area, therefore this configuration is the optimum option in this limited urbanized area.

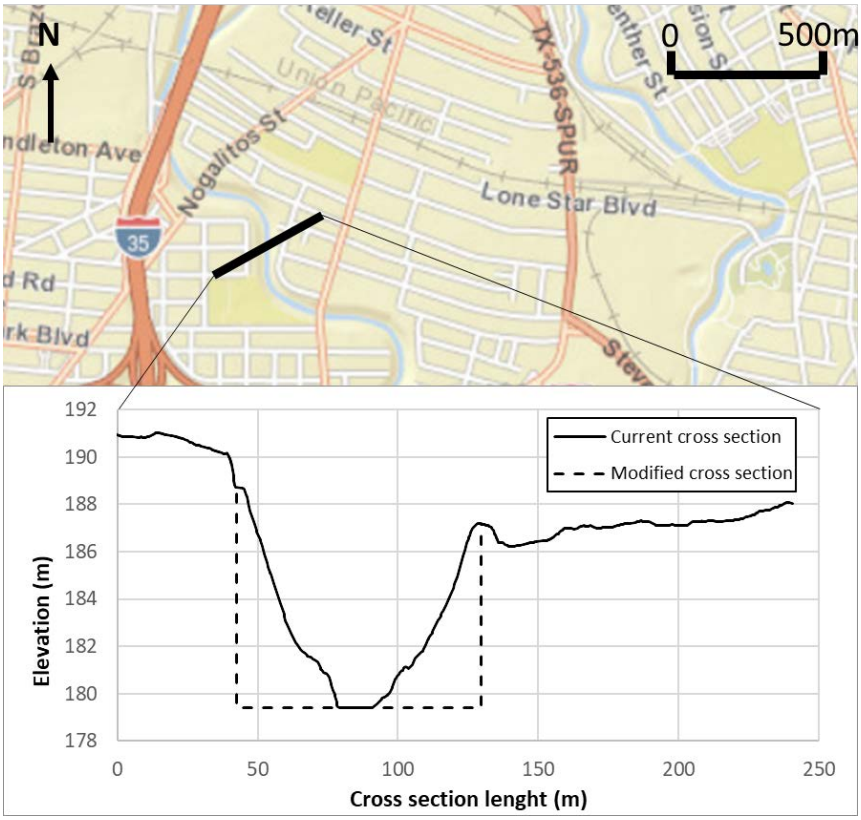

Figure 13. River cross-section modification.

The DEM terrain was also modified to access floodplain widening impacts with HEC-RAS 2D. The original river characteristics was replaced by a rectangular shaped channel (see Figure 14(b)). The Manning's roughness of the river was set as 0.011 $s/m^{1/3}$ to represent a smooth concrete channel.

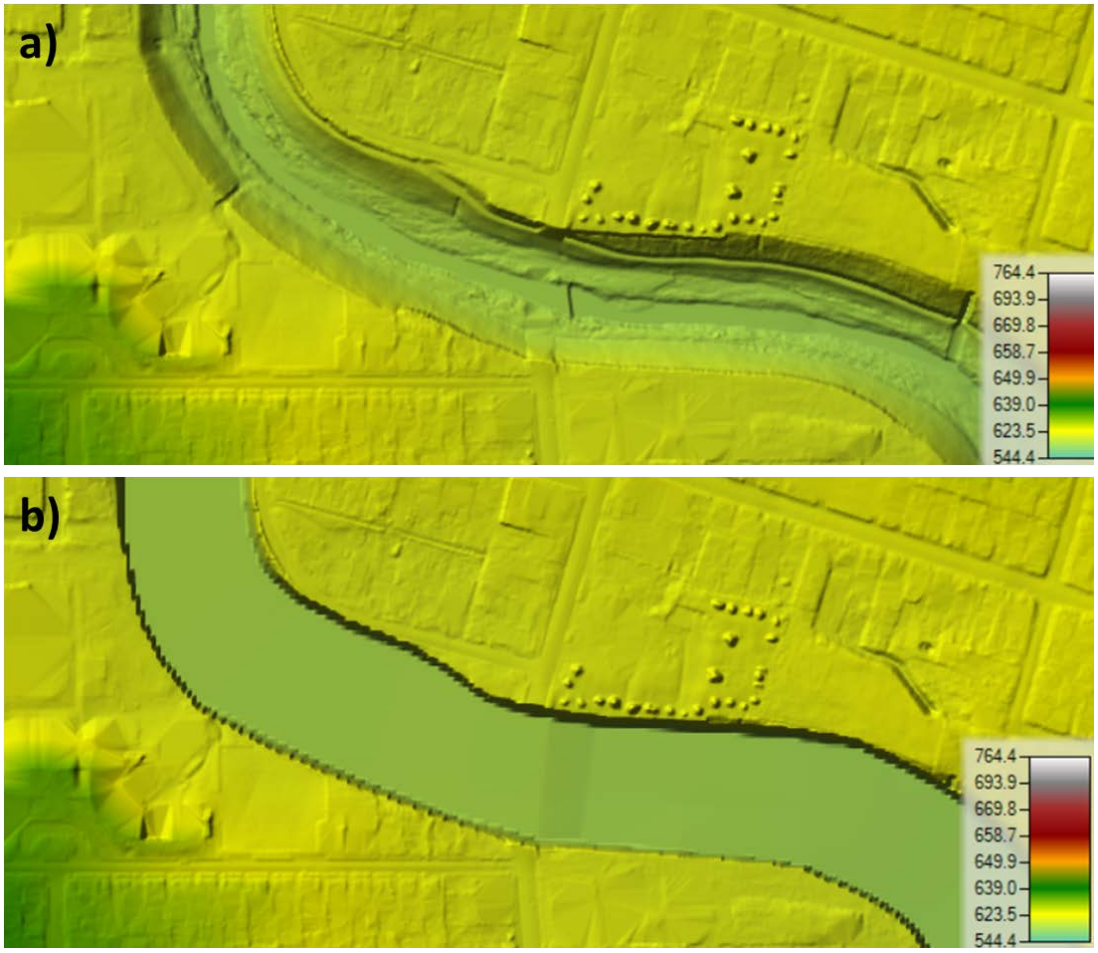

Figure 14. Flood plain terrain modification.

4.8. Olmos Dam Modification

The existing Olmos Dam (described in Subsection 4.1) was modified to analyze its ability to mitigate the impacts of climate change. We have simulated an increase on its crest to enhance its storage and prevent overflow with a 500-year storm. First, we have identified the extent of flood plain for water surface elevation of 222, 223, 225 and 227 m and what would be the affected land. This investigation was used to determine where embankments should be constructed to protect the surrounding area.

The discharge-elevation and the storage elevation curves (Figure 5) were modified in HEC-HMS. The increase in the storage was estimated by multiplying the maximum area within the embankments by the elevation. The discharge in the gates was extrapolated considering a linear relation between discharge and water surface elevation. The modified curves are shown in Figure 15.

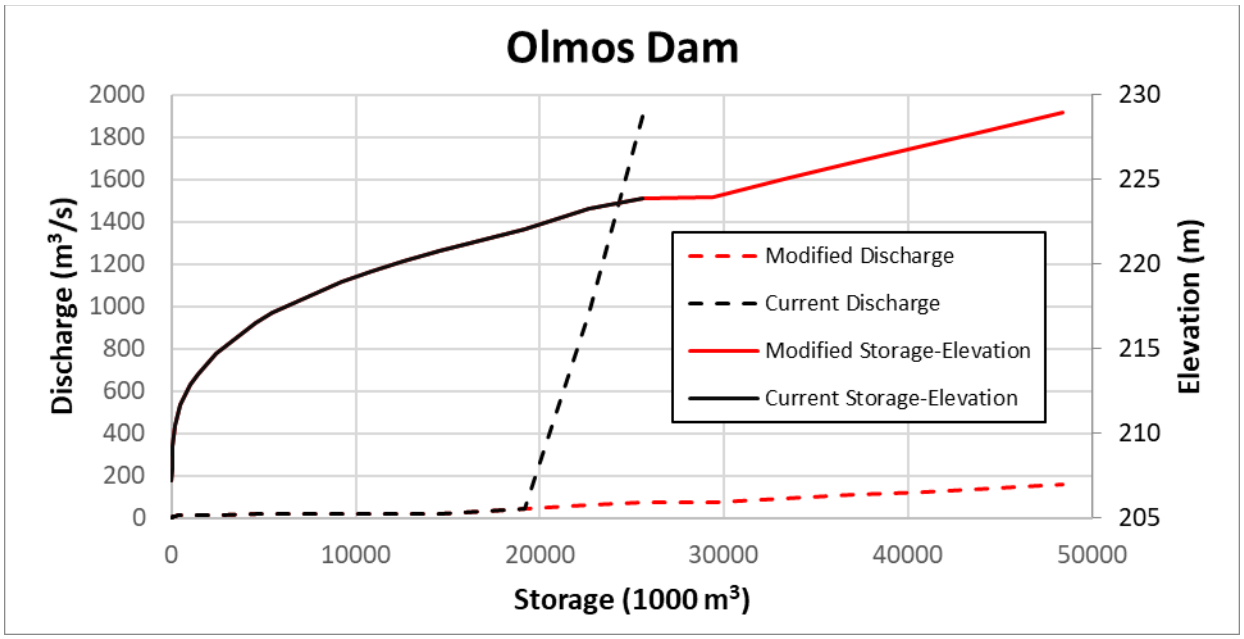

Figure 15. Storage and discharge improvement of Olmos Dam.

The simulation in HEC-HMS were performed with 100-year and 500-year storm with current and near future (RCP. 4.5) climate conditions. The effect of this modification on water level at the target bridges and on the floodplains was evaluated though HEC-RAS 1D and 2D respectively.

4.9. Levees

The minimum elevation of levees and their location were calculated for the 100-year storm in the near future with the climate conditions projected for RCP 4.5. The levees height for 100-year storm is required by FEMA for Special Flood Hazard Areas. Mobile barriers need to be installed to connect the levees between the bridges where necessary, as fixed levees may not be installed in these places. Therefore, traffic in such bridges should be ceased during the superstorms events. The bridges to be closed, where these barriers would be placed, was indicated by HEC-RAS 1D, described in Subsection 4.4.2.

The HEC-RAS 2D model was used to estimate the levees height along the river sides. The terrain was modified with barriers along the riversides with extreme heights to guarantee that no overflow would occur. Then the 100-year storm was simulated in this terrain to estimate the water surface elevation along the reach in four profiles (Figure 16). The levees elevation was set to be the same as the water surface elevation where it is higher than the ground elevation. Finally, the terrain was modified to include the levees. The 500-year storm flooding was tested with this configuration with the HEC-RAS 2D model. Levees were tested only in Upper San Antonio Watershed, as the area in Leon Creek is very low urbanized and the protection would be minimum.

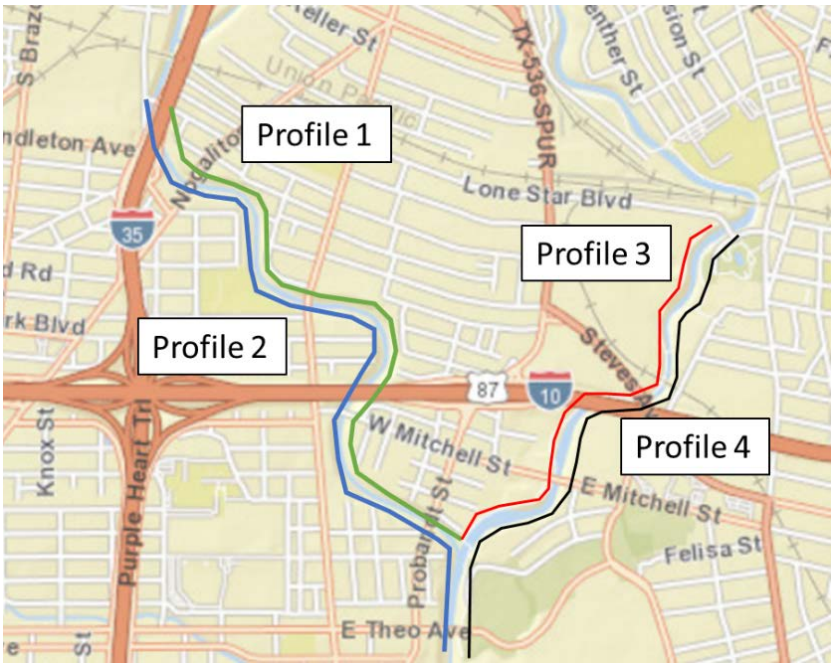

Figure 16. Profiles for levees estimation.

5. ANALYSIS AND FINDINGS

This section presents the main analysis and results and it is divided into ten main sub-sections. First, the climate change projections are analyzed and the error of these projections are quantified. Then, Subsection 5.2 presents new IDF curves calculated for the near, middle and far future. Subsection 5.3 describes the performance of the developed hydrologic models. With the models successfully calibrated and validated, analysis begins by showing how floodplains are affected and how they differ from FEMA maps (Subsection 5.4). Subsequently, the impacts of climate change are assessed in terms of increased peak flows on Subsection 5.5, and how bridges would be affected on Subsection 5.6, and how much area and extended roads would flood on Subsection 5.7. The following subsections (Subsections 5.8–5.10) include results of flood mitigation scenarios, such as implementation of LID, channel widening and use of levees.

5.1. Climate Change Projections

The climate change models were compared with historic observations from the period of 1975 to 1999. Figure 17 presents the relative error of the models for four metrics: maximum rainfall depth (Max), 99th, 95th and 90th percentiles (P99, P95 and P90, respectively), and the number of wet days (NWet). The metric Max is the index with highest error, whose median prediction underestimates in more than 40%, indicating that projections generated by GCMs are under predicting very rainy days. The GCMs downscaled by LOCA had more proximity to the observed, but also presented higher variation possibly due to the greatest number of models. The metrics P99, P95 and P90, however, proved to be more accurate than the maximum rainfall depth estimate and in general had the third quartile of the models matched the observed rain record. A relative high number of models still under predicts these five metrics, with some model generating errors near 20%. On the other hand, some models also show errors around 20% of over-prediction with respect to the observed rainfall time series of the region.

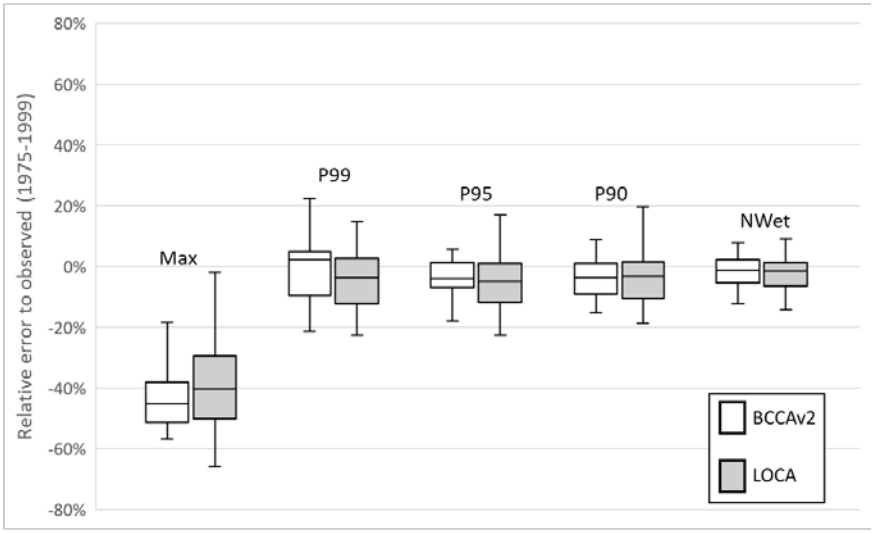

Figure 17. Relative error of maximum rainfall depth (Max), 99th, 95th and 90th percentiles (P99, P95 and P90), and the number of wet days (NWet).

To assess a band of uncertainty in terms of intensity for different durations, IDF curves using 51 GCM models for the historic period of 1950 to 1975 were generated. Figure 18 shows the predicted IDFs from all the 51 models for the 100-year return period and from the Texas Department of

Transportation (TxDOT), developed by USGS as shown in Figure 3. The errors discussed in Figure 17 seems to have propagated to the generated IDFs. The TxDOT and USGS IDFs are closer to the third quartile of projections for 1 day of duration or below. This IDF is close to the median for rainfall duration of 2 days, and lower for longer durations. *(48)* found that the choice of the historical period to adjust the bias correction can be a great source of uncertainty. Here we have used only one period (1950-1975) and might be relevant to test the calibration of the bias correction in multiple periods.

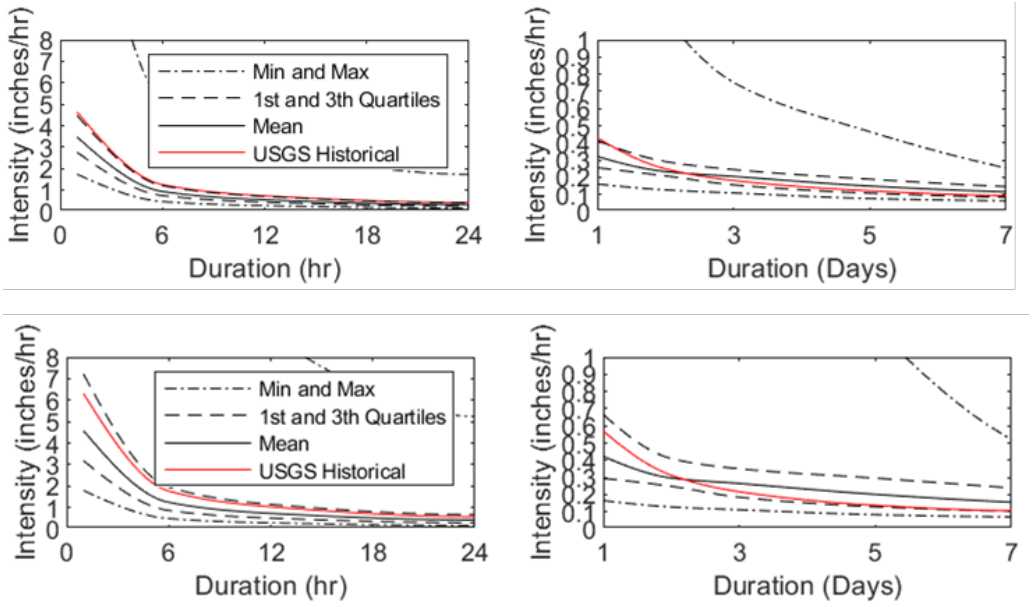

Figure 18. IDF generation from the GCMs and from TxDOT for 100 years (top) and 500 years (bottom) return period for the historic validation period (1975 – 1999).

5.2. Future IDFs

The estimated IDF curves for the future periods (near, medium and far future) for the 100- and 500-year storms for both RCP 4.5 and 8.5 scenarios are shown in the Figures 19 to 22. The results show a clear increase in the rainfall intensity caused by climate change, especially for the farther future. Similar results were also observed by *(49)*. RCP 4.5 scenario had greater intensities when compared to RCP 8.5 for 100-year storm. For 500-year, RCP 8.5 present more intense rainfall for durations shorter than 1 day. The intensities for durations below or equal one day were below the third quartile of all projections and durations above or equal 2 days were usually below the 1st quartile. Therefore, these figures suggest that the intensity might increase for all duration of storms with 100- and 500-year return period.

Figure 23 shows the standard deviation in percentage of the mean (relative standard error to the mean), for RCPs 4.5 (a) and 8.5 (b) for 1 and 7 days of rainfall duration. It shows that the discrepancy between the models are greater for the farther future, except for duration of one day under RCP 4.5 scenario. The figure shows that the relative standard error is greater for lower durations, in agreement with the results found by *(15, 50)*. Surprisingly, this error was greater in the historical period than some future ones (e.g. RCP 4.5 intensities for duration of 1 day). The uncertainty increases with return period, also found by *(51)*, showing how the target superstorm events are harder to project.

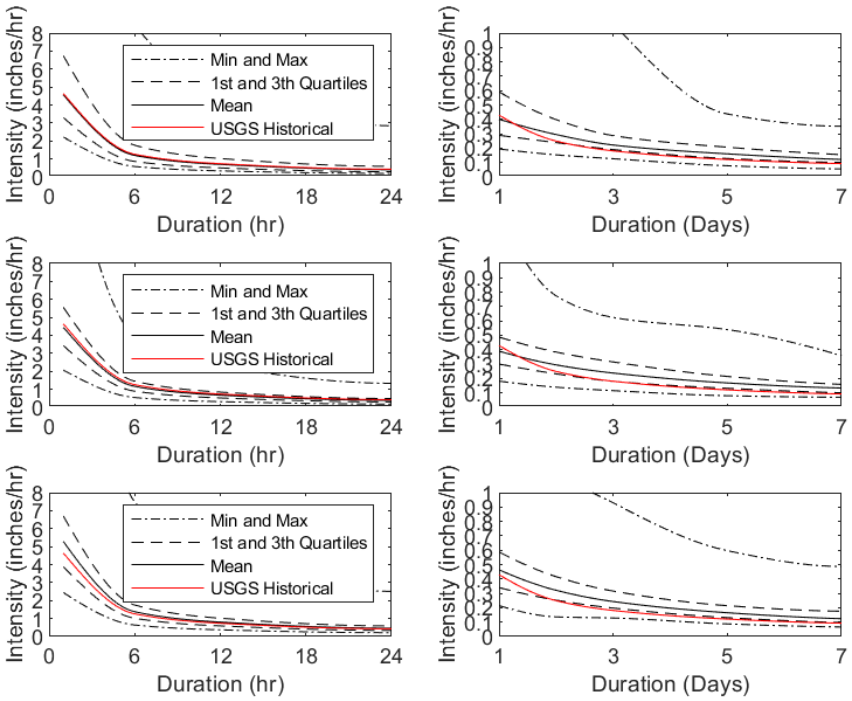

Figure 19. IDF curves for the 100-year return period for RCP 4.5 for 2025-2049 (top), 2050-2074 (mid) and 2075-2099 (bottom).

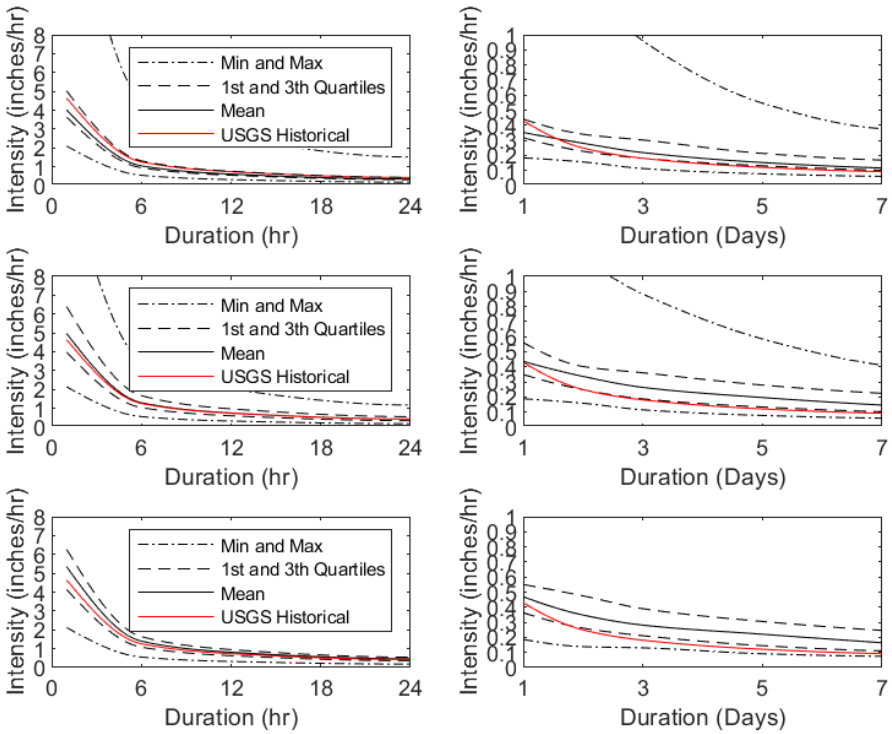

Figure 20. IDF curves for the 100-year return period for RCP 8.5 for 2025-2049 (top), 2050-2074 (mid) and 2075-2099 (bottom).

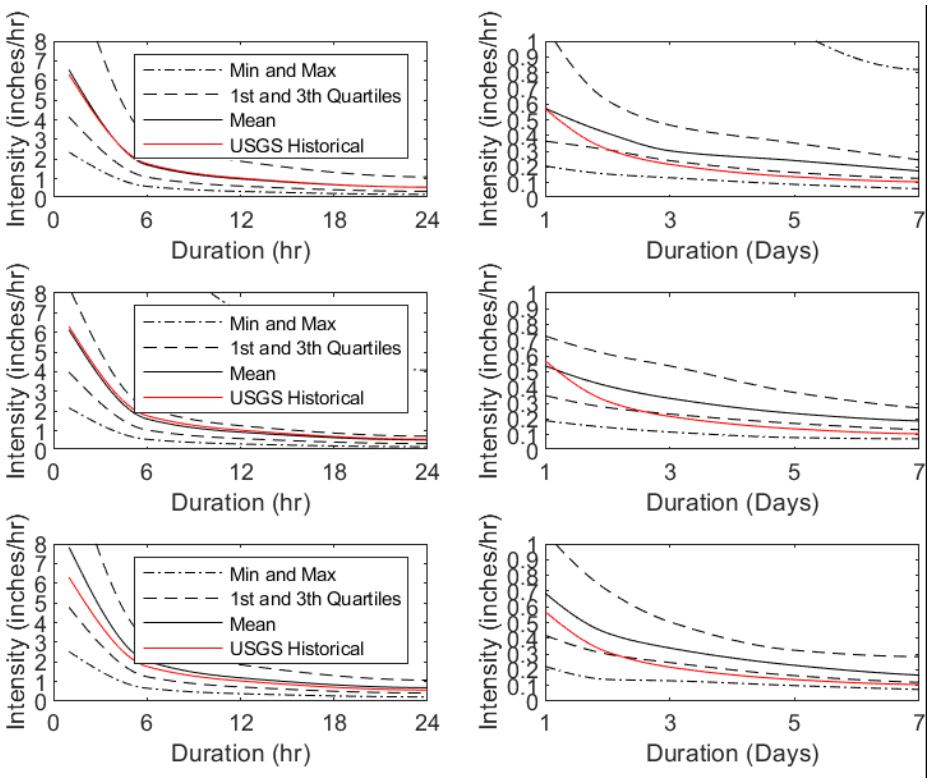

Figure 21. IDF curves for the 500-year return period for RCP 4.5 for 2025-2049 (top), 2050-2074 (mid) and 2075-2099 (bottom).

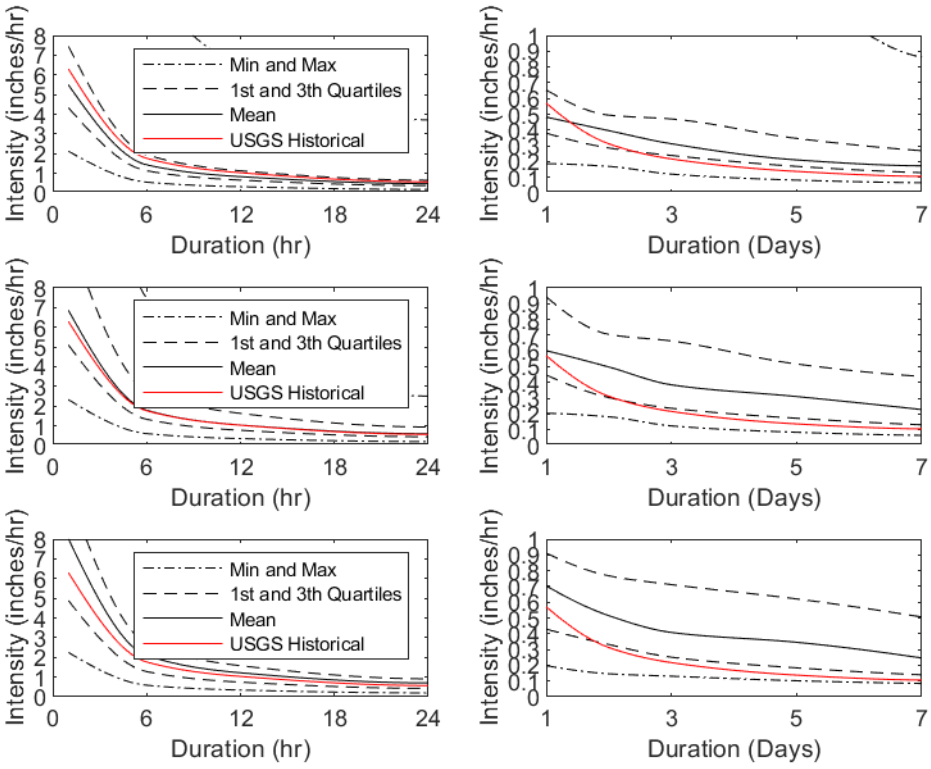

Figure 22. IDF curves for the 500-year return period for RCP 8.5 for 2025-2049 (top), 2050-2074 (mid) and 2075-2099 (bottom).

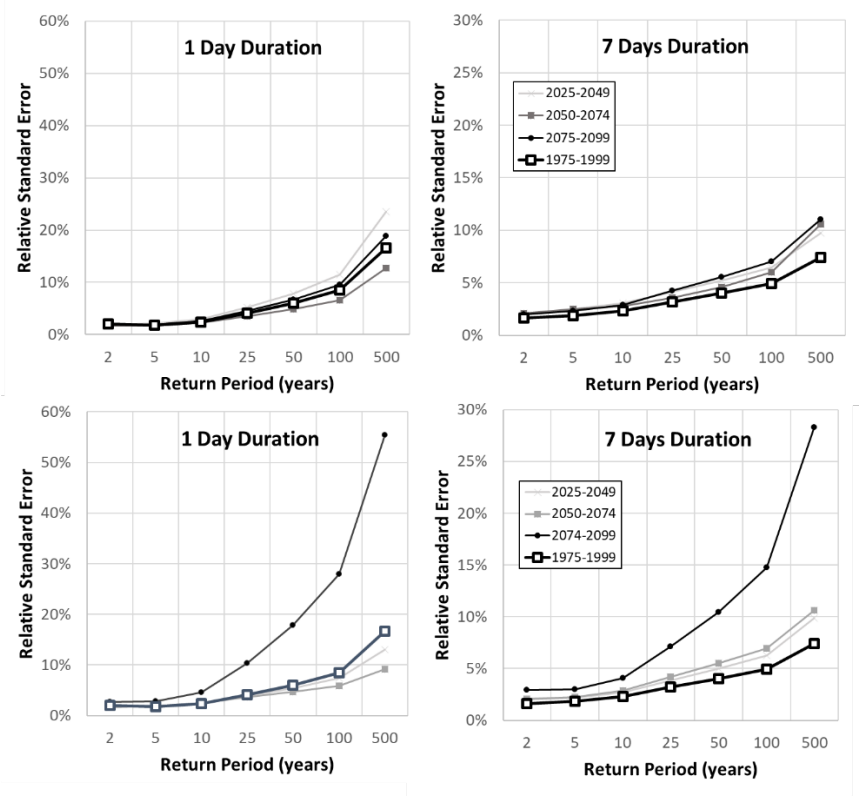

Figure 23. Relative standard error for RCPs 4.5 (a) and 8.5 (b).

The 3rd quartile was used to simulate future conditions, as it was closer to the historical IDF on bias-correction validation. The intensity values used on simulations are shown in Table 9.

Table 9. Average intensities (in/hr) used on simulations for a duration of 24 hrs.

	Historical	RCP 4.5			RCP 4.5		
	USGS	2025-2049	2050-2075	2075-2099	2025-2049	2050-2075	2075-2099
100-year	0.45	0.63	0.52	0.62	0.47	0.59	0.58
500-year	0.60	1.16	0.77	1.14	0.69	1.00	0.96

5.3. Performance of the Hydrologic Models

The calibrated land use parameters for GSSHA are shown in Table 10. This table shows that the roughness of the developed grids had to be greatly reduced to properly represent the flow conveyance. Tables 11 and 12 are the calibrated soil parameters for Leon Creek and Upper San Antonio, respectively. The bedrock hydraulic conductivity was significantly reduced in Leon Creek, but still in the limits suggested by *(42).*

Table 10. Calibrated land use parameters.

Land Use	Roughness (s/m$^{1/3}$)		Impervious Area (%)	
	Leon Creek	Upper San Antonio	Leon Creek	Upper San Antonio
Open Water	0.008	0.009	99.99	99.99
Developed, Open Space	0.008	0.009	47.0	29.0
Developed, Low Intensity	0.007	0.008	75.0	49.0
Developed, Medium Intensity	0.006	0.007	84.0	82.0
Developed, High Intensity	0.006	0.007	92.0	91.0
Barren Land (Rock/Sand/Clay)	0.04	0.4	9.0	4.0
Deciduous Forest	0.29	0.4	7.0	3.0
Evergreen Forest	0.15	0.42	5.0	3.0
Mixed Forest	0.16	0.42	6.0	3.0
Shrub/Scrub	0.19	0.32	9.0	3.0
Grassland/Herbaceous	0.13	0.41	6.0	3.0
Pasture/Hay	0.12	0.41	4.0	3.0
Cultivated Crops	0.09	0.41	4.0	3.0
Woody Wetlands	0.13	0.41	4.0	3.0

Table 11. Calibrated soil parameters for Leon Creek.

Soil	Hydraulic Conductivity (cm/hr)	Suction Head (cm)	Total Porosity (cm^3/cm^3)	Effective Porosity (cm^3/cm^3)	Residual Saturation (cm^3/cm^3)	Field Capacity Saturation (cm^3/cm^3)	Wilting Point Saturation (cm^3/cm^3)
Bedrock	0.001	0.8	0.06	0.05	0.01	0.01	0.004
Clay	0.018	22.63	0.48	0.39	0.09	0.40	0.27
Clay loam	0.079	18.08	0.46	0.39	0.08	0.32	0.20
Fine sandy loam	0.71	10.15	0.45	0.41	0.04	0.21	0.10
Gravelly clay loam	0.09	16.9	0.46	0.39	0.08	0.32	0.20
Loam	0.043	6.89	0.46	0.43	0.03	0.27	0.12
Sandy clay	0.037	19.9	0.43	0.32	0.11	0.34	0.24
Silty clay	0.031	24.22	0.48	0.42	0.06	0.39	0.25
Variable	0.19	12.2	0.42	0.36	0.06	0.28	0.17
Very gravelly loam	0.43	7.1	0.46	0.43	0.03	0.27	0.12

Table 12. Calibrated soil parameters for Upper San Antonio.

Soil	Hydraulic Conductivity (cm/hr)	Suction Head (cm)	Total Porosity (cm^3/cm^3)	Effective Porosity (cm^3/cm^3)	Residual Saturation (cm^3/cm^3)	Field Capacity Saturation (cm^3/cm^3)	Wilting Point Saturation (cm^3/cm^3)
Bedrock	0.008	0.71	0.06	0.05	0.01	0.01	0.004
Clay	0.027	31.63	0.48	0.39	0.09	0.40	0.27
Clay loam	0.09	20.88	0.46	0.39	0.08	0.32	0.20
Fine sandy loam	0.88	8.95	0.45	0.41	0.04	0.21	0.10
Gravelly clay loam	0.07	18.9	0.46	0.39	0.08	0.32	0.20
Loam	0.34	8.89	0.46	0.43	0.03	0.27	0.12
Sandy clay	0.05	23.9	0.43	0.32	0.11	0.34	0.24
Silty clay	0.028	29.22	0.48	0.42	0.06	0.39	0.25
Variable	0.18	15	0.42	0.36	0.06	0.28	0.17
Very gravelly loam	0.42	6.5	0.46	0.43	0.03	0.27	0.12

The ability of the developed models to predict observed storm events was tested and the results are presented next. Figure 24 shows the hydrographs for Upper San Antonio watershed and Table 13 contains the goodness-of-fit metrics of the models: peak flow error, volume error, Nash-Sutcliff Efficiency (NSE) and coefficient of determination (R^2). We observe that the predicted peak flows are well represented by the models. GSSHA tends to have a faster peak than HEC-HMS, which in turn has its peak occurring earlier than the observed.

The values of NSE and R2 greater than 0.5 can be consider satisfactory according to *(52–54).* Most of the R2 are above 0.5, except for the GSSHA model of event 5. NSE, however, shows poorer results and the reason is the timing of the peak. Efforts to match the timing were performed, but the difference in peak or in volume would be greater. The primary aim of the calibration in this study was to match the peak values, as it has the greatest effects on floodplains. One potential explanation of the difficulties in matching the times of the peaks are the rainfall radar time resolution, which is coarser than in the model run time steps. GSSHA simulations typically generated peaks earlier than HEC-HMS, indicating that overland flow velocity is high. In general, the model tends to over predict the total volume; however, the peak flow values seems to not have a well defined bias, with some events over-predicting and other events under-predicting.

The calibration for Leon Creek watershed was performed using the largest rainfall event, which can be seen in Figure 24. The calibration using other events were not successful, producing significant errors in volume and peak. The models presented acceptable R^2 and NSE values. HEC-HMS over estimated the peak in 11% and underestimated the volume in 22%. On the other hand, GSSHA model underestimated the peak in 21.9%, with a volume 8.8% higher than the observed. The five events used in validation are showed an overestimation of both models, that did not represent the observed hydrograph.

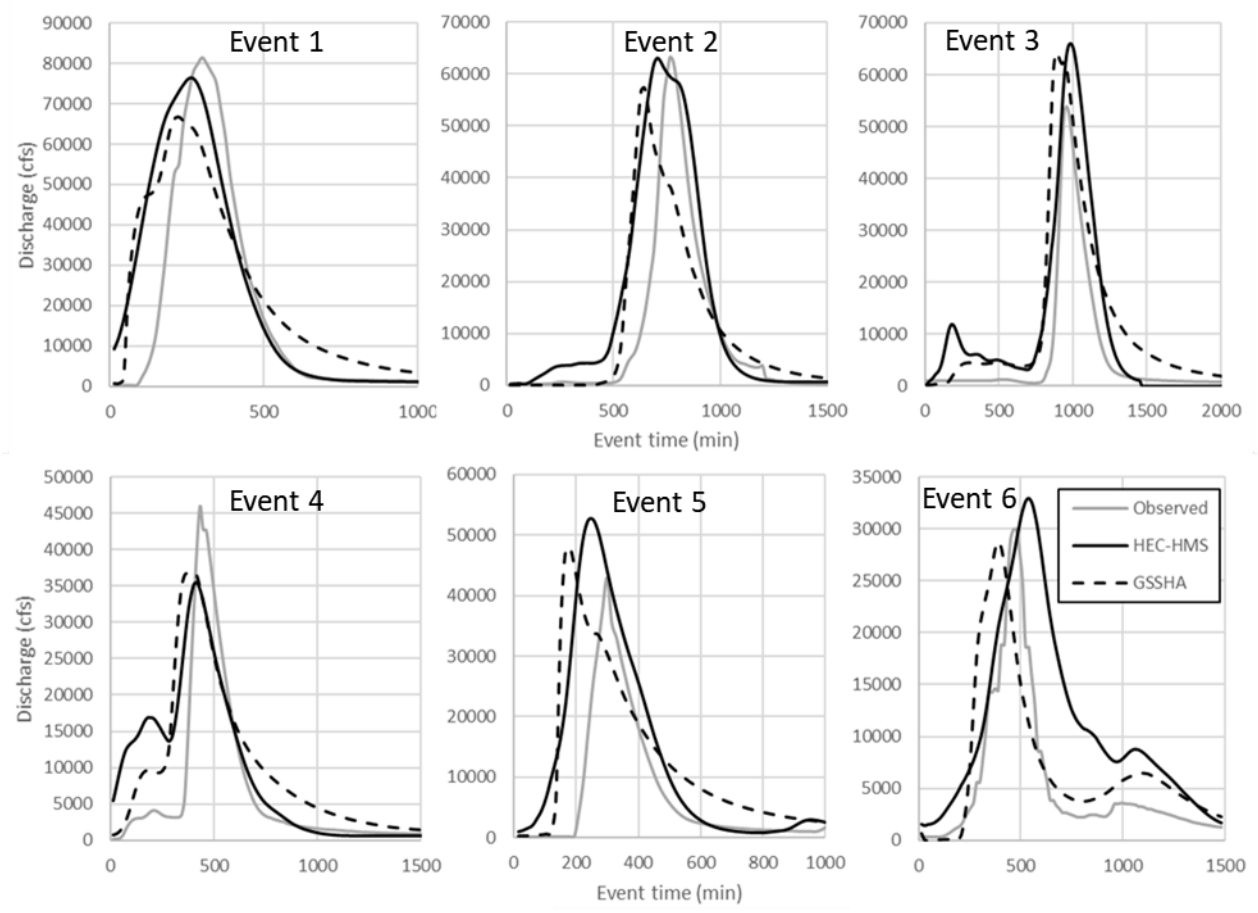

Figure 24. Predicted and observed hydrographs for Upper San Antonio watershed.

Table 13. HEC-HMS and GSSHA goodness-of-fit metrics (peak flow error, error in volume, NSE and R^2).

	HEC-HMS				GSSHA			
Events	**Peak (%)**	**Volume (%)**	**NSE**	**R2**	**Peak (%)**	**Volume (%)**	**NSE**	**R2**
1	-6.26	22.08	0.67	0.72	-17.96	26.29	0.63	0.66
2	-0.5	60.3	0.56	0.80	-9.3	20.4	0.69	0.54
3	22.6	80.4	0.55	0.91	19.1	103.8	0.51	0.77
4	-22.8	36.7	0.59	0.66	-20.1	48.9	0.51	0.62
5	22.3	86.3	-0.14	0.65	11.5	79.9	-0.35	0.33
6	10.1	99.5	-0.10	0.66	-4.0	31.8	0.49	0.61

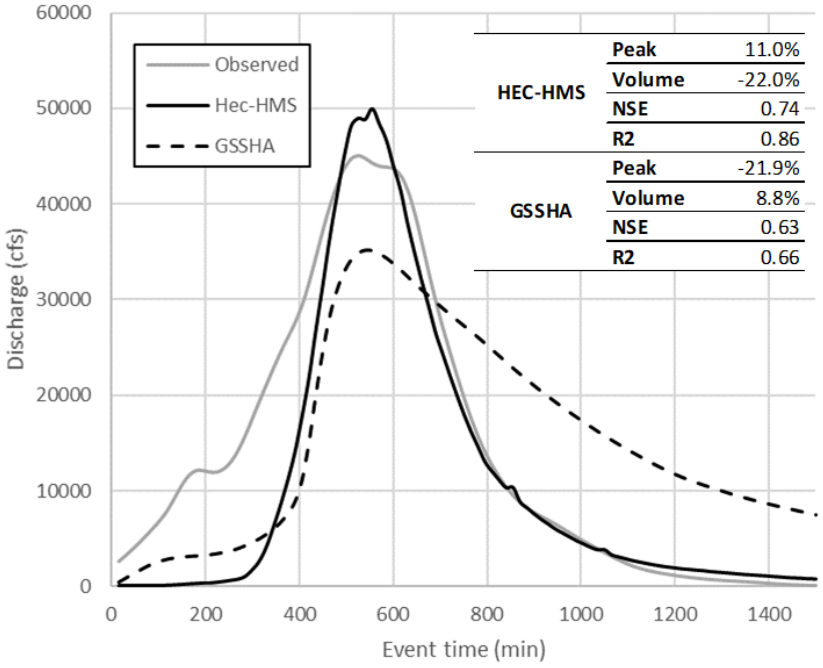

Figure 25. Calibrated hydrograph during rain Event 1 for Leon Creek watershed.

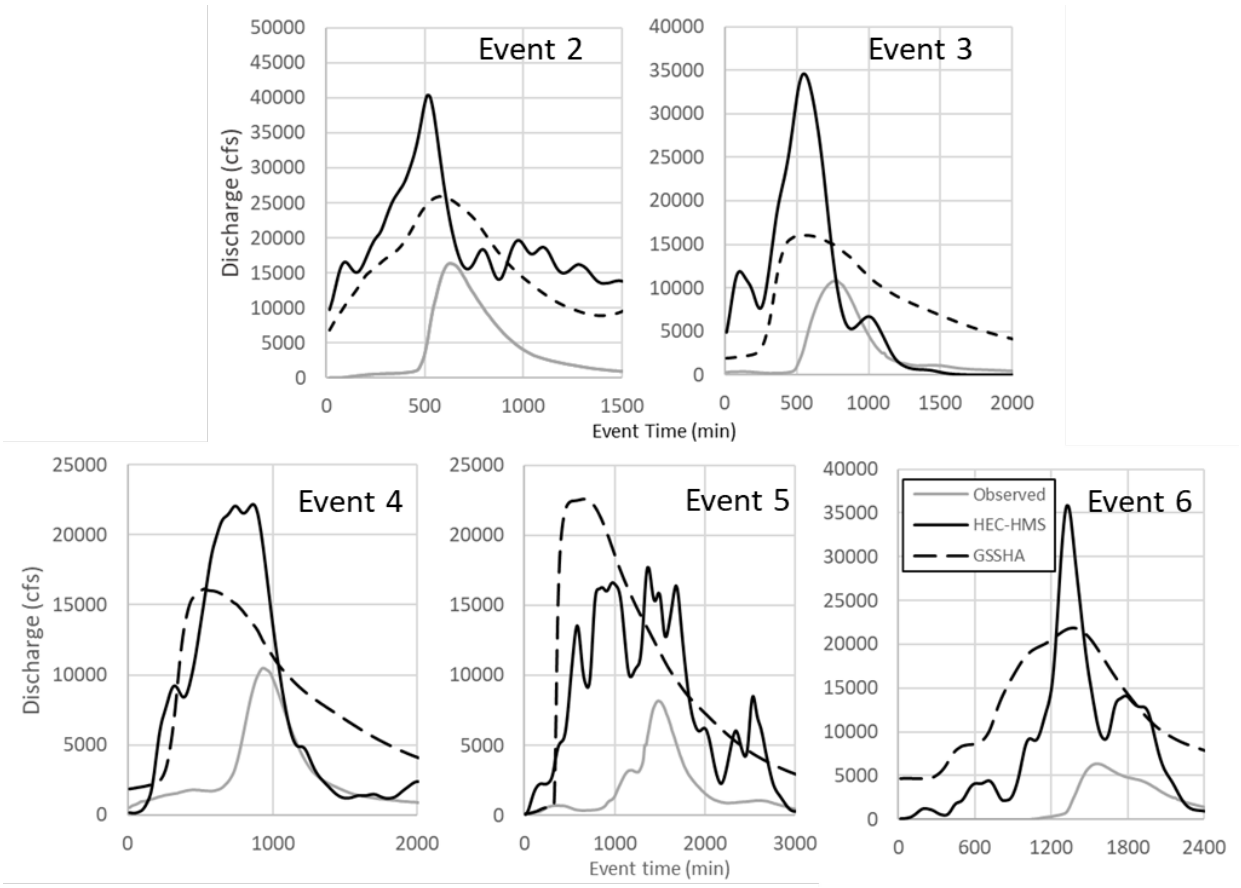

Figure 26. Validation hydrographs for Leon Creek.

The observed runoff coefficient was calculated for each of the five events, showed in Figure 27. The runoff coefficient was calculated using radar data at a middle location of the Leon Creek Watershed. This figure shows that the runoff coefficient of Event 1 is significantly higher than the other events, which can explain failure of the models to reproduce the observed hydrograph. The reason is possibly the radar rainfall estimation, which could be affected by the more irregular elevation of this watershed when compared to Upper San Antonio.

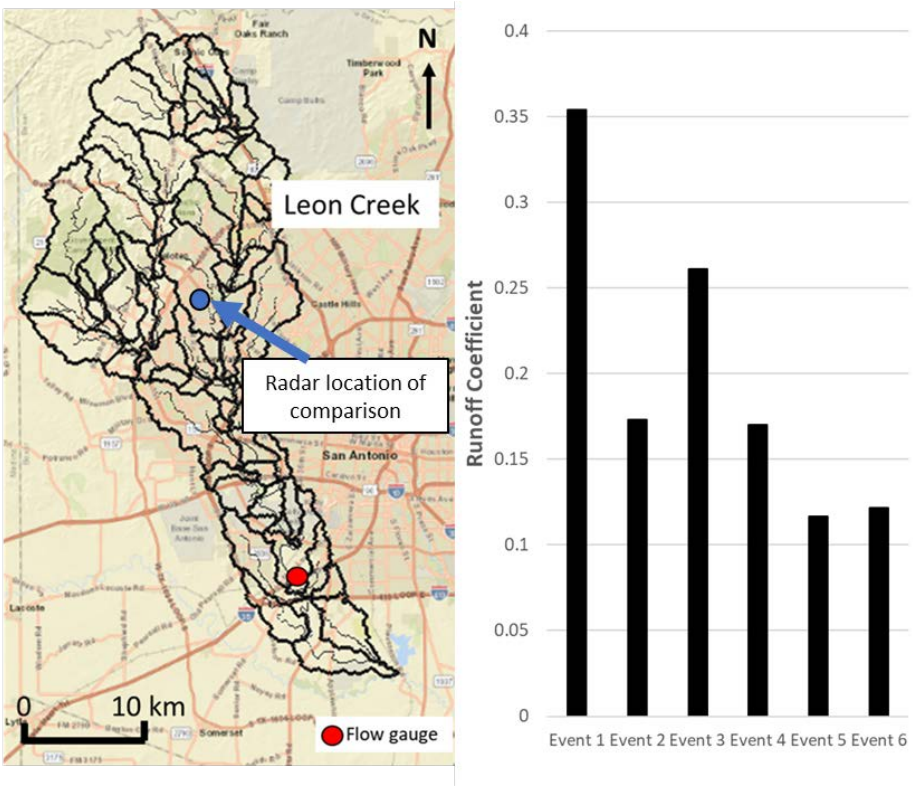

Figure 27. Radar data location and runoff coefficients of the six rain events.

5.4. Watershed Scale Floodplain Analysis

This section presents a visual and comparative analysis of the floodplain generated by GSSHA and the floodplains published by FEMA for the entire extension of the selected watersheds. Figure 28 shows the entire flood map for GSSHA for a storm of 100-year return period in Leon Creek and Upper San Antonio with 0.1m depth or higher. Figure 29 to 34 are zooms to critical points related to the transportation infrastructure in San Antonio. These are compared to FEMA prediction flood of 1% frequency (100-year return period).

5.4.1. GSSHA

The GSSHA model typically presented wider floodplains in some areas (and some isolated flood points) that did not occur in FEMA's map. The GSSHA model also flooded the golf field near the Olmos Dam, which did not occur with FEMA's results (Figure 34). The areas however area similar and both floodplains indicate the same flooded points at the major highways. The comparison of flood maps shows that there is an agreement between FEMA and the GSSHA model prediction of 1% chance of flood. It indicates that the model is suitable to project future climate change impacts. The wider flooded area resulted from GSSHA is due to its coarser resolution, indicating that higher resolutions models are required. Higher resolution modeling, however, comes with a significant increase of computational effort.

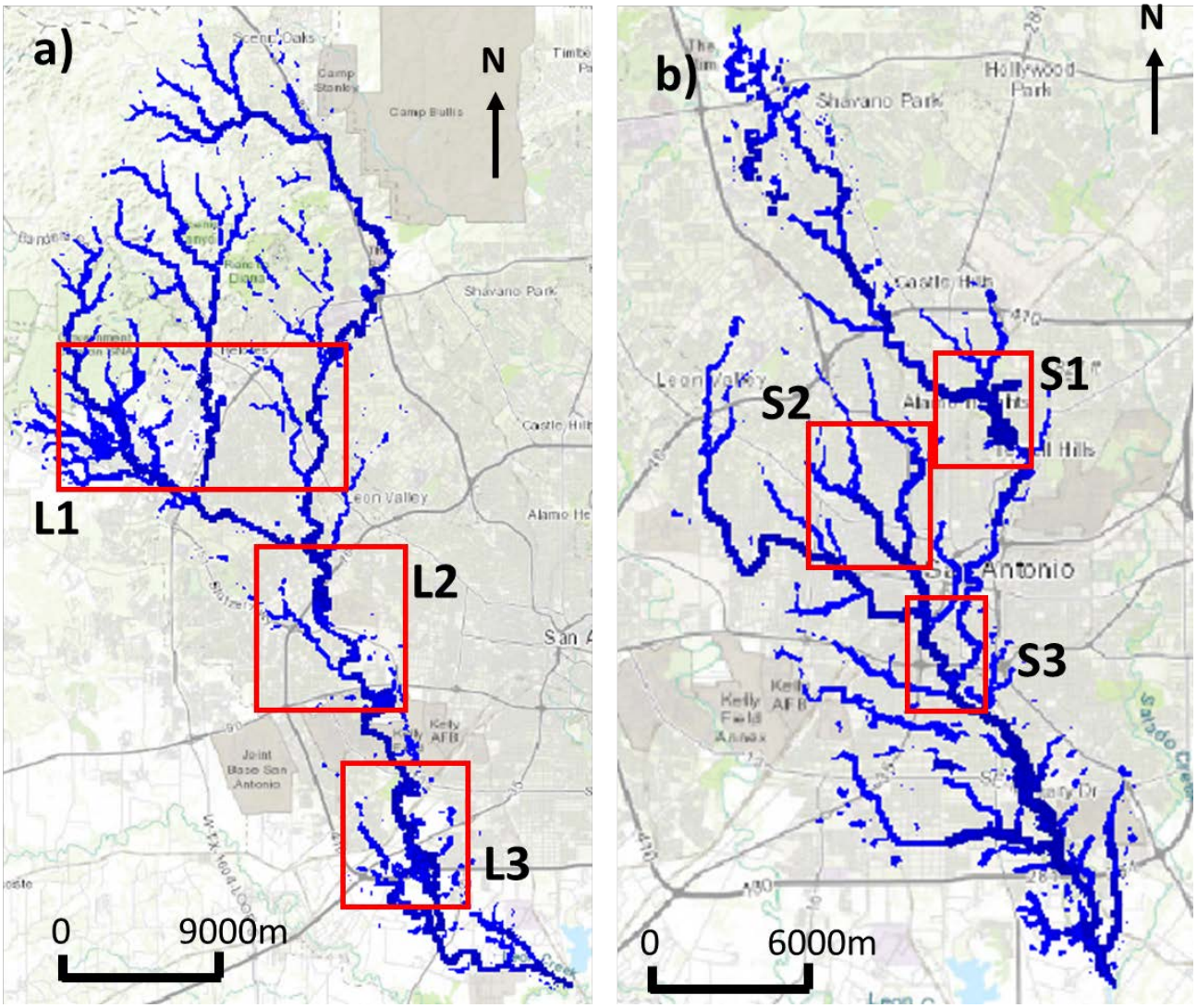

Figure 28. Floodplains in Leon Creek (a) and Upper San Antonio (b) watersheds generated by GSSHA (Note: GSSHA results are too coarse to identify flood risk areas.)

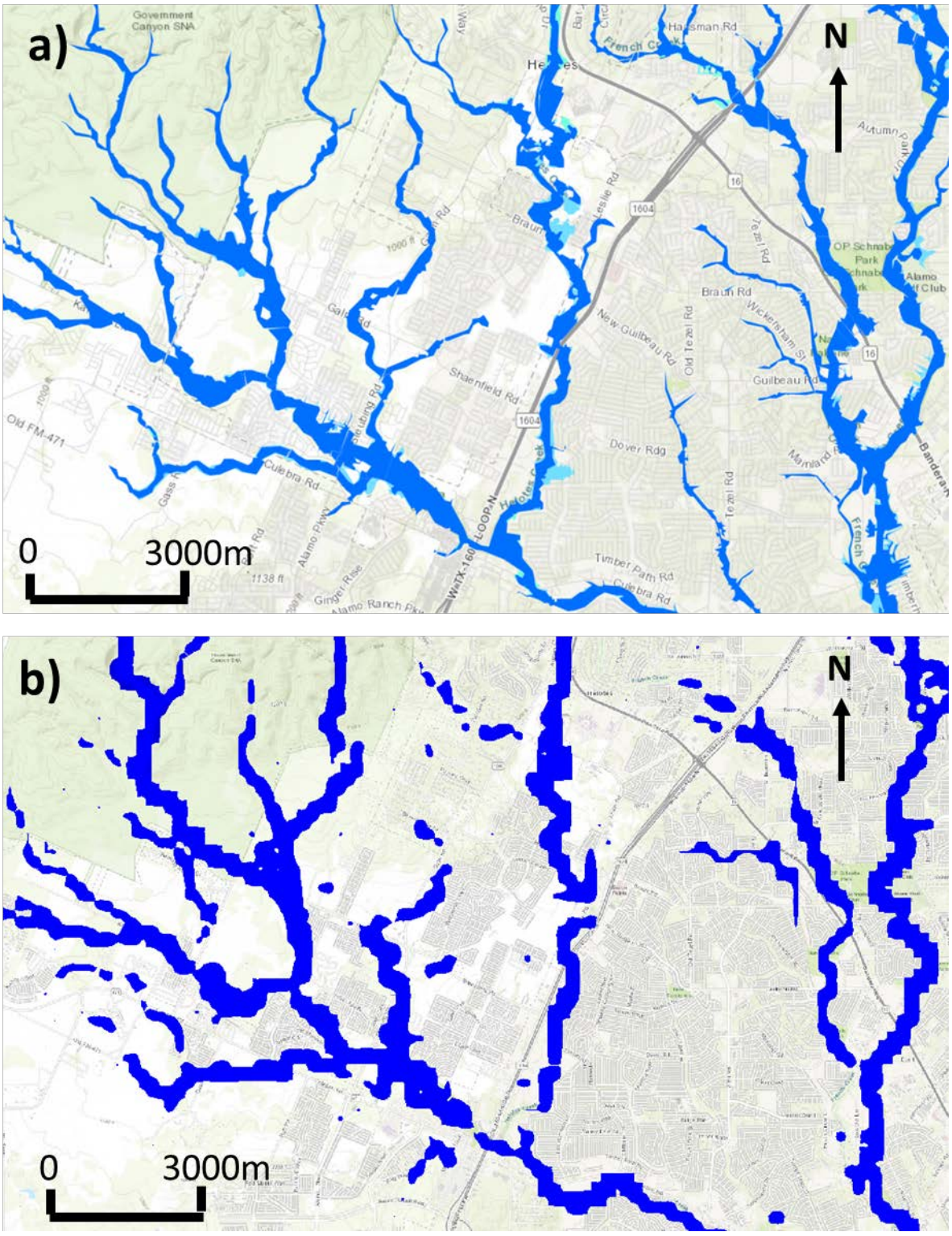

Figure 29. Comparison between (a) FEMA and (b) GSSHA floodplains in area L1. (Note: GSSHA results are too coarse to identify flood risk areas).

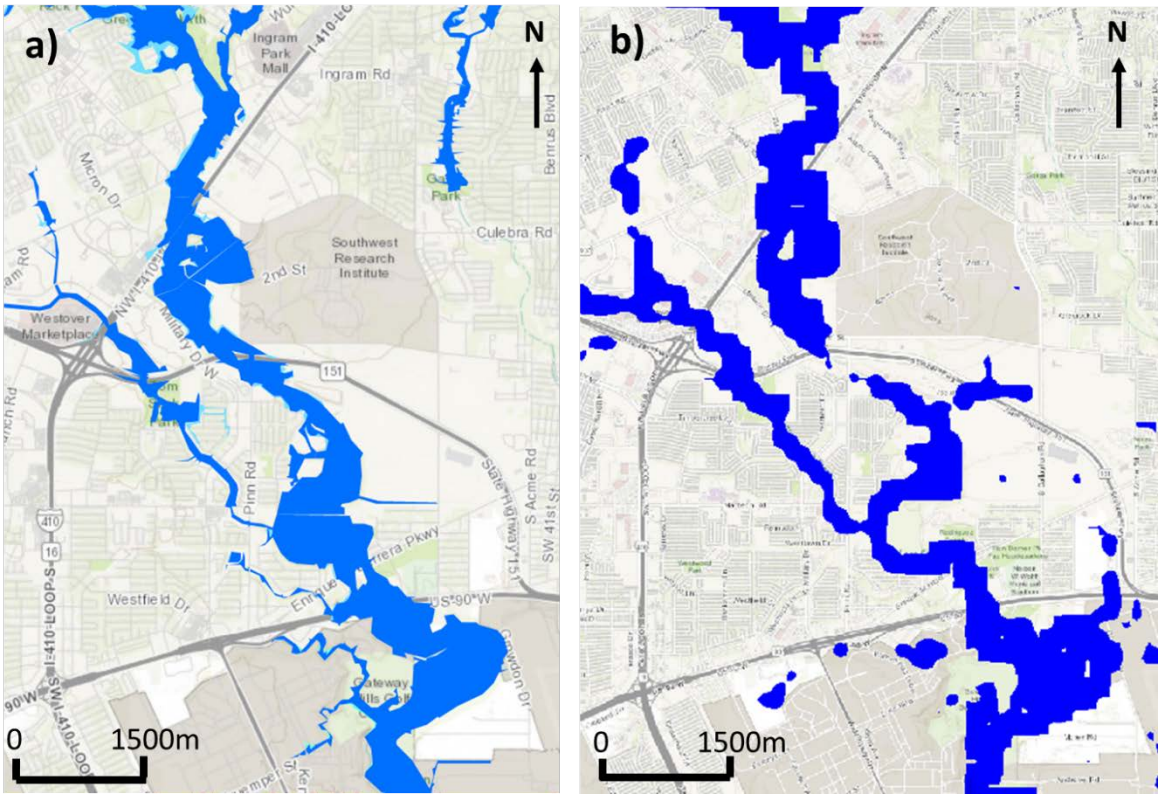

Figure 30. Comparison between (a) FEMA and (b) GSSHA floodplains in area L2. (Note: GSSHA results are too coarse to identify flood risk areas).

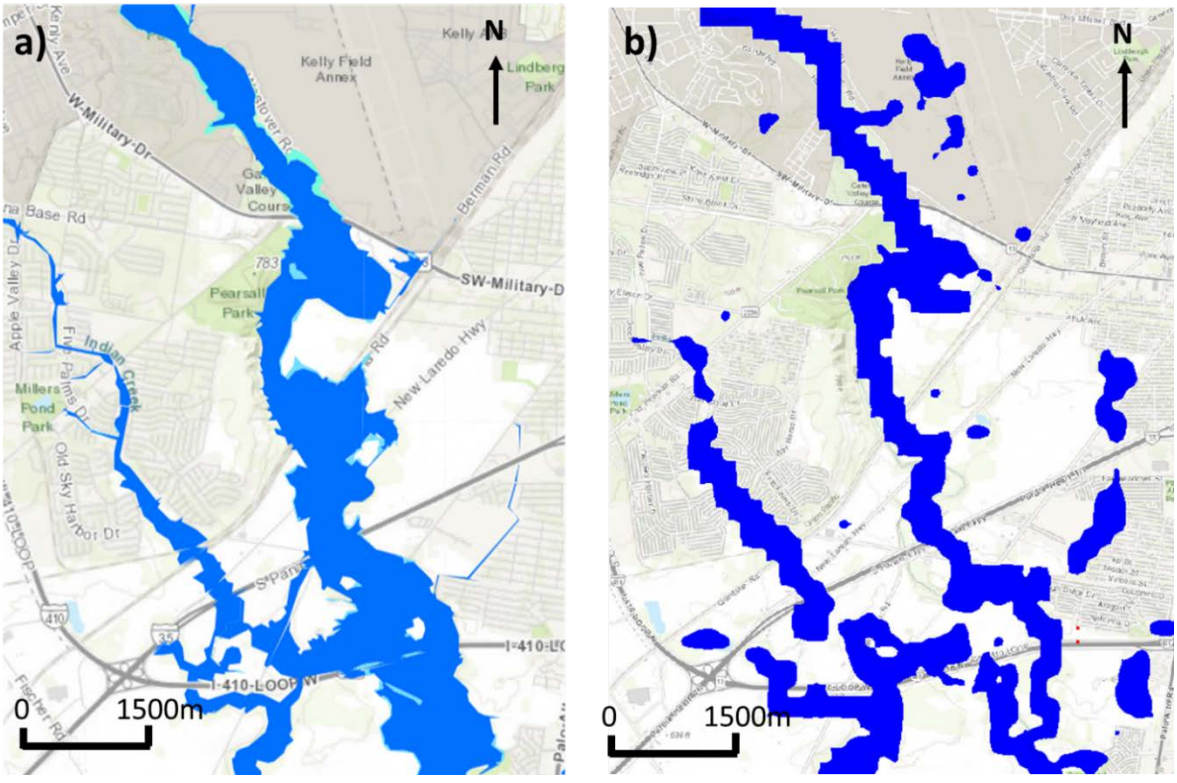

Figure 31. Comparison between (a) FEMA and (b) GSSHA floodplains in area L3. (Note: GSSHA results are too coarse to identify flood risk areas).

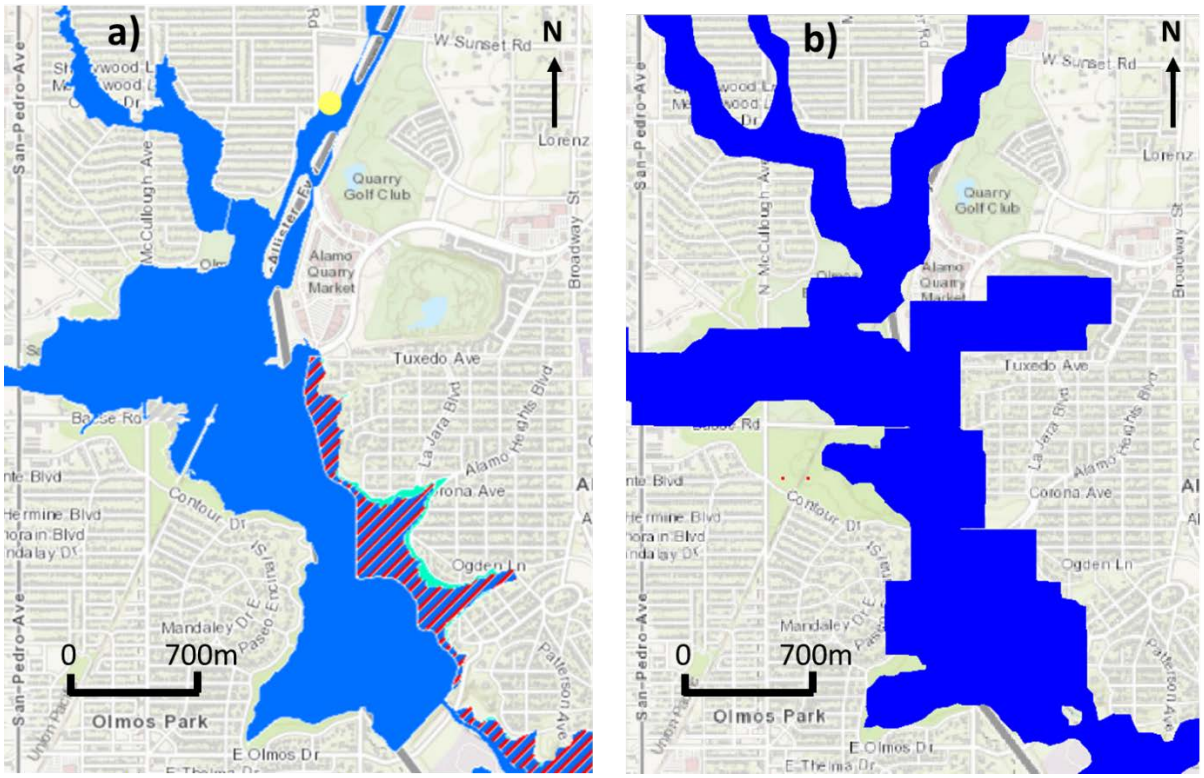

Figure 32. Comparison between (a) FEMA and (b) GSSHA floodplains in area S1. (Note: GSSHA results are too coarse to identify flood risk areas).

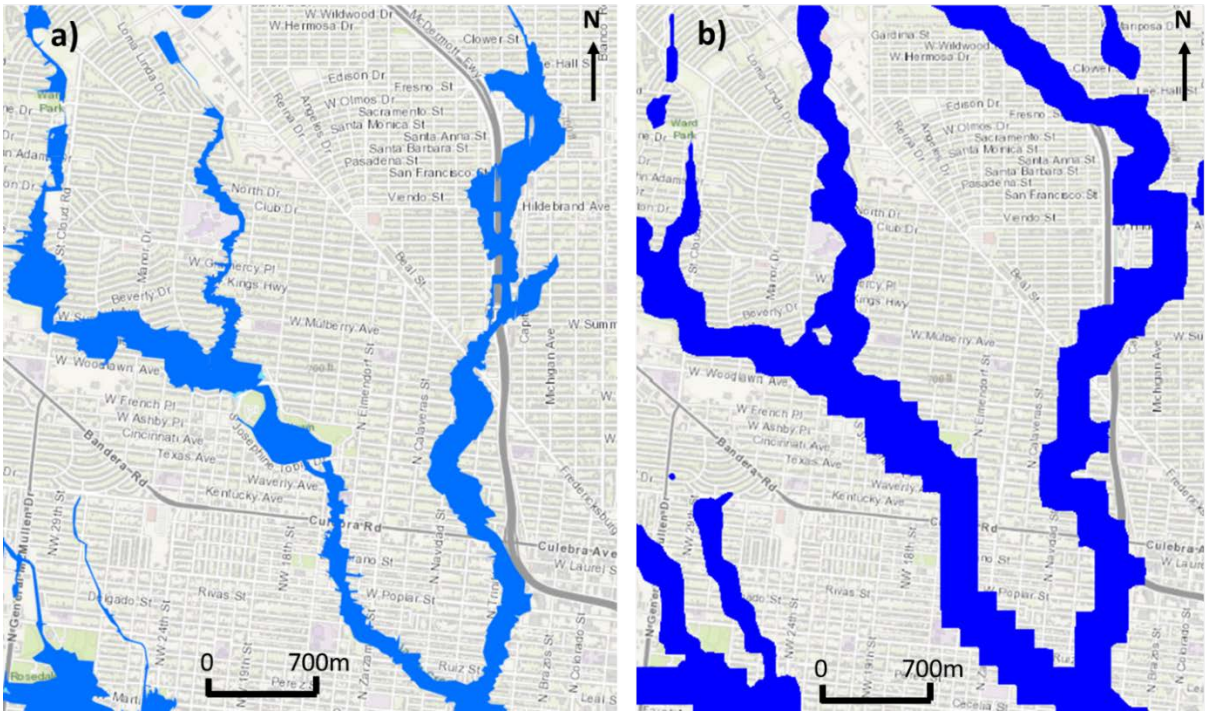

Figure 33. Comparison between (a) FEMA and (b) GSSHA floodplains in area S2. (Note: GSSHA results are too coarse to identify flood risk areas).

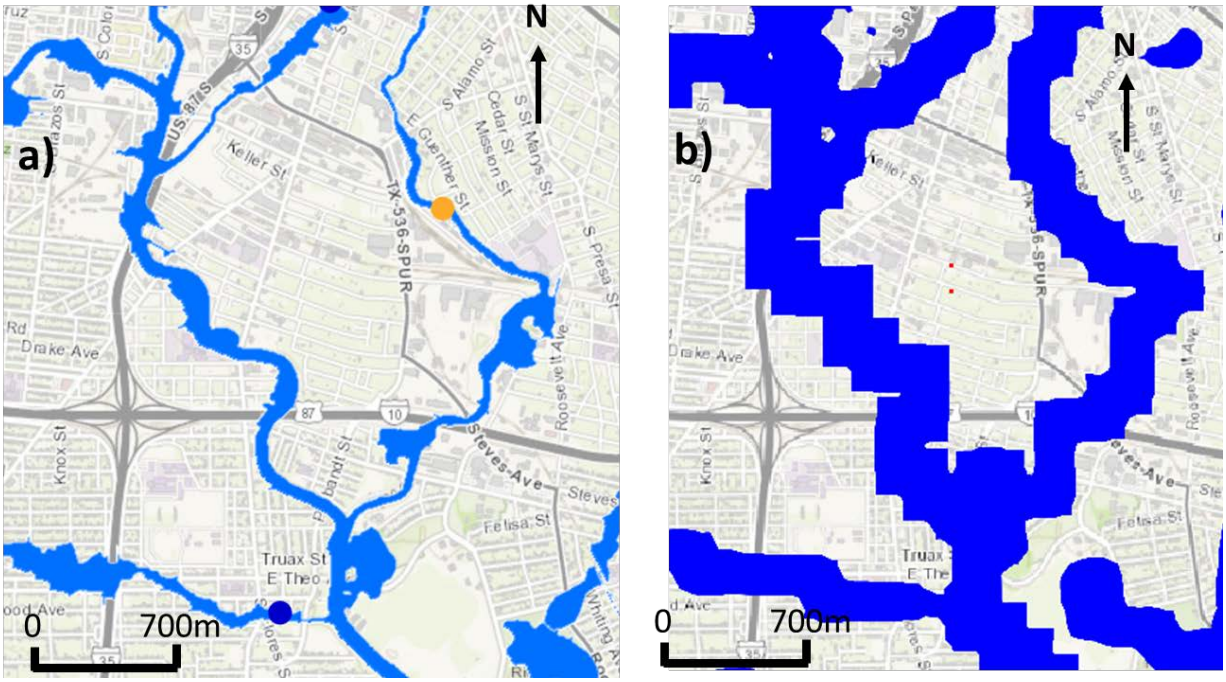

Figure 34. Comparison between (a) FEMA and (b) GSSHA floodplains in area S3. (Note: GSSHA results are too coarse to identify flood risk areas).

5.4.2. HEC-RAS 2D

The results with HEC-RAS 2D model presented more consistent results in Upper San Antonio (Figure 35). The HEC-RAS 2D presented larger floodplains in San Pedro Creek and lower on San Antonio River when compared to FEMA. The major difference is the flooded area south of the I-10. This is a low depression area that is likely to be flooded when the river overflows. Figure 36 details de flood area highlighted in Figure 35. It can be seen how the high resolution DEM contributes to a precise floodplain generation. The floodplain generated for Leon Creek is significantly overestimating the flood extent. This is probably due to the poor calibration of HEC-HMS in Leon Creek.

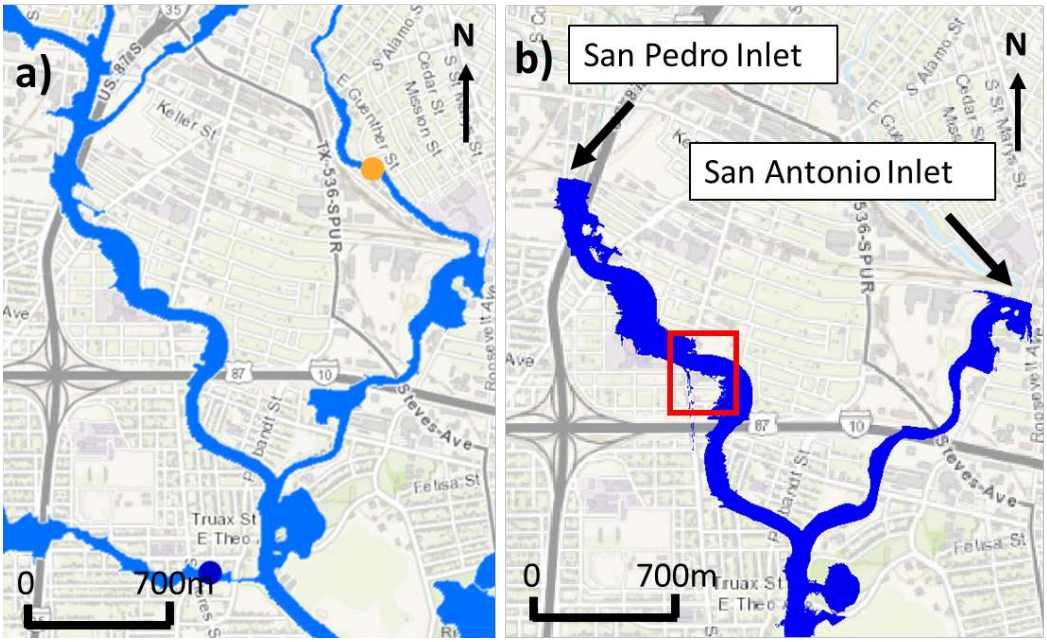

Figure 35. Comparison between (a) FEMA and (b) HEC-RAS2 2D in Upper San Antonio.

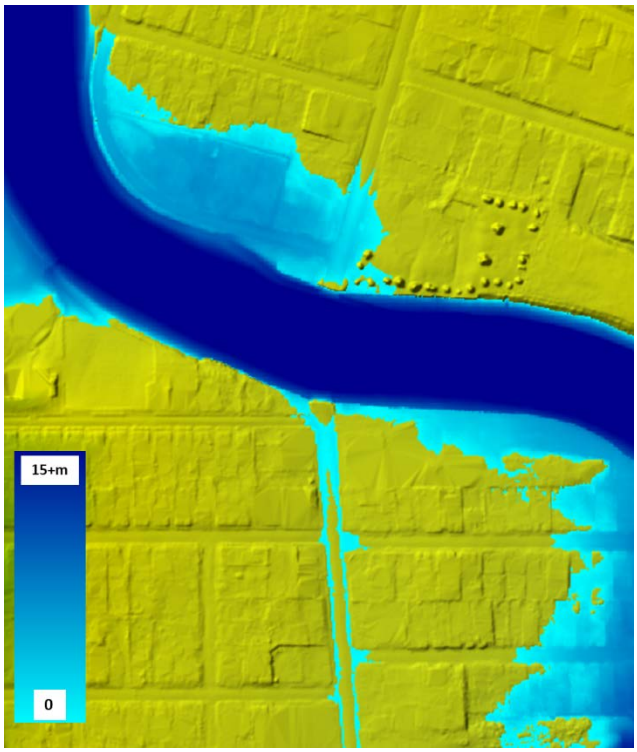

Figure 36. Detailed floodplain in high resolution DEM.

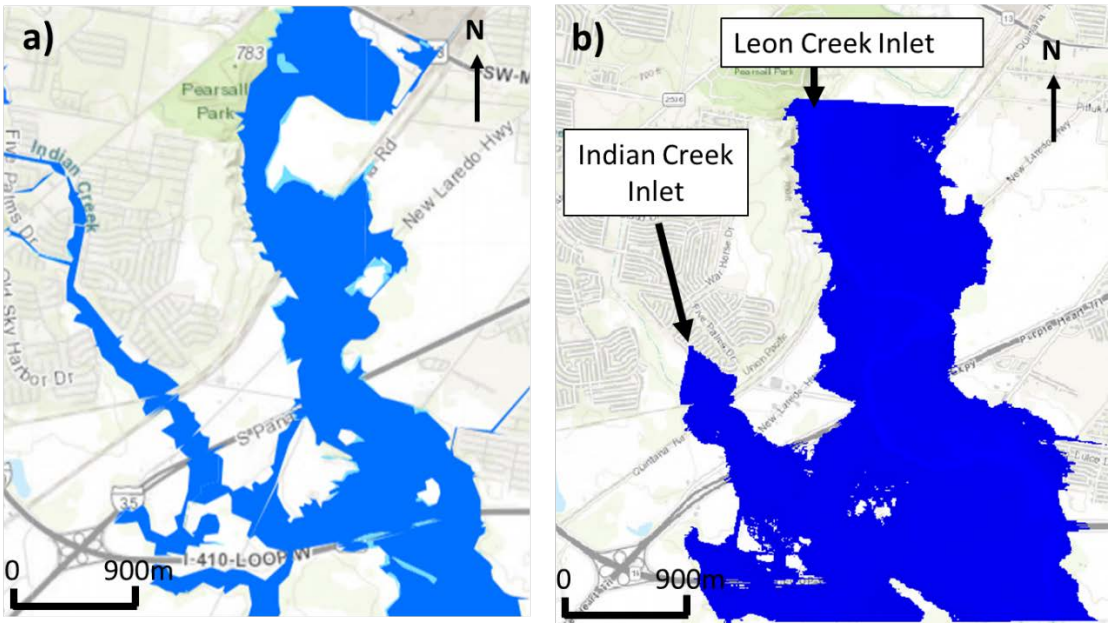

Figure 37. Comparison between (a) FEMA and (b) HEC-RAS2 2D in Leon Creek Watershed.

5.5. Future Peak Flows, Flooded Areas and Roads

The change in peak flows, flooded areas and roads caused by climate change is analyzed next. Figure 38 and Figure 39 shows the projected peak flows generated by the HEC-HMS for Upper San Antonio River and Leon Creek watersheds, respectively. Peaks generated with 1st quartile precipitation is always lower in the future when compared to present estimations. The peaks with the 1st quartile and median precipitation tend to increase in the future. The peak flows with the 3rd quartile, which better match historic conditions are shown in the section 5.2, varies with climate scenario. The RCP 4.5 scenario presented the highest peak in the near future, while the RCP 8.5 is more critical between 2050 and 2074. The uncertainties, measured as the difference between the 1st and 3rd quartiles, of RCP 4.5 are larger than RCP 8.5. These observations are valid for both 100- and 500-years storms.

The impacts of flooding caused by the 3rd quartile precipitation was evaluated for entire Upper San Antonio and Leon Creek watershed with GSSHA (Tables 14 and 15). The results show that this precipitation can generate greater floodplains with 1% frequency in the future than 0.2% probability in present days, except for the period of 2050-2074 under RCP 4.5 and 2025-2049 RCP 8.5. These results show how climate change can increase the impacts of floods in transportation infrastructure, especially the near future under RCP4.5 scenario.

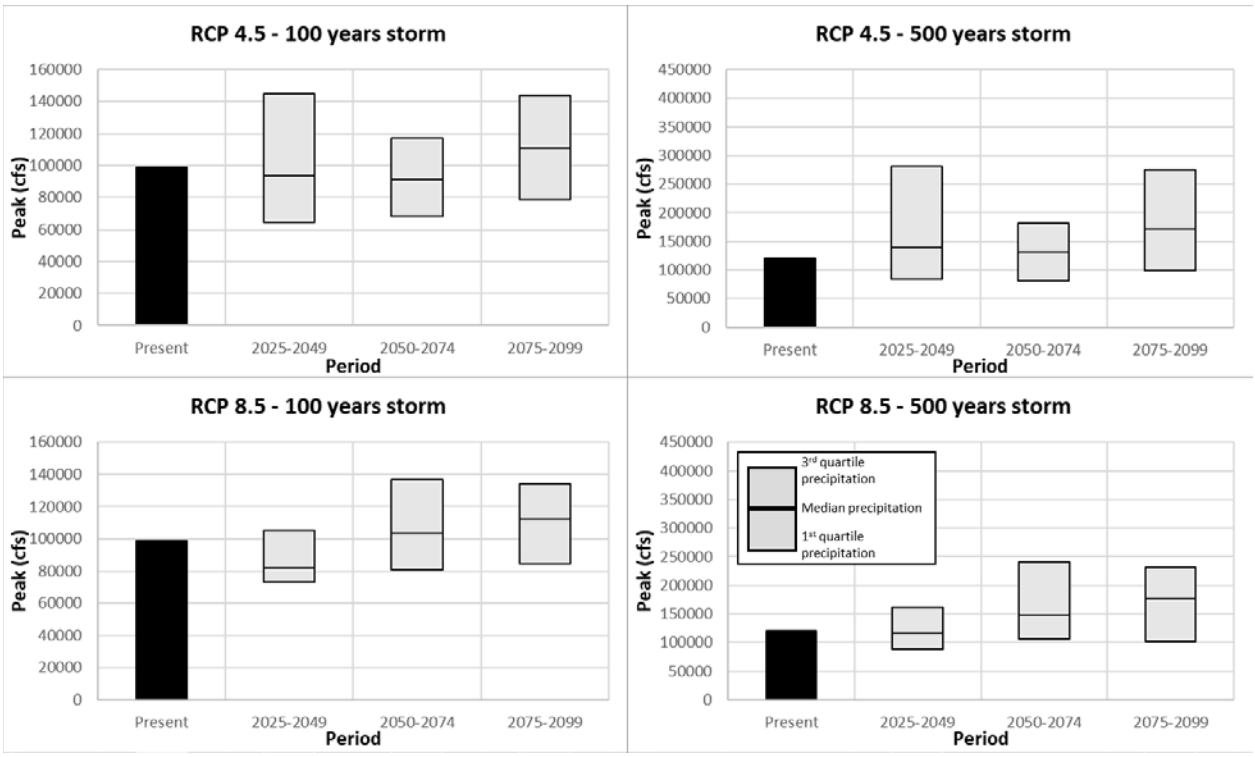

Figure 38. Peak flow projections generated by HEC-HMS models in the Upper San Antonio watershed.

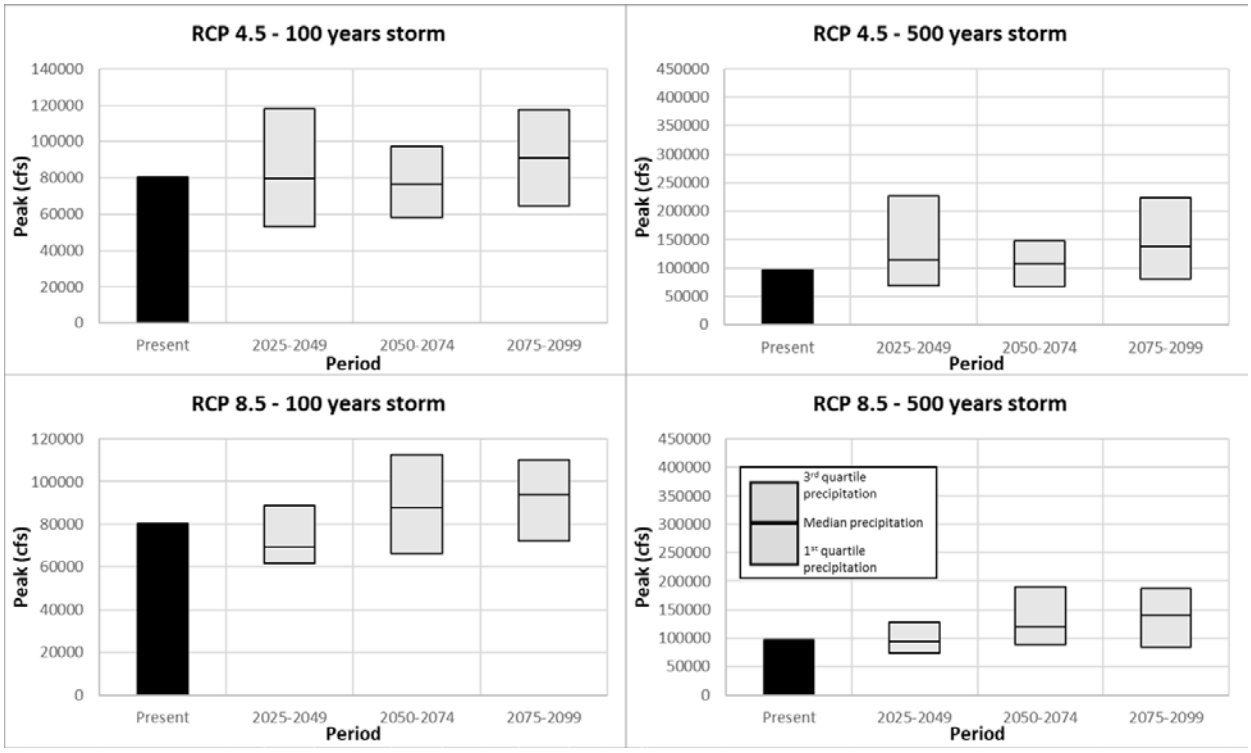

Figure 39. Peak flow projections generated by HEC-HMS models in the Leon Creek watershed.

Table 14. Flooded area and length of roads for the 100 and 500 years return period in Upper San Antonio watershed.

Scenario	Period	100-Year Storm		500-Year Storm	
		Flooded Area (km2)	Flooded Roads (km)	Flooded Area (km2)	Flooded Roads (km)
	Historical	33.4	231	38.1	266
RCP 4.5	2025-2049	40.4	283	55.0	419
	2050-2074	36.2	250	45.3	329
	2075-2099	40.2	282	54.5	414
RCP 8.5	2025-2049	34.1	235	43.1	309
	2050-2074	39.3	273	51.3	384
	2075-2099	38.8	270	52.5	379

Table 15. Flooded area and length of roads for the 100 and 500 years return period in the Leon Creek watershed.

Scenario	Period	100-Year Storm		500-Year Storm	
		Flooded Area (km2)	Flooded Roads (km)	Flooded Area (km2)	Flooded Roads (km)
	Historical	83.6	241	93.4	277
RCP 4.5	2025-2049	101.6	311	142.1	504
	2050-2074	90.7	267	114.0	364
	2075-2099	101.2	310	140.6	497
RCP 8.5	2025-2049	85.1	247	107.4	336
	2050-2074	98.6	299	131.2	447
	2075-2099	97.5	294	128.8	434

Figure 40 and Figure 41 shows the percentage increase of flooded area and roads compared to present probability of 100- and 500-year storms. The figures shows that the increase in flooded road varies with flooded area. In general, the percentage increase on flooded is greater than in flooded area. The exception are lower increases in flooded area that reach smaller extent of flooded roads, observed during mid future (RCP 4.5) and near future (RCP 8.5) in Upper San Antonio. The relative change in flooded area and roads are greater for 500-year return period storm. This is related to the greater difference on 500-year storm compared to the 100-year. The increase in flooded area and flooded roads is greater in Leon Creek, which can have an increase of more than 80% in flooded roads in the near future under RCP 4.5.

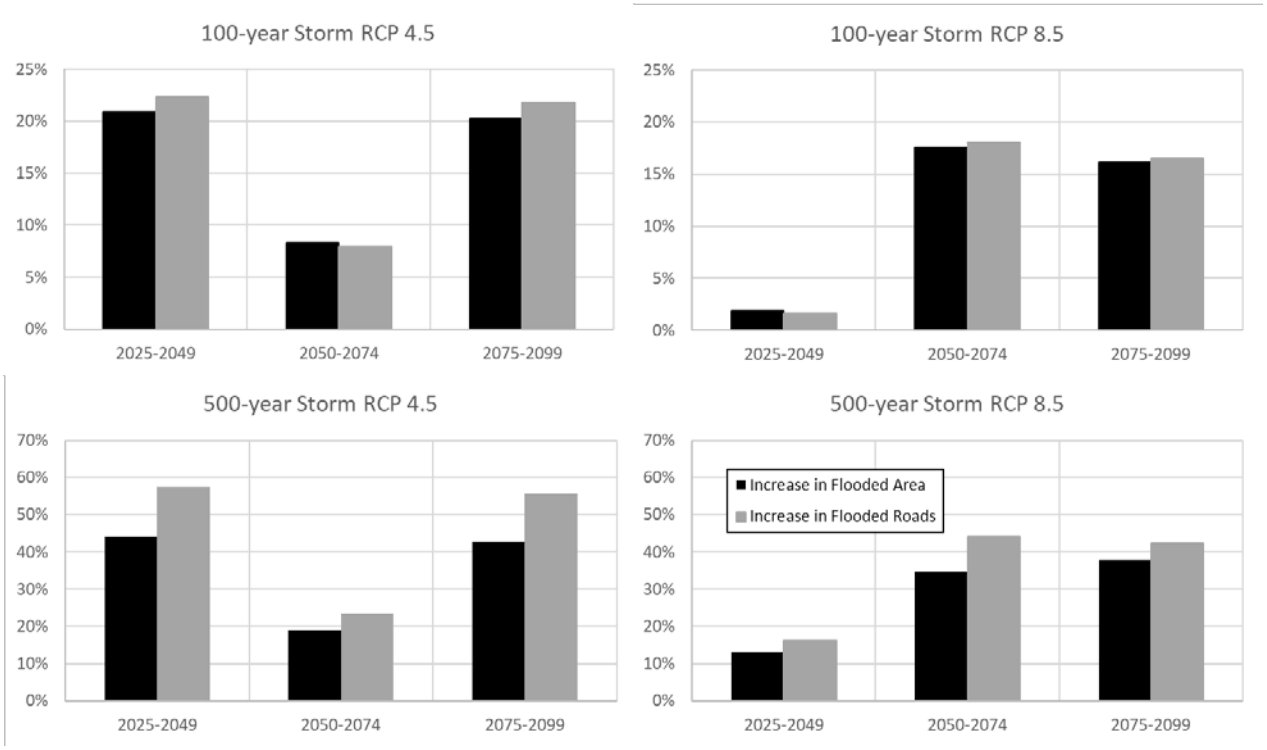

Figure 40. Projected flooded area and roads extent relative to present conditions in Upper San Antonio watershed.

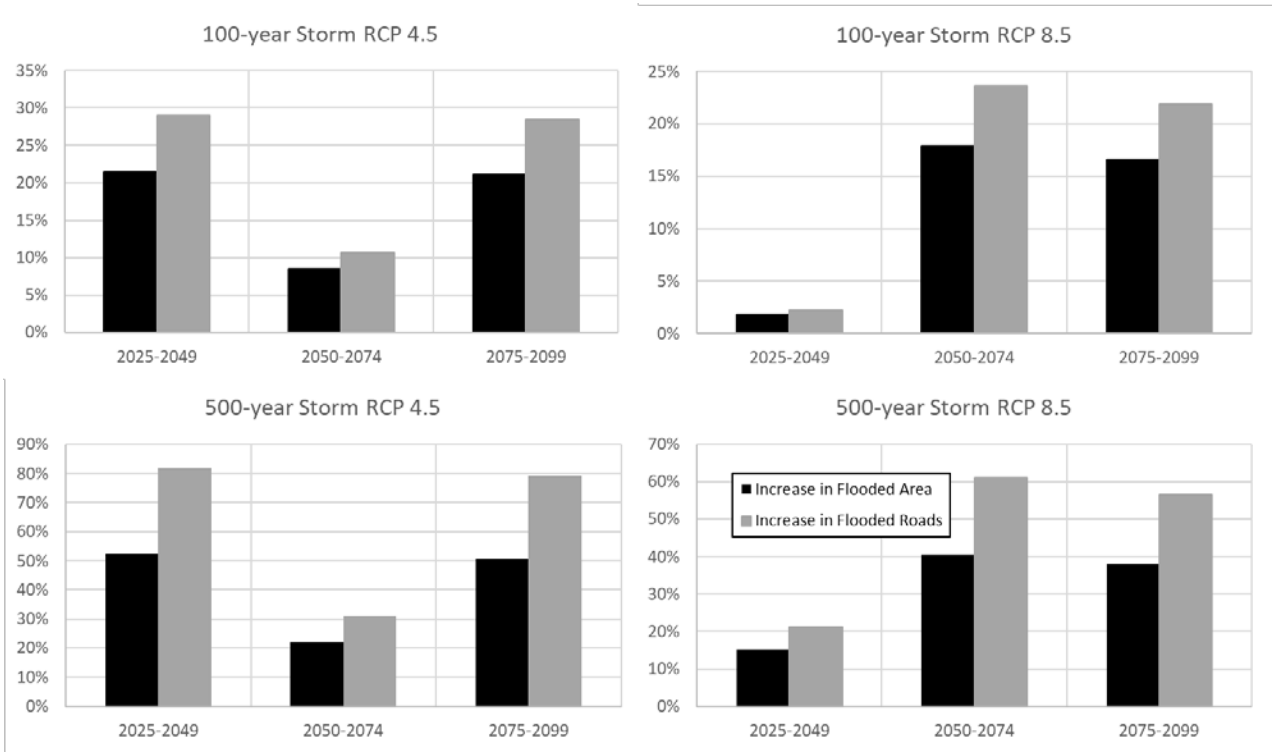

Figure 41. Projection of flooded area and roads extent relative to present conditions in Leon Creek watershed.

Upper San Antonio is more urbanized and has a higher density of roads, as Figure 42 shows. The extent of flooded roads per flooded area in Upper San Antonio watershed is twice higher than Leon Creek. Figure 42 shows that the relationship between flooded roads and the percentage of watershed that is flooded is linear. The slope of the trendline in Upper San Antonio is higher, which means that the increase in flooded area is more significant to transportation infrastructure. These findings show that the more developed the watershed is, the greater is the impact of floods on transportation infrastructure. The reason that Leon creek presented a higher increase in flooded roads is due to larger increase area in flooded areas. This figure shows that the difference between the maximum and minimum percentages of flooded area is greater in Leon Creek.

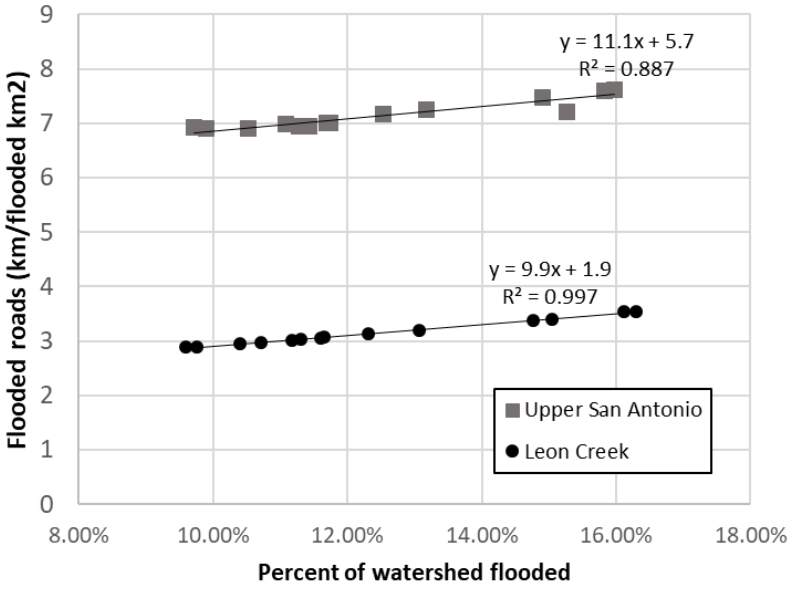

Figure 42. Relationship between relative flooded area (%) and flooded roads extension (km/flooded km²).

5.6. HEC-RAS 1D Analysis on Bridges

This section presents an analysis of the impact of the increase of flooding caused by climate change on a selected number of bridges in the Upper San Antonio River and Leon Creek watershed. The analysis was performed using HEC-RAS 1D model. Figure 43, Figure 44 and Figure 45 present the analysis made with HEC-RAS for the bridges located in the target area for Leon Creek (Figure 7), San Antonio River and San Pedro Creek (Figure 8). This chart shows the depth of water relative to the bottom of the bridged deck. Positive values mean that the flood wave is above the bridge bottom and therefore is flooding. In Leon Creek, the seven bridges that are located upstream are already vulnerable to the current 100- and 500-year storms, including the bridge on IH-35 south and its access roads. South West Loop 410 and the State Highway 16 would not be affected by flood with current extreme rainfall frequency. However, the near future projection indicates that the two roads can be affected by floods with 100- and 500-year storms. The greatest difference is observed for HEC-RAS simulation of 500-year water level, that can reach over 4m above State Highway 16.

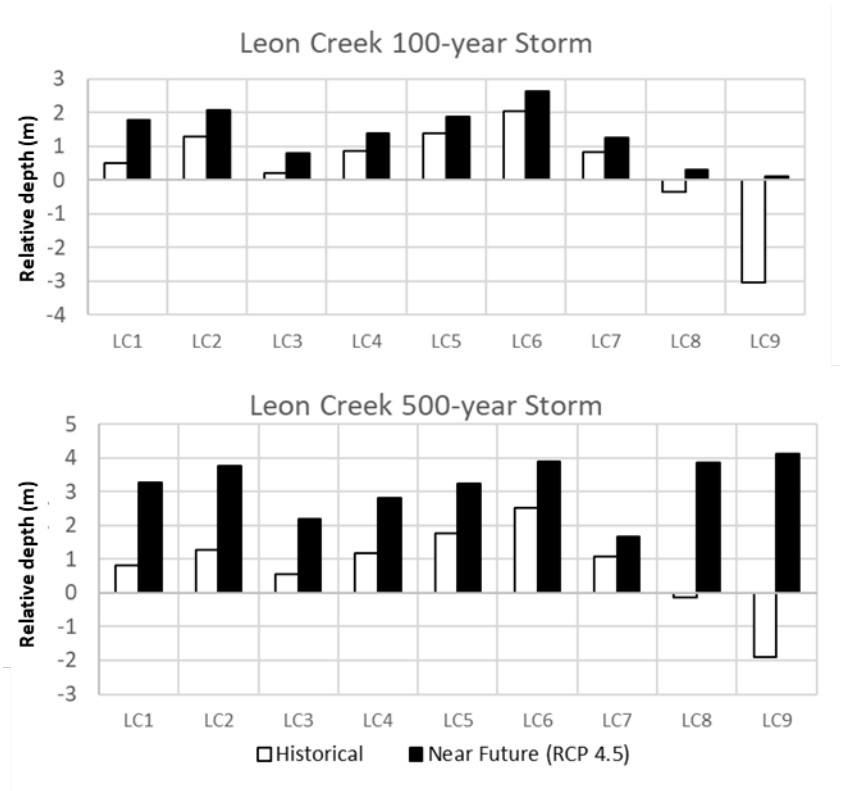

Figure 43. Depth of water above bottom of bridges at Leon Creek for the 100- and 500- year storms for historical and near future conditions (RCP 4.5).

In the San Antonio River, most of the bridges are safe against flood events with those two storms, except for Lone Star Boulevard with the 500-year. The projected near future 100-year storm will affect the Lone Star Boulevard bridge if compared to current conditions. The future 500-year storm, however, is likely to flood all bridges within the studied area according to the HEC-RAS 1D results. Bridges in San Pedro Creek are more susceptible to flooding when compared to the ones analyzed in San Antonio River and in Leon Creek. All the bridges all likely to be flooded with current 500-year storm and four out of five in the 100-year case. All the bridges in the area can be affected by project future floods. Of the 20 bridges evaluated in two regions, 9 and 5 bridges were not subjected to flooding under current condition if subjected to the 100- and 500-year storms. In the near future, only 5 bridges were safe with 100-year storm and all bridges are likely to flood with 500-year storm.

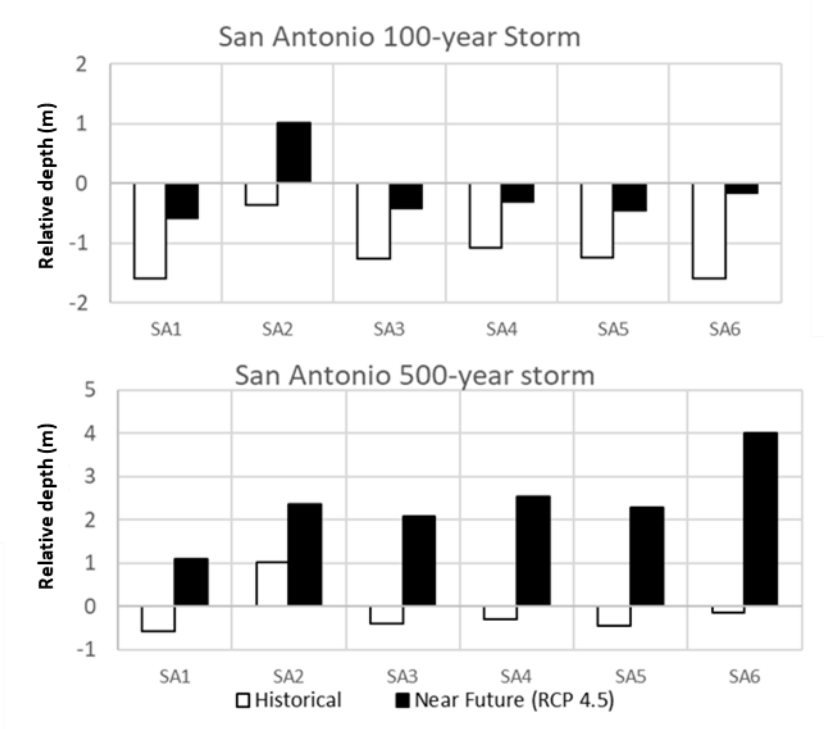

Figure 44. Depth of water above bottom of bridges at Upper San Antonio river for the 100- and 500- year storms for historical and near future conditions (RCP 4.5).

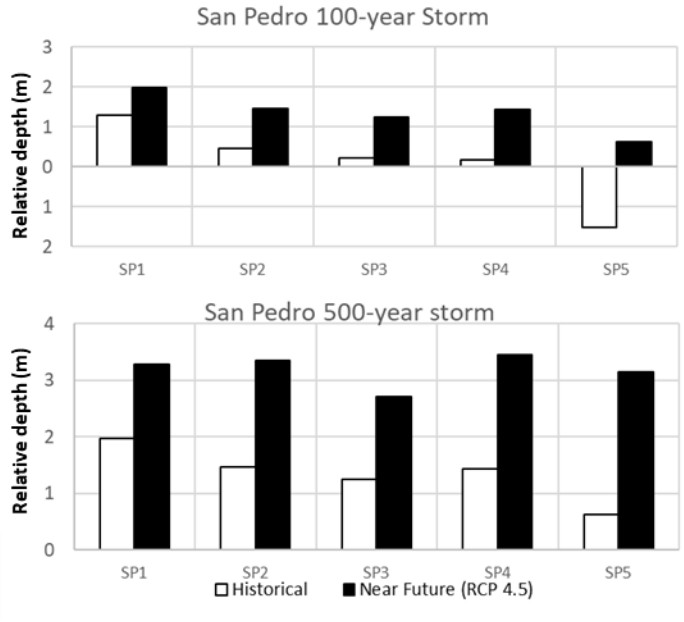

Figure 45. Depth of water above bottom of bridges at San Pedro Creek for the 100- and 500- year storms for historical and near future conditions (RCP 4.5).

5.7. HEC-RAS 2D Analysis

The extent of flooded roads was higher in Leon Creek than in Upper San Antonio due to a larger floodplain that reached closed highway (Table 16). The roads in this area of Leon Creek are concentrated in limited areas and increase in flooded area can not effect any roads. This is showed on the equal extent of flooded roads in near future (RCP 4.5, 100-year storm) and historical (500-year storm) with different flooded area.

Table 16. HEC-RAS 2D analysis on flooded area and roads.

Design Storm	Period	Leon Creek		Upper San Antonio	
		Flooded Area (km^2)	Flooded Roads (km)	Flooded Area (km^2)	Flooded Roads (km)
100-year	Historical	35.21	57.03	0.62	5.00
	Near Future 4.5	37.06	57.81	0.80	10.06
500-year	Historical	37.02	57.81	0.98	7.58
	Near Future 4.5	49.40	72.06	2.25	29.33

This larger open space in the Leon Creek watershed resulted in larger increases in flooded area than roads, as Figure 46 demonstrates. The Upper San Antonio is more urbanized as has a larger roads grids around the rivers. Increase in flooded area in this watershed, in this particular region, had larger impact on the transportation infrastructure. This figure also shows that the extent of flooded area is significantly higher in Upper San Antonio, specially from the 500-year storm. The affected roads with current conditions and with climate change can be observed in figures 40 and 41.

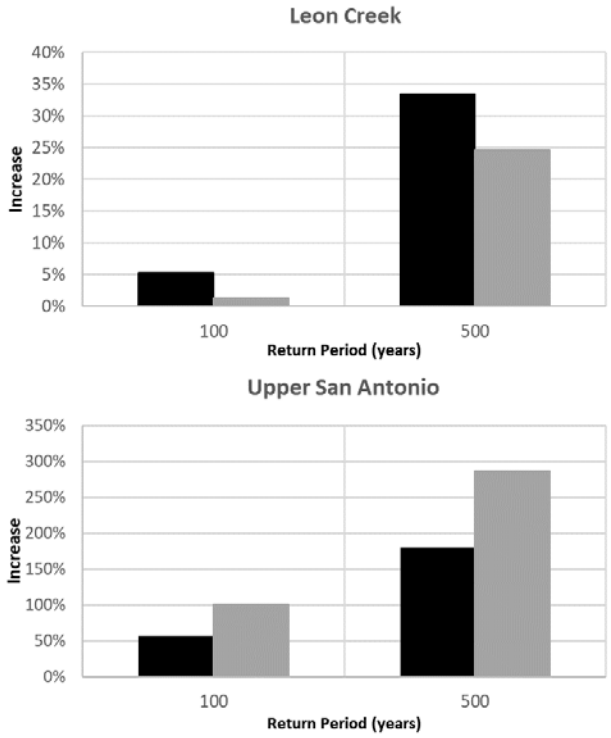

Figure 46. Projection of flooded area and roads extent with HEC-RAS 2D.

Figure 47. Affected roads modeled with HEC-RAS 2D in Upper San Antonio with 100-year (left) and 500-year storm.

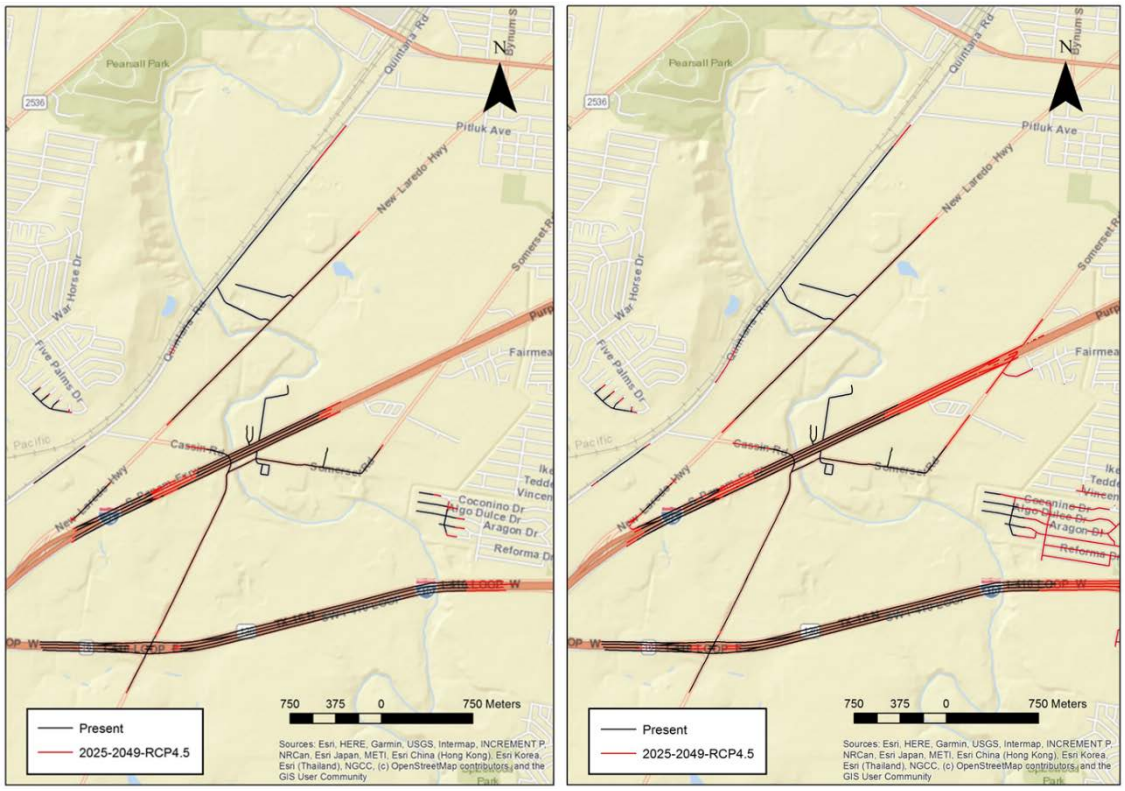

Figure 48. Affected roads modeled with HEC-RAS 2D in Leon Creek with 100-year (left) and 500-year storm.

5.8. LID Implementation Scenarios

The potential benefits of implementing LID stormwater controls in a watershed scale were assessed for the San Antonio River, Leon Creek, San Pedro Creek and the Apache Creek, which is a tributary of the Upper San Antonio River. This analysis evaluated the relative reduction of peak flow with respect to the historical 100-year and 500-year return period storms for three scenarios of LID implementation (5, 10 and 15% of LID in each sub-basins) (Figure 49). The results indicate that the peak reduction is less effective for the 500-year storm, which remains almost constant in San Antonio River and San Pedro Creek. Even with 15% of the area occupied by LID, all peaks were still more than the double than the peak generated with current 500-year storm. The peak reduction is more significant for 100-year storm, as this generates lower runoff that have greater capacity to be retained by LIDs. Peaks at San Antonio River and Leon Creek presented the greatest reduction of more than 10% the relative increase in peak by climate changes. However, the scenario with 15% LID occupation still have all the peaks more than 27% greater than it was predicted with todays' conditions.

(55) analyzed the efficiency of LIDs in reducing peak flows in a 0.58 km^2 urban watershed and how it is influenced by intensity and duration. They modified the CN in the watershed to represent the LID placement. Their results showed that the structures can significantly reduce peak flows for less intense (2 years of return period) and longer rainfalls (up to 72% reduction). Their results also showed that LID performed poorly for heavier storms, with no more than 20.2% peak reduction for 100-year storm. *(47)* modeled LID performance in a 0.26 km^2 watershed using GSSHA. They increased the storage and infiltration of the grids where a LID was supposed to be located. Their results also showed that peak reduction is dependent on intensity. While the 2-year storm reached 25% in peak reduction, the 100-year presented a maximum reduction of 9.4%. However, the lower reduction was observed for a 50-year storm with a maximum of 5.5%. The reason might be a more realistic representation of LID placement when compared to *(55)* and this report. Grid representation can catch the influence of one LID into another, which might decrease the overall capacity under certain circumstances.

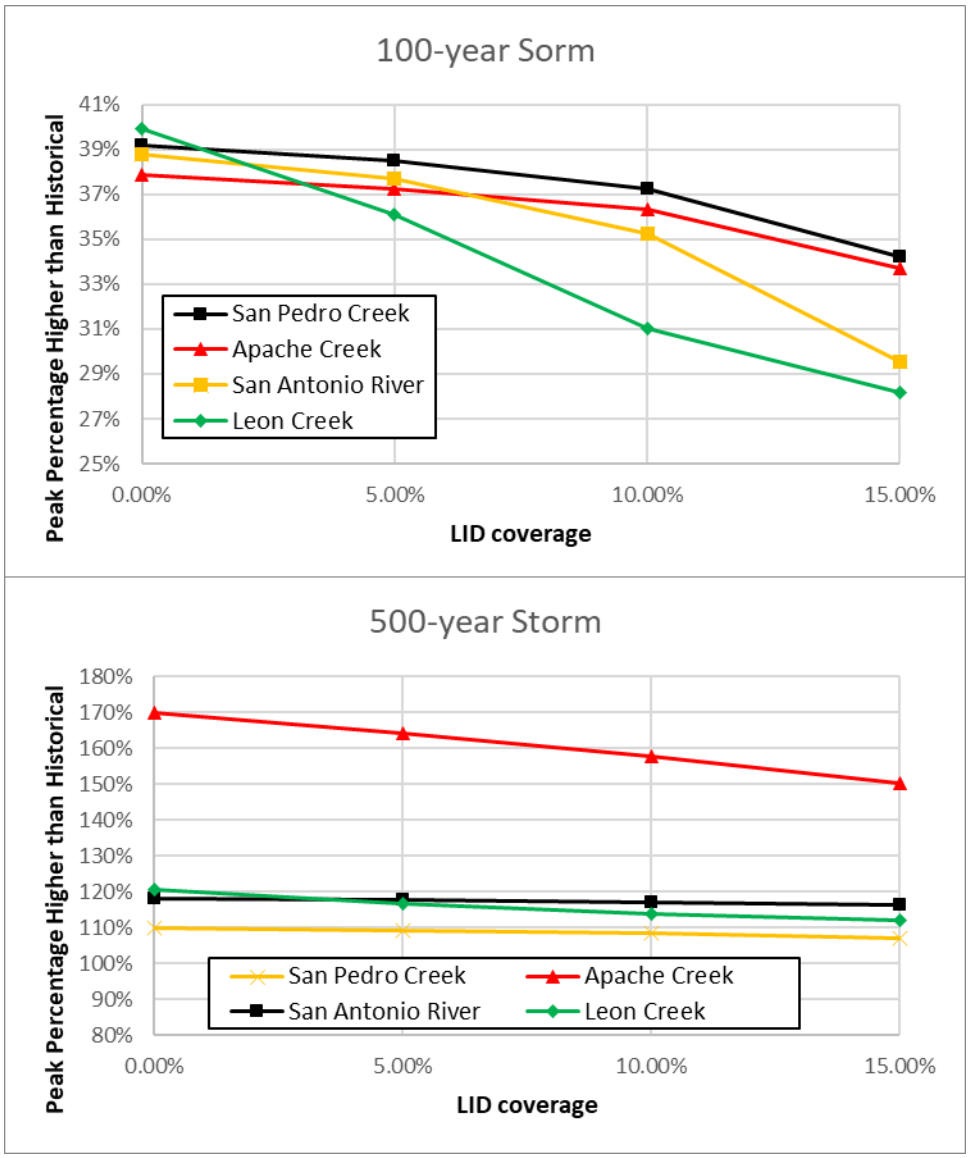

Figure 49. Peak flow reduction for different levels of LID implementation for the 100- and 500-year return period storms.

The effectiveness of peak flow reduction is depicted in Figures 50, 51 and 52 in the bridges at San Antonio River, San Pedro Creek and Leon Creek, respectively. The flood depth in bridges decline in most cases for LID scenarios simulations. This approach was not enough to convert climate change impacts on the transportation infrastructure in San Pedro Creek and San Antonio River. However, the application of LID scenarios can reduce the water level below bridge elevation for SW Loop 410 (LC 8) and State Highway 16 (LC9) at Leon Creek (Figure 52) for the 100-year storm.

LID application scenarios showed that this method is less efficient in mitigating climate change impacts from floods generated by super storms when compared to other methods (described in the following sections). Simulations were taken in HEC-HMS to predict the percentage the watershed to be composed of LID to reduce to peak to its current condition for 100-year storm in Leon Creek and San Antonio River downstream to San Pedro Creek. It is estimated that a total of 22% of the

area in Leon Creek and 37% in Upper San Antonio would be required to be transformed into LID practices so the climate change effects are minimized. These percentages are high and might be difficult to be applied due to the large area of the watersheds, particularly because of high costs of retrofitting and operating LID controls *(47, 56).*

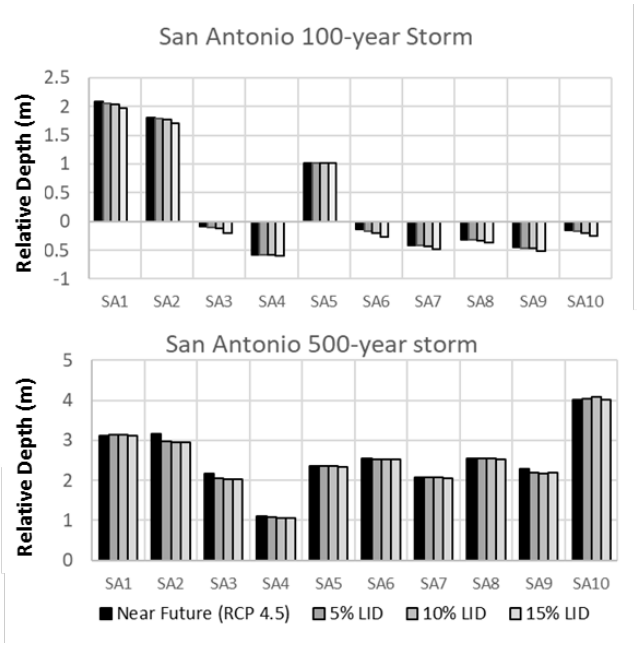

Figure 50. LID scenarios effects on bridges at San Antonio River.

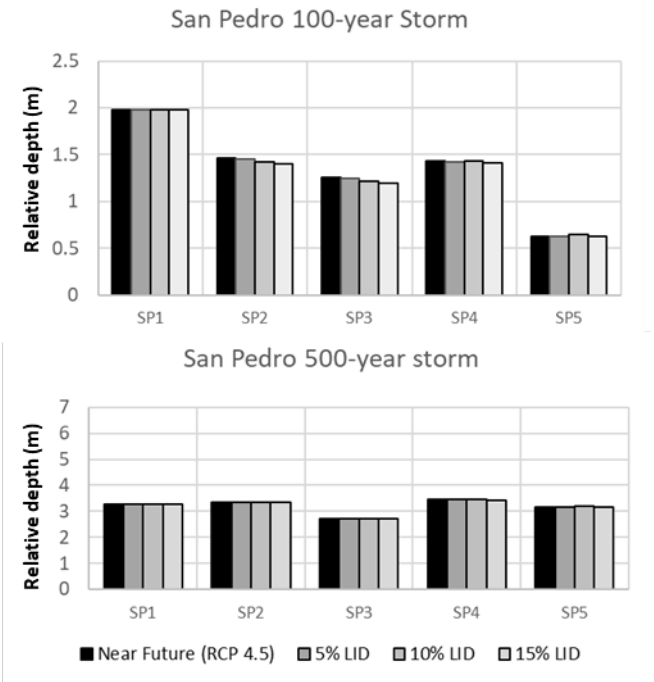

Figure 51. LID scenarios effects on bridges at San Pedro Creek.

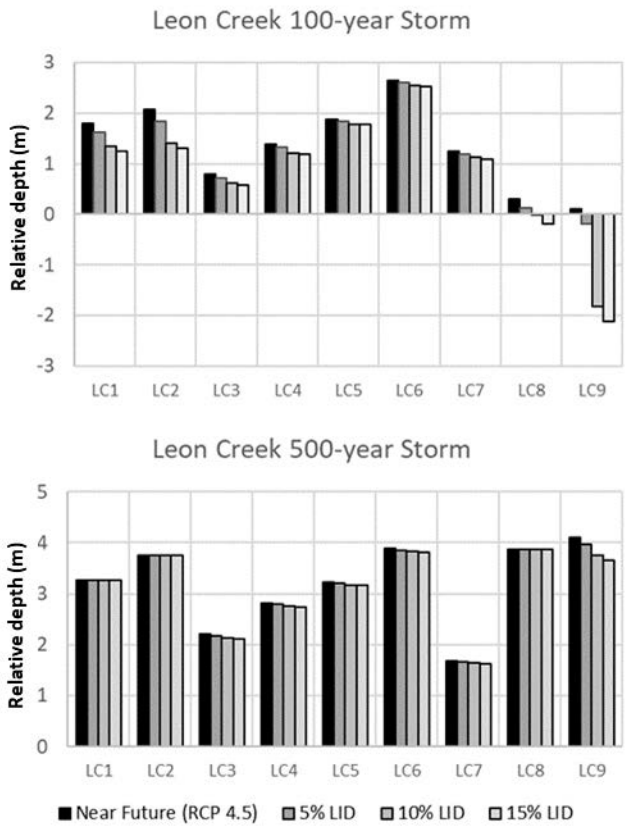

Figure 52. LID scenarios effects on bridges at Leon Creek.

5.9. Channel Widening

Widening the main channel can help protect all bridges from 100-year storm in the near future RCP 4.5, except for Furnish Street at San Pedro Creek (Figures 53 and 54). HEC-RAS 1D results show that this channel widening reduces the water level at all bridges for the 100-year storm. However, the bridges were still underwater with the 500-year storm in the near future RCP 4.5. In this case, channelizing the streams increases the water level at downstream bridges. The reason is that this configuration increases the flow capacity due to the larger cross-sectional area and lower roughness. Therefore, the water accumulation downstream can be intensified consequently. The major benefits are observed in the bridges the middle of the channel modification (e.g. SA3 and SP2).

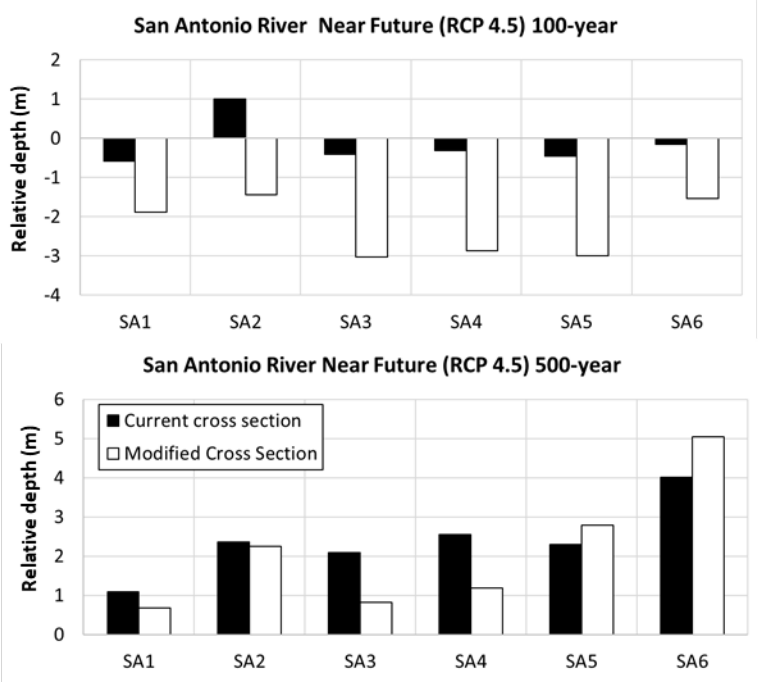

Figure 53. Channel widening benefits on bridges at San Antonio River.

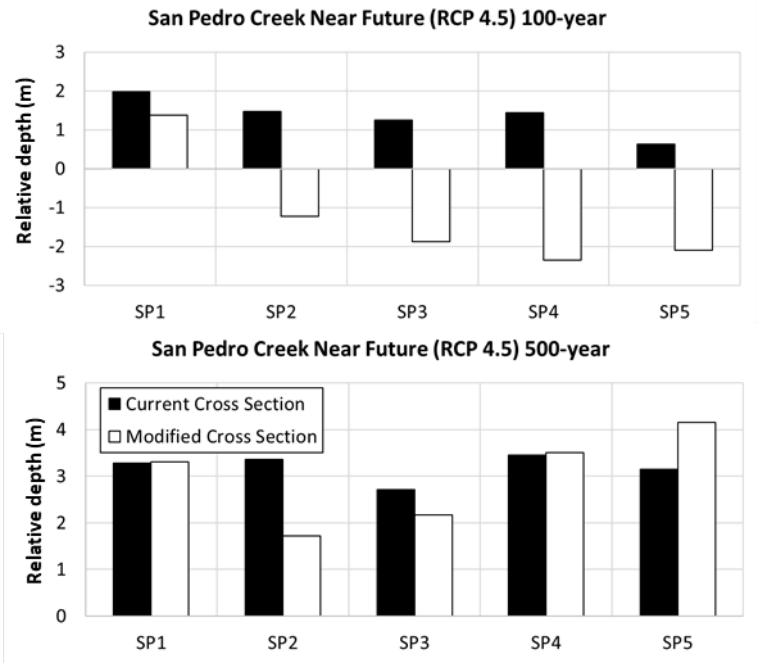

Figure 54. Bridge widening impacts on bridges at San Pedro Creek.

HEC-RAS 2D results show that the flooded area and roads can be significantly reduced, as shown in Table 17. This reduction approximates the extent of flooded area and roads to its current condition for the 100-year storm, as presented in Figure 55. This figure also shows that the 500-year floodplain in the near future RCP 4.5 continued to be considerably higher than its current conditions.

Table 17. Comparison between flooded area and roads with current and modified channel.

Design Storm	Scenario	Flooded Area (km^2)	Flooded Roads (km)
100-year	Near Future 4.5	0.80	7.58
	Modified Channel 100-year	0.65	5.10
500-year	Near Future 4.5	2.25	29.33
	Modified Channel 500-year	1.62	19.28

The comparison between the affected roads with current condition streams and flood widening is shown in Figure 56. This measurement shows the substantial decrease in flooded roads discussed in Figure 55. The poorer effectiveness of channelization in downstream area for 500-year storm is also observed in the flooded roads, where there was little reduction on the affected roads.

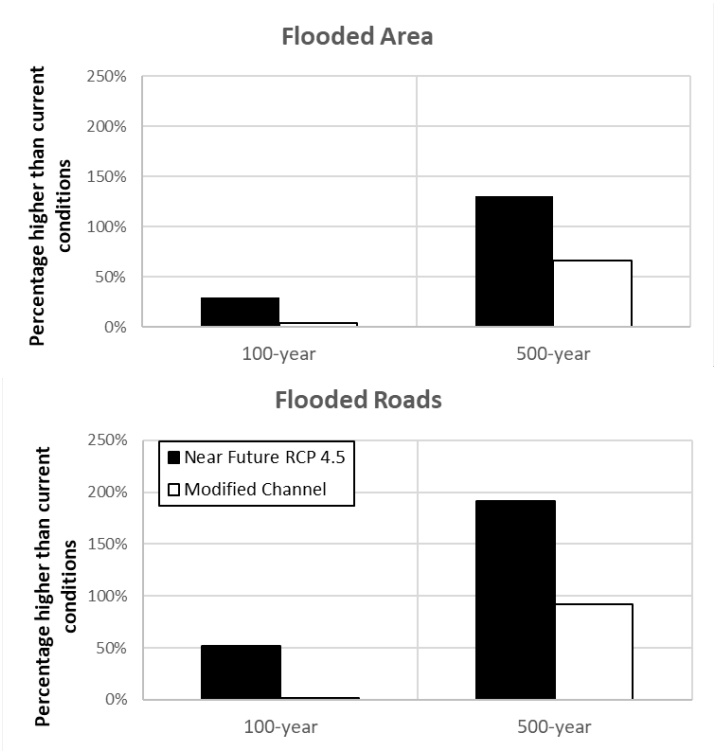

Figure 55. Flood widening impacts flooded area and roads.

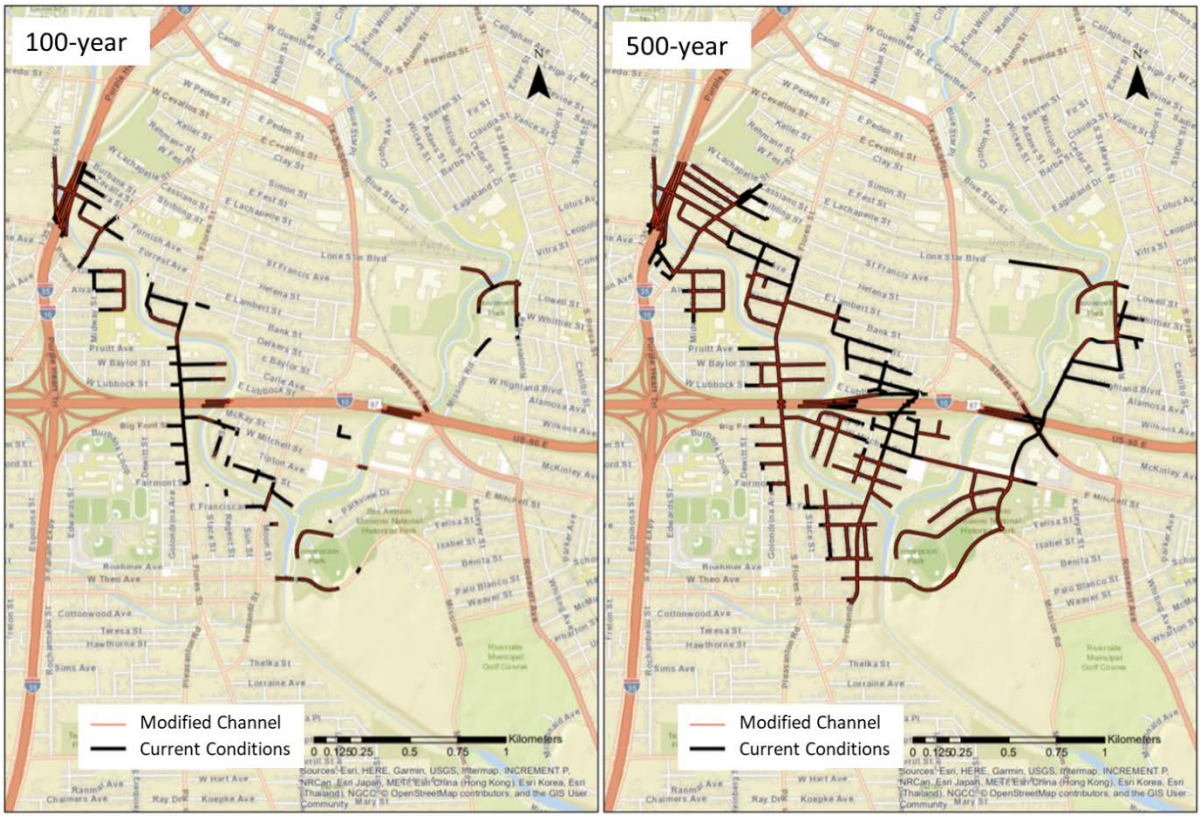

Figure 56. Map of flooded roads with and without channelization.

5.10. Olmos Dam Modification

In this analysis, a scenario where the storage capacity of the Olmos Dam is enhanced. The first step was to analyze how much area surrounding the dam would be affected when the crest height is elevated. The flooded area with a crest elevation of 222m is mainly the green area reserved to the Olmos Dam (Figure 57(a)). Roads surrounding this area would be flooded if the crest is increased to 223m as Figure 57(b) shows. The flooded area in Olmos Dam would affected surrounding neighborhood with a crest elevation of 225m and 227m, in Figures 57(c) and 57(d) respectively. Therefore, the increase on the Olmos Dam's crest was here simulated by considering the construction of an embankment to restrict the floodplain to the 222m extent.

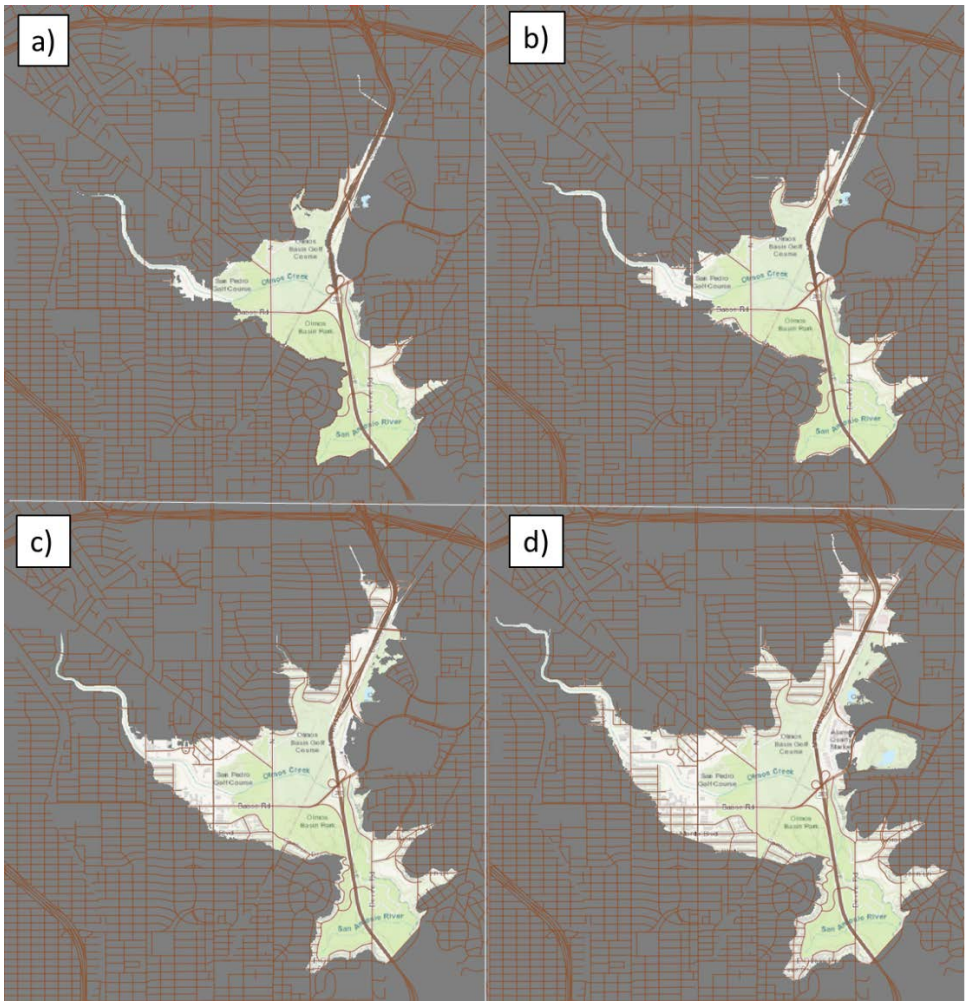

Figure 57. Flood extent with 222m (a) 223m (b) 225m(c) and 227m (d) Olmos Dam's crest.

The peak flow reduction and the maximum elevation reached during a 100-year and 500-year storms are presented in Table 18. Results show that elevating the crest can significantly reduce the events that caused overflow in the system. This configuration reduced the 500-year peak in the near future almost to its current conditions. However, it would be necessary to increase the Dam's crest in more than 5m. The future 500-year peak with the modified dam is still higher than the one generated with historical records, even the simulation showing that the Olmos Dam overflowed by 10cm. The reason is the greater hydraulic pressure increasing the flow through the gates.

Table 18. Comparison of peaks and water surface elevation with current and modified Olmos Dam.

Period	Design Storm	Existing		Modified	
		Outflow (m^3/s)	Max. Elevation (m)	Outflow (m^3/s)	Max. Elevation (m)
Historical	100-year	32.3	221.3	32.3	221.3
	500-year	133.3	222.0	47.9	222.3
Near Future (RCP 4.5)	100-year	370.1	222.3	63.7	223.3
	500-year	1490.8	223.4	133.4	227.5

Simulation on HEC-RAS 1D and 2D were conducted to verify how this modification could contribute to reduce climate change impacts on the transportation infrastructure. The results showed no difference in the water surface elevation on bridges and in flooded area and roads, even with the reduction on the Dam's outflow.

The Dam's outflow was still lower than the peak resulted from other areas where San Pedro Creek reaches the San Antonio River during the 100-year storm (see Figure 57). Therefore, the peak reduction did not affect the maximum flood plain area. The peak flow from Olmos Dam was higher than the first peak at the confluence for the 500-year storm. However, the first peak is closer to the San Pedro's, and these two combined are more significantly the area than the outflow peak from Olmos Dam isolated. The discharge at San Pedro Creek is much smaller when the Olmos Dam's outflow peak reaches the area. These results show how delaying the peaks can be effective to flood control.

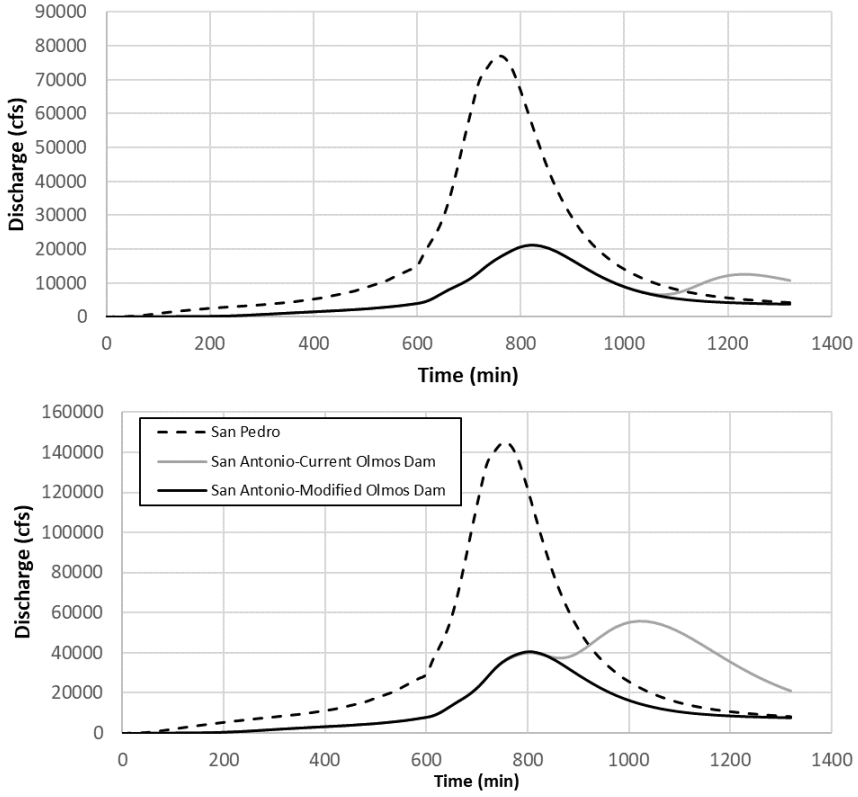

Figure 58. Peak reduction from Olmos Dam modification.

5.11. Implementation of Levees

The ground and water surface elevation in the four profiles (Figure 16) is shown in Figure 59. The downstream profiles (e.g. profiles 2 and 4) are more vulnerable to overflow. The difference between water surface and ground elevations corresponds to the levee height in the models. The levee indicated in profile two is exemplified in Figure 60. This figure also shows that the other riverside (Profile 1) do not need a levee in this same area. Figures 44 and 45 shows the bridges underwater with the 100-year storm, indicating the bridges where mobile barriers should be placed.

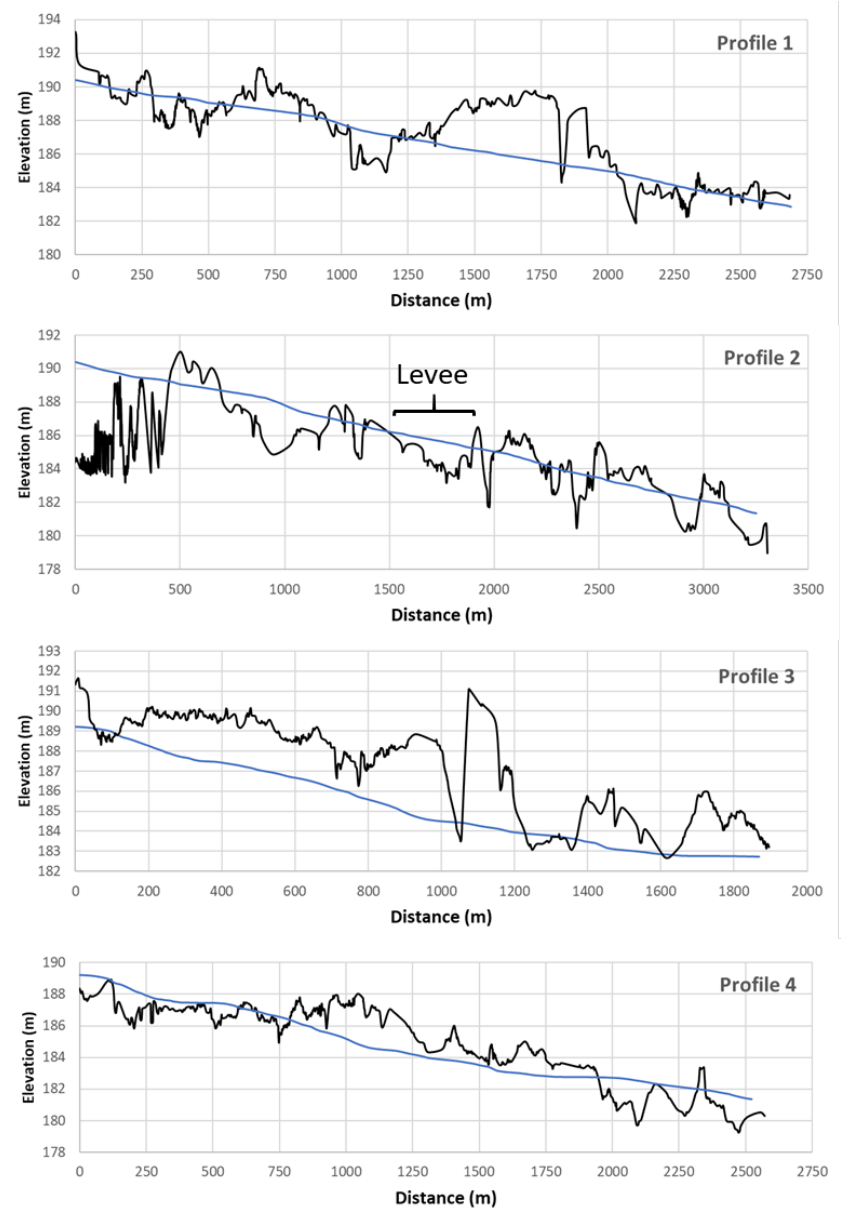

Figure 59. Water surface and ground elevation at each profile.

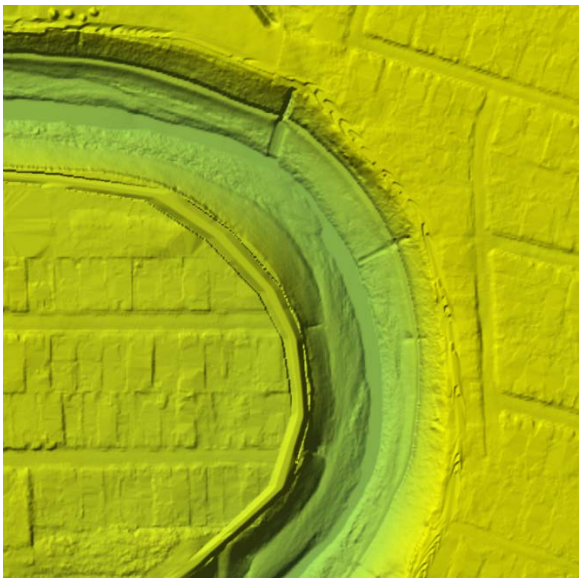

Figure 60. Example of terrain modification to include levees in HEC-RAS 2D.

The application of levees was effective in reducing the flood in Upper San Antonio for 500-year storm in the near future, shown in Table 19. The extent of flooded roads and area is lower for this storm and scenario among all flood control measurements.

Table 19. Flooded area and roads with and without levees in Near Future RCP 4.5.

Scenario	Flooded Area (km^2)	Flooded Roads (km)
No Levees	2.25	29.33
Levees Applied	1.29	13.99

The extent of flooded roads and area continued to be higher than flood from current 500-year storm, as presented in Figure 61. The map of affected roads in Upper San Antonio watershed is presented in Figure 62. This figure and Table 19 shows that the flooding in this area approximated to the 100-year storm in the near future with no levees (see Table 16 and Figure 42).

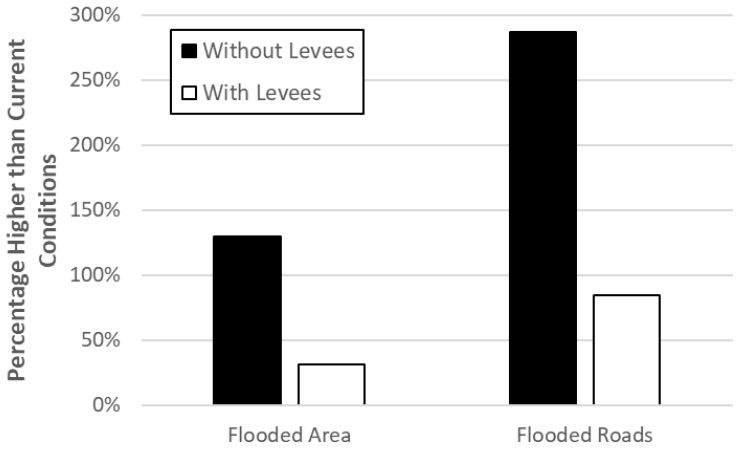

Figure 61. Performance of levees for 500-year storm in near future RCP 4.5.

Figure 62. Flooded roads with a 500-year storm in near future RCP 4.5.

6. CONCLUSIONS

This study analyzed 51 combinations of future projections for representative concentration pathways (RCP) 4.5 and 8.5 scenarios and three future periods (2025-2049, 2050-2074 and 2075-2099) in the City of San Antonio, TX. The future projections were calibrated and validated with 50 years of observed precipitation records. The future intensity-duration-frequency curves (IDF) were estimated with the generalized extreme value (GEV) method. The 1st and 3rd quartiles, median, minimum and maximum intensities of the projections combination were determined for both scenario and each period. A GSSHA, HEC-HMS, and HEC-RAS 1D and 2D models were built for the Leon Creek and Upper San Antonio watersheds. These models combined were used to evaluate climate change impacts on transportation infrastructure. Moreover, scenarios to mitigate climate change impacts were tested with LIDs, levees, flood widening, and Olmos Dam modification to enhance its capacity.

The rainfall analysis shows that the 3rd quartile of projected IDF is closest to the one originated with observed precipitation. The 3rd quartile intensity is likely to increase in the future, especially for storms with duration longer than 1 day. The near future (2025-2049) under RCP 4.5 scenario presented the greatest increase in intensity.

The historic and projected IDFs were used to generate design storms and evaluate the runoff generation for the 100- and 500-year return period storm. HEC-HMS model shows that discharge peak will increase for all future periods under both scenarios, for the 100- and 500-years storms. Flood projections generated by GSSHA for 100- and 500-years and future precipitation showed that flooded area can increase significantly. For instance, the increase in flooded roads can be more than 80% in near future for 500-year storm in Leon Creek watershed.

LID implementation, Olmos Dam increased capacity, levees and channel widening mitigating strategies were tested to address the increase in flood impacts from climate change. Olmos Dam modification have shown no effectiveness in reducing the flood plains to its current conditions. LID implementation would only be effective with large percentages occupation in both watersheds, which would be very costly. Levees significantly reduced the 100-year storm damages. However, the 500-year flooding impact in the near future continued to be considerably higher than the one predicted with current conditions. None of the strategies were able to mitigate the climate change impact of the 500-year storm.

The results generated here illustrate how potential climate change can impact urban watersheds and the transportation infrastructure. The results, also, show that climate projections uncertainties are still significantly high, which is also supported by many studies in the literature. Nonetheless, this study illustrates the need for watershed, floodplain, city and transportation officials to evaluate potential impacts of climate change and investigate what alternative adaptation and mitigation strategies can be implemented to decrease the potential risks of devastating flooding events in the built environment.

REFERENCES

1. Aich, V., Liersch, S., Vetter, T., Fournet, S., Andersson, J. C. M., Calmanti, S., and Paton, E. N. (2016). Flood projections within the Niger River Basin under future land use and climate change. *Science of The Total Environment*, 562, 666-677. doi:10.1016/j.scitotenv.2016.04.021.

2. Clavet-Gaumont, J., Huard, D., Frigon, A., Koenig, K., Slota, P., Rousseau, A., and Larouche, B. (2017). Probable maximum flood in a changing climate: An overview for Canadian basins. *Journal of Hydrology*: Regional Studies, 13, 11-25. doi:10.1016/j.ejrh.2017.07.003.

3. Gao, C., He, Z., Pan, S., Xuan, W., & Xu, Y.-P. (2018). Effects of climate change on peak runoff and flood levels in Qu River Basin, East China. *Journal of Hydro-environment Research*. doi:10.1016/j.jher.2018.02.005.

4. Shrestha, S., & Lohpaisankrit, W. (2017). Flood hazard assessment under climate change scenarios in the Yang River Basin, Thailand. *International Journal of Sustainable Built Environment*, 6(2), 285-298. doi:10.1016/j.ijsbe.2016.09.006.

5. Yin, J., Guo, S., He, S., Guo, J., Hong, X., & Liu, Z. (2018). A copula-based analysis of projected climate changes to bivariate flood quantiles. *Journal of Hydrology*, 566, 23-42. doi:10.1016/j.jhydrol.2018.08.053.

6. NOAA National Centers for Environmental Information (NCEI). (2018). U.S. Billion-Dollar Weather and Climate Disasters https://www.ncdc.noaa.gov/billions/. Accessed Oct. 3, 2018.

7. Liu, Z., Lao, J., Zhang, Y., Liu, Y., Zhang, J., Wang, H., & Jiang, B. (2018). Association between floods and typhoid fever in Yongzhou, China: Effects and vulnerable groups. *Environmental Research*, 167, 718-724. doi:10.1016/j.envres.2018.08.030.

8. Wijerathne, K. B. P. C. A., & Senevirathna, E. M. T. K. (2018). Identify the risk for leptospirosis disease during flooding periods (Special reference to Medirigiriya Divisional Secretariat Division in Polonnaruwa district). *Procedia Engineering*, 212, 101-108. doi:10.1016/j.proeng.2018.01.014.

9. van der Wiel, K., Kapnick, S. B., van Oldenborgh, G. J., Whan, K., Philip, S., Vecchi, G. A., . . . Cullen, H. (2017). Rapid attribution of the August 2016 flood-inducing extreme precipitation in south Louisiana to climate change. *Hydrol. Earth Syst. Sci.*, 21(2), 897-921. doi:10.5194/hess-21-897-2017.

10. Karamouz, M., Razmi, A., Nazif, S., & Zahmatkesh, Z. (2017). Integration of inland and coastal storms for flood hazard assessment using a distributed hydrologic model. *Environmental Earth Sciences*, 76(11), 395. doi:10.1007/s12665-017-6722-6.

11. Downer, C. W., and Ogden, F. L. (2006). Gridded Surface Subsurface Hydrologic Analysis (GSSHA) User's Manual, US Army Corp of Engineers, Engineering Research and Development Center.

12. Lawrence, J., Reisinger, A., Mullan, B., & Jackson, B. (2013). Exploring climate change uncertainties to support adaptive management of changing flood-risk. *Environmental Science & Policy*, 33, 133-142. doi:10.1016/j.envsci.2013.05.008.

13. Shen, M., Chen, J., Zhuan, M., Chen, H., Xu, C.-Y., & Xiong, L. (2018). Estimating uncertainty and its temporal variation related to global climate models in quantifying climate change impacts on hydrology. *Journal of Hydrology*, 556, 10-24. doi:10.1016/j.jhydrol.2017.11.004.

14. Sillmann, J., Kharin, V. V., Zhang, X., Zwiers, F. W., & Bronaugh, D. (2013). Climate extremes indices in the CMIP5 multimodel ensemble: Part 1. Model evaluation in the present climate. *Journal of Geophysical Research: Atmospheres*, *118*(4), 1716-1733.

15. Chandra, R., Saha, U., & Mujumdar, P. P. (2015). Model and parameter uncertainty in IDF relationships under climate change. *Advances in water resources*, *79*, 127-139.

16. Kundzewicz, Z. W., Krysanova, V., Benestad, R. E., Hov, Ø., Piniewski, M., & Otto, I. M. (2018). Uncertainty in climate change impacts on water resources. *Environmental Science & Policy*, 79, 1-8. doi:10.1016/j.envsci.2017.10.008.

17. DeGaetano, A. T., & Castellano, C. M. (2017). Future projections of extreme precipitation intensity-duration-frequency curves for climate adaptation planning in New York State. *Climate Services*, *5*, 23-35.

18. Agilan, V., & Umamahesh, N. V. (2016). Is the covariate based non-stationary rainfall IDF curve capable of encompassing future rainfall changes?. *Journal of Hydrology*, *541*, 1441-1455.

19. Ganguli, P., & Coulibaly, P. (2017). Does nonstationarity in rainfall require nonstationary intensity–duration–frequency curves?. *Hydrology and Earth System Sciences*, *21*(12), 6461-6483.

20. Shrestha, A., Babel, M., Weesakul, S., & Vojinovic, Z. (2017). Developing Intensity–Duration–Frequency (IDF) curves under climate change uncertainty: the case of Bangkok, Thailand. *Water*, *9*(2), 145.

21. Vu, M. T., Raghavan, S. V., Liu, J., & Liong, S. Y. (2018). Constructing short-duration IDF curves using coupled dynamical–statistical approach to assess climate change impacts. *International Journal of Climatology*, *38*(6), 2662-2671.

22. Rodríguez, R., Navarro, X., Casas, M. C., Ribalaygua, J., Russo, B., Pouget, L., & Redaño, A. (2014). Influence of climate change on IDF curves for the metropolitan area of Barcelona (Spain). *International Journal of Climatology*, *34*(3), 643-654.

23. Suarez, P., Anderson, W., Mahal, V., & Lakshmanan, T. R. (2005). Impacts of flooding and climate change on urban transportation: A systemwide performance assessment of the Boston Metro Area. *Transportation Research Part D: transport and environment*, *10*(3), 231-244.

24. Chang, H., Lafrenz, M., Jung, I. W., Figliozzi, M., Platman, D., & Pederson, C. (2010). Potential impacts of climate change on flood-induced travel disruptions: a case study of Portland, Oregon, USA. *Annals of the Association of American Geographers*, *100*(4), 938-952.

25. Miao, Q., Feeney, M. K., Zhang, F., Welch, E. W., & Sriraj, P. S. (2018). Through the storm: Transit agency management in response to climate change. *Transportation Research Part D: Transport and Environment*, 63, 421-432.

26. TWDB. (2012). "Water for Texas 2012 State Water Plan." Texas Water Development Board, Austin, TX.

27. Sharif, H., Jackson, T., Hossain, M., and Zane, D. (2014). "Analysis of Flood Fatalities in Texas." Natural Hazards Review, 0(0), 04014016.

28. Bonnin, G. M., Martin, D., Lin, B., Parzybok, T., Yekta, M., & Riley, D. (2006). Precipitation-frequency atlas of the United States. *NOAA atlas*, *14*(2), 1-65.

29. Asquith, W.H., and Roussel, M.C., 2004, Atlas of depth-duration frequency of precipitation annual maxima for Texas: U.S. Geological Survey Scientific Investigations Report 2004–5041, 106 p., http://pubs.usgs.gov/sir/2004/5041/.

30. Cleveland, T. G., Herrmann, G. R., Tay, C. C., Neale, C. M., Schwarz, M. R., & Asquith, W. H. (2015). *New rainfall coefficients: including tools for estimation of intensity and hyetographs in Texas* (No. FHWA/TX-15/0-6824-1). Texas. Dept. of Transportation. Research and Technology Implementation Office.

31. Lin, Y. (2019, August 13). GCIP/EOP Surface: Precipitation NCEP/EMC 4KM Gridded Data (GRIB) Stage IV Data, Version 1.0, UCAR/NCAR–Earth Observing Laboratory. Retrieved from http://data.eol.ucar.edu/cgi-bin/codiac/fgr_form/id=21.093.

32. City of San Antonio. (2019, August 13). GIS data. Retrieved from https://www.sanantonio.gov/GIS/GISData.

33. Reclamation (2013). 'Downscaled CMIP3 and CMIP5 Climate and Hydrology Projections: Release of Downscaled CMIP5 Climate Projections, Comparison with preceding Information, and Summary of User Needs', prepared by the U.S. *Department of the Interior, Bureau of Reclamation, Technical Services Center*, Denver, Colorado. 47pp.

34. Schmidli, J., Goodess, C. M., Frei, C., Haylock, M. R., Hundecha, Y., Ribalaygua, J., & Schmith, T. (2007). Statistical and dynamical downscaling of precipitation: An evaluation and comparison of scenarios for the European Alps. *Journal of Geophysical Research: Atmospheres*, *112*(D4).

35. Mpelasoka, F. S., & Chiew, F. H. (2009). Influence of rainfall scenario construction methods on runoff projections. *Journal of Hydrometeorology*, *10*(5), 1168-1183.

36. Hosking, J.R.M., 1990, L-moments—Analysis and estimation of distributions using linear combinations of order statistics: Journal Royal Statistical Society B, v. 52, no. 1, p. 105–124.

37. U.S. Weather Bureau. 1953. Rainfall Intensities for Local Drainage Design in the United States. Technical Paper No. 24, Part I, U.S. Department of Commerce, Weather Bureau, Washington, DC, 19 p.

38. Garbrecht, J., & MARTZ, L. W. (2004). TOPAZ user manual.

39. Green, W. H., & Ampt, G. A. (1911). Studies on Soil Phyics. The Journal of Agricultural Science, 4(1), 1-24. https://doi.org/10.1017/S0021859600001441.

40. Pradhan, N. R., & Loney, D. (2018). An analysis of the unit hydrograph peaking factor: A case study in Goose Creek Watershed, Virginia. *Journal of Hydrology: Regional Studies*, *15*, 31-48.

41. Rawls, W. J., Brakensiek, D. L., & Miller, N. (1983). Green-Ampt infiltration parameters from soils data. *Journal of hydraulic engineering*, *109*(1), 62-70.

42. Domenico, P.A. and F.W. Schwartz, (1990). Physical and Chemical Hydrogeology, John Wiley & Sons, New York, 824 p.

43. Harmsen, E. (Ed.), Goyal, M. (Ed.). (2018). Flood Assessment. New York: Apple Academic Press, https://doi.org/10.1201/9781315365923.

44. Maclay, R. W. (1995). Geology and hydrology of the Edwards Aquifer in the San Antonio area, Texas (No. 95-4186). US Geological Survey.

45. Prince-George's County. (2000). "Low-Impact Development Design Manual." Dept. of Environmental Resources, Prince George's County, Laurel, MD.

46. US EPA. (2000). "Low Impact Development: A Literature Review." Office of Water, Washington, D.C.

47. Fry, T. J., & Maxwell, R. M. (2017). Evaluation of distributed BMP s in an urban watershed—High resolution modeling for stormwater management. *Hydrological processes*, *31*(15), 2700-2712.

48. Fadhel, S., Rico-Ramirez, M. A., & Han, D. (2017). Uncertainty of intensity–duration–frequency (IDF) curves due to varied climate baseline periods. *Journal of hydrology*, *547*, 600-612.

49. Alam, M. S., & Elshorbagy, A. (2015). Quantification of the climate change-induced variations in Intensity–Duration–Frequency curves in the Canadian Prairies. *Journal of Hydrology*, *527*, 990-1005.

50. So, B. J., Kim, J. Y., Kwon, H. H., & Lima, C. H. (2017). Stochastic extreme downscaling model for an assessment of changes in rainfall intensity-duration-frequency curves over South Korea using multiple regional climate models. *Journal of Hydrology*, *553*, 321-337.

51. Willems, P. (2013). Revision of urban drainage design rules after assessment of climate change impacts on precipitation extremes at Uccle, Belgium. *Journal of Hydrology*, *496*, 166-177.

52. Moriasi, D. N., Arnold, J. G., Van Liew, M. W., Bingner, R. L., Harmel, R. D., & Veith, T. L. (2007). Model evaluation guidelines for systematic quantification of accuracy in watershed simulations. Transactions of the ASABE, 50(3), 885-900.

53. van der Wiel, K., Kapnick, S. B., van Oldenborgh, G. J., Whan, K., Philip, S., Vecchi, G. A., . . . Cullen, H. (2017). Rapid attribution of the August 2016 flood-inducing extreme precipitation in south Louisiana to climate change. *Hydrol. Earth Syst. Sci.*, 21(2), 897-921. doi:10.5194/hess-21-897-2017.

54. Santhi, C., Arnold, J. G., Williams, J. R., Dugas, W. A., Srinivasan, R., & Hauck, L. M. (2001). validation of the swat model on a large RWER basin with point and nonpoint sources 1. JAWRA *Journal of the American Water Resources Association*, 37(5), 1169-1188.

55. Hu, M.; Zhang, X.; Li, Y.; Yang, H.; Tanaka, K.; Tanka, K. Flood mitigation performance of low impact development technologies under different storms for retrofitting an urbanized area. *J. Clean. Prod.* 2019, *222*, 373–380.

56. McPherson, E. G. (1992). Accounting for benefits and costs of urban greenspace. *Landscape and Urban Planning*, *22*(1), 41-51.

57. SARA. *About/Projects*. San Antonio River Authority. https://www.sara-tx.org/about/projects. Accessed Aug. 23, 2019.

58. NOAA. *NOAA's Weather and Climate Tool Kit*. National Oceanic and Atmospheric Administration (NOAA). https://www.ncdc.noaa.gov/wct/index.php. Accessed Aug. 23, 2019.

APPENDIX A: LEON CREEK CALIBRATION OF HEC-HMS

Table A1. Calibration of the Lean Creek HEC-HMS model.

	Initial Value			Calibrated		
Subbasin ID	**Suction Head (cm)**	**Hydraulic Conductivity (cm/hr)**	**Impervious Area (%)**	**Suction Head (cm)**	**Hydraulic Conductivity (cm/hr)**	**Impervious Area (%)**
1	6.01	0.0191	12.48	7.81	0.016	2.16
2	6.26	0.0196	3.12	8.14	0.016	0.54
3	7.02	0.0219	7.28	9.13	0.018	1.26
4	4.79	0.0161	11.44	6.22	0.013	1.98
5	6.02	0.0369	57.20	7.83	0.030	29.29
6	6.68	0.0360	57.20	8.69	0.029	29.29
7	6.52	0.0270	61.88	8.48	0.022	31.68
8	5.45	0.0270	67.60	7.08	0.022	34.61
9	6.81	0.0307	71.76	8.85	0.025	36.74
10	4.56	0.0208	1.60	5.93	0.017	0.28
11	3.96	0.0131	61.54	5.15	0.011	31.51
12	6.37	0.0245	71.76	8.28	0.020	36.74
13	5.33	0.0223	70.72	6.93	0.018	36.21
14	4.56	0.0190	69.68	5.93	0.016	35.68
15	4.71	0.0225	57.20	6.13	0.018	29.29
16	4.96	0.0228	58.24	6.44	0.019	29.82
17	4.06	0.0232	51.32	5.28	0.019	26.28
18	6.68	0.0360	65.52	8.69	0.029	33.55
19	6.52	0.0270	1.60	8.48	0.022	0.28
20	4.17	0.0183	59.28	5.42	0.015	30.35
21	4.10	0.0170	1.60	5.33	0.014	0.28
22	5.48	0.0272	54.08	7.12	0.022	27.69
23	4.09	0.0133	67.60	5.32	0.011	34.61
24	4.55	0.0193	59.28	5.92	0.016	30.35
25	7.55	0.0291	59.28	9.82	0.024	30.35
26	4.09	0.0133	61.36	5.32	0.011	31.42
27	5.35	0.0196	58.24	6.96	0.016	29.82
28	5.42	0.0210	44.72	7.05	0.017	7.73
29	4.43	0.0189	67.60	5.76	0.016	34.61
30	5.42	0.0210	67.60	7.05	0.017	34.61
31	5.52	0.0246	1.60	7.18	0.020	0.28
32	4.73	0.0153	59.28	6.15	0.012	30.35
33	3.49	0.0152	60.32	4.54	0.012	30.88
34	3.96	0.0131	43.27	5.15	0.011	7.48
35	5.23	0.0186	58.86	6.80	0.015	30.14
36	5.77	0.0220	67.60	7.50	0.018	34.61
37	7.61	0.0242	62.40	9.89	0.020	31.95
38	5.23	0.0186	41.60	6.80	0.015	7.19
39	3.96	0.0131	57.20	5.15	0.011	29.29
40	4.29	0.0166	76.00	5.58	0.014	38.91
41	5.31	0.0185	64.48	6.90	0.015	33.01
42	5.85	0.0225	69.68	7.61	0.018	35.68
43	4.85	0.0167	65.52	6.30	0.014	33.55

Subbasin ID	Initial Value			Calibrated		
	Suction Head (cm)	Hydraulic Conductivity (cm/hr)	Impervious Area (%)	Suction Head (cm)	Hydraulic Conductivity (cm/hr)	Impervious Area (%)
44	3.93	0.0150	67.60	5.11	0.012	34.61
45	7.75	0.0230	67.60	10.07	0.019	34.61
46	6.35	0.0197	2.08	8.26	0.016	0.36
47	4.73	0.0153	22.88	6.15	0.012	3.95
48	4.65	0.0168	11.44	6.04	0.014	1.98
49	5.31	0.0185	37.44	6.90	0.015	6.47
50	4.61	0.0149	47.84	5.99	0.012	8.27
51	5.79	0.0182	2.08	7.52	0.015	0.36
52	6.70	0.0208	3.12	8.71	0.017	0.54
53	3.96	0.0131	46.80	5.15	0.011	8.09
54	4.49	0.0146	65.52	5.84	0.012	33.55
55	5.76	0.0198	2.08	7.49	0.162	0.36
56	5.71	0.0203	67.60	7.43	0.017	34.61
57	6.35	0.0197	35.36	8.26	0.016	6.11
58	4.53	0.0160	1.60	5.89	0.013	0.28
59	4.61	0.0149	57.20	5.99	0.012	29.29
60	4.80	0.0155	2.08	6.24	0.013	0.36
61	5.49	0.0174	13.52	7.13	0.014	2.34
62	6.25	0.0194	2.08	8.12	0.016	0.36
63	3.93	0.0150	3.12	5.11	0.012	0.54
64	5.49	0.0227	30.16	7.14	0.019	5.21
65	5.15	0.0191	77.60	6.70	0.016	39.73
66	2.76	0.0116	23.92	3.59	0.009	4.13
67	5.86	0.0348	1.60	7.62	0.028	0.28
68	5.29	0.0220	78.00	6.88	0.018	39.94
69	4.82	0.0162	58.24	6.26	0.013	29.82
70	6.24	0.0211	17.68	8.11	0.017	3.06
71	7.76	0.0452	73.60	10.09	0.037	37.68
72	6.35	0.0013	36.40	8.26	0.001	6.29
73	4.75	0.0158	69.68	6.18	0.013	35.68
74	6.19	0.0193	12.48	8.04	0.016	2.16
75	6.24	0.0211	71.22	8.11	0.017	36.46
76	5.14	0.0170	75.93	6.68	0.014	38.88
77	5.56	0.0223	72.55	7.23	0.018	37.15
78	4.61	0.0149	57.20	5.99	0.012	29.29
79	5.75	0.0013	56.16	7.48	0.001	28.75
80	5.02	0.0357	58.24	6.53	0.029	29.82
81	4.00	0.0186	5.20	5.20	0.015	0.90
82	6.04	0.0369	58.24	7.85	0.030	29.82
83	7.32	0.0284	32.94	9.52	0.023	5.69
84	4.27	0.0184	67.60	5.55	0.015	34.61
85	5.75	0.0250	54.08	7.48	0.020	27.69
86	6.48	0.0417	54.08	8.42	0.034	27.69
87	4.06	0.0201	64.96	5.27	0.016	33.26
88	6.11	0.0315	51.12	7.94	0.026	26.17
89	7.05	0.0951	68.54	9.17	0.078	35.09
90	8.65	0.0507	77.79	11.24	0.042	39.83

Subbasin ID	Initial Value			Calibrated		
	Suction Head (cm)	Hydraulic Conductivity (cm/hr)	Impervious Area (%)	Suction Head (cm)	Hydraulic Conductivity (cm/hr)	Impervious Area (%)
91	5.86	0.0348	59.16	7.62	0.028	30.29
92	7.32	0.0284	69.13	9.52	0.023	35.39
93	4.26	0.0176	31.97	5.54	0.014	5.52
94	4.40	0.0190	54.08	5.72	0.016	27.69
95	5.89	0.0250	43.36	7.65	0.020	7.49
96	6.74	0.0295	53.04	8.76	0.024	27.16
97	5.70	0.0337	54.08	7.41	0.028	27.69
98	6.15	0.0220	40.56	8.00	0.0137	7.01

APPENDIX B: UPPER SAN ANTONIO CALIBRATION OF HEC-HMS

Table B1. Calibration of the Upper San Antonio HEC-HMS model.

	Initial Value			Calibrated		
Subbasin ID	**Suction Head (cm)**	**Hydraulic Conductivity (cm/hr)**	**Impervious Area (%)**	**Suction Head (cm)**	**Hydraulic Conductivity (cm/hr)**	**Impervious Area (%)**
1	3.44	0.016	67.20	4.12	0.012	70.34
2	2.68	0.037	57.54	3.21	0.028	50.76
3	4.07	0.037	57.54	4.89	0.028	68.50
4	5.19	0.047	67.20	6.23	0.036	80.00
5	5.94	0.045	67.20	7.12	0.035	80.00
6	5.02	0.042	64.67	6.03	0.033	76.99
7	5.41	0.039	66.67	6.49	0.030	79.37
8	5.61	0.040	65.91	6.74	0.030	78.46
9	6.39	0.047	66.65	7.67	0.036	79.34
10	8.87	0.051	67.20	10.65	0.039	80.00
11	8.79	0.048	62.30	10.55	0.037	79.73
12	8.89	0.048	67.20	10.67	0.037	80.00
13	8.16	0.029	65.76	9.80	0.023	78.29
14	7.64	0.038	65.86	9.16	0.029	78.40
15	7.96	0.041	67.20	9.56	0.031	80.00
16	7.63	0.041	66.91	9.16	0.031	79.65
17	9.17	0.038	69.72	11.01	0.030	80.00
18	6.43	0.033	67.20	7.71	0.026	80.00
19	7.58	0.046	66.78	9.10	0.036	79.50
20	4.27	0.041	45.31	5.13	0.032	53.94
21	6.28	0.046	58.56	7.53	0.035	69.71
22	6.47	0.044	61.98	7.77	0.034	73.79
23	3.57	0.047	60.95	4.29	0.036	72.56
24	7.42	0.037	63.95	8.90	0.029	76.13
25	7.55	0.040	65.30	9.06	0.031	77.74
26	8.95	0.047	67.20	10.74	0.036	80.00
27	6.35	0.036	66.01	7.61	0.027	78.58
28	8.79	0.040	65.86	10.55	0.031	78.40
29	5.64	0.037	47.70	6.76	0.029	56.79
30	4.08	0.042	25.27	4.89	0.032	30.08
31	6.98	0.046	39.22	8.38	0.035	46.69
32	5.51	0.048	57.22	6.62	0.037	68.12
33	3.00	0.047	18.56	3.61	0.036	22.10
34	3.02	0.046	0.07	3.62	0.035	70.32
35	3.81	0.044	67.20	4.58	0.034	57.50
36	6.72	0.047	56.00	8.07	0.036	64.30
37	2.71	0.045	62.80	3.25	0.035	74.76
38	3.17	0.042	65.61	3.81	0.032	78.11
39	2.93	0.036	66.30	3.52	0.028	78.93

Subbasin ID	Initial Value			Calibrated		
	Suction Head (cm)	Hydraulic Conductivity (cm/hr)	Impervious Area (%)	Suction Head (cm)	Hydraulic Conductivity (cm/hr)	Impervious Area (%)
40	3.02	0.037	66.58	3.62	0.028	79.26
41	3.81	0.037	67.12	4.58	0.029	79.91
42	6.72	0.048	67.07	8.07	0.037	79.84
43	7.41	0.037	66.66	8.89	0.028	79.36
44	3.82	0.033	66.98	4.58	0.025	79.45